Identification of novel clinical applications for acid sphingomyelinase inhibitors

Inaugural-Dissertation

zur

Erlangung des Doktorgrades

Dr. rer. nat.

der Fakultät für

Biologie

an der

Universität Duisburg-Essen

vorgelegt von

Nadine Beckmann

aus Haan (Rheinland), Deutschland

im Juni 2017

Die der vorliegenden Arbeit zugrundeliegenden Experimente wurden am Institut für Molekularbiologie, Universität Duisburg-Essen durchgeführt.

1. Gutachter: Prof. Dr. Erich Gulbins

2. Gutachter: Prof. Dr. Dirk M. Hermann

3. Gutachter: Prof. Dr. Florian Lang

Vorsitzender des Prüfungsausschusses: Prof. Dr. Ralf Küppers

Tag der mündlichen Prüfung: 25.09.2017

Index

Abbreviations

AC	Acid ceramidase (human AC, murine Ac)
ACPA	Anti-citrullinated protein antibody
AIA	Antigen induced arthritis
ASAH1	N-acylsphingosine amidohydrolase 1 (human gene *ASAH1*, murine *Asah1*)
ASM	Acid sphingomyelinase (human ASM, murine Asm)
bSM	Bacterial sphingomyelinase
CF	Cystic fibrosis
CFA	Complete Freud's adjuvant
CXCL	Chemokine C-X-C motif ligand
DMARD	Disease modifying anti rheumatic drug
ELISA	Enzyme-linked immunosorbent assay
FCS	Fetal calf serum
FD	Farber disease
FDA	Food and drug administration agency
FIASMA	Functional inhibitor of acid sphingomyelinase
GALT	Gut-associated lymphoid tissue
GC	Glucocorticoid
GPT	Glutamic-pyruvic transaminase (also known as alanine transaminase)
GOT	Glutamic oxaloacetic transaminase (also known as aspartate transaminase)
HLA	Human leukocyte antigen
i.m.	Intramuscular
i.p.	Intraperitoneally
i.v.	Intravenously
IL	Interleukin
iNOS	Inducible NO synthase
LAMP-1	Lysosomal-associated membrane protein 1
L-ASM	Lysosomal acid sphingomyelinase
LDH	Lactate dehydrogenase
MAPK	Mitogen-activated protein kinase
mBSA	Methylated bovine serum albumin
MCP-1	Monocyte chemoattractant protein 1

MMP	Matrix metalloproteinase
MTX	Methotrexate
NK	Natural killer cells
NO	Nitric oxide
PBMC	Peripheral blood mononuclear cell
PBS	Phosphate-buffered saline
PFA	Paraformaldehyde
PHA	Phytohaemagglutinin
RA	Rheumatoid arthritis
RF	Rheumatoid factor
rhAC	Recombinant human acid ceramidase
RNS	Reactive nitrogen species
ROS	Reactive oxygen species
S-ASM	Secretory acid sphingoymelinase
SMPD1	Sphingomyelin phosphodiesterase 1 (human gene *SMPD1*, murine *Smpd1*)
SGLT	Sodium-glucose linked transporters
SSZ	Sulfasalazine
TGFß	Transforming growth factor ß
TLC	Thin layer chromatography
TNF-α	Tumor necrosis factor α
VEGF	Vascular endothelial growth factor

List of figures

List of tables

1. Abstract

Acid sphingomyelinase is a lysosomal enzyme that catalyzes the hydrolysis of sphingomyelin to ceramide. Acid sphingomyelinase/ceramide have been implicated in the pathogenesis of a number of different diseases. Pharmacological inhibitors of acid sphingomyelinase are already in clinical use and are well tolerated. Thus, this study aimed to expand the existing applications of known acid sphingomyelinase inhibitors to acid sphingomyelinase/ceramide-related diseases with a currently unmet clinical treatment need.

Farber disease is a rare lysosomal storage disorder caused by ceramide accumulation due to acid ceramidase deficiency. This study introduces a new mouse model to study FD that mirrors the human disease closely. Cross-breeding of these mice to acid sphingomyelinase-deficient mice reduced ceramide accumulation, improved disease manifestations and prolonged survival. Pharmacological inhibition of acid sphingomyelinase, however, failed due to unexpected, genotype-specific toxicity.

In rheumatoid arthritis, an autoimmune disorder affecting predominantly the joints, ceramide levels in the synovial fluid of patients have been reported to be elevated. Using a mouse model of inflammatory arthritis, this study analyzed the role of acid sphingomyelinase in joint inflammation and shows that both genetic ablation and pharmacological inhibition of acid sphingomyelinase ameliorates arthritis severity.

Zusammenfassung

Das Enzym Saure Sphingomyelinase katalysiert die Hydrolyse von Sphingomyelin zu Ceramid. Saure Sphingomyelinase und Ceramid spielen eine Rolle in der Pathogenese einer Reihe verschiedener Erkrankungen. Pharmakologische Inhibitoren der Sauren Sphingomyelinase werden bereits in der Klinik eingesetzt und sind gut verträglich. Das Ziel dieser Arbeit war es deshalb, die Anwendungsgebiete dieser bereits eingesetzten Inhibitoren auf Erkrankungen zu erweitern, bei denen die Saure Sphingomyelinase und/oder Ceramid eine Rolle spielen und die bislang nur unzureichend behandelt werden können.

Farber Lipogranulomatose ist eine seltene lysosomale Speichererkrankung, bei der es aufgrund einer Sauren Ceramidase-Defizienz zu einer Anreicherung von Ceramid kommt. Diese Arbeit stellt ein neues Mausmodell zur Erforschung der Erkrankung vor, dass den Phänotyp der humanen Erkrankung wiederspiegelt. Die Kreuzung dieser Mäuse mit Saure Sphingomyelinase-defizienten Mäusen reduzierte die Ceramid-Akkumulation, verbesserte die Symptome und verlängerte das Überleben der Farber-Mäuse. Die pharmakologische Inhibition scheiterte jedoch aufgrund unerwarteter, Genotyp-spezifischer Toxizität.

Rheumatoide Arthritis ist eine Autoimmunerkrankung, die vor allem die Gelenke betrifft. In der Synovialflüssigkeit von Patienten mit dieser Erkrankung wurden erhöhte Ceramid-Spiegel festgestellt. Mithilfe eines Mausmodells für entzündliche Arthritis wurde in dieser Arbeit die Rolle der Sauren Sphingomyelinase bei Gelenkentzündungen untersucht. Sowohl durch genetische Deletion als auch durch pharmakologische Inhibition der sauren Sphingomyelinase konnte die Gelenkentzündung reduziert werden.

2. Introduction

2.1 Acid sphingomyelinase

2.1.1 Structure and maturation

Acid sphingomyelinase (human ASM, murine Asm; Enzyme Commission Classification number 3.1.4.12) catalyzes the hydrolysis of sphingomyelin to phosphorylcholine and ceramide with an acidic pH optimum. It is encoded by one conserved gene (human *SMPD1*, murine *Smpd1*) of 5-6 kb located on the p15.1-p15.4 region of chromosome 11. The gene encompasses 6 exons and yields 7 isoforms, of which only the one containing all six exons is catalytically active (Rhein et al. 2012; Schuchman et al. 1991).

The nascent polypeptide (pre-pro-ASM) contains a signal peptide, saposin-domain, proline-rich linker, catalytic metallophosphatase (phosphodiesterase) domain and a carboxy-terminal region (Fig. 1). The signal peptide targets pre-pro-ASM to the endoplasmatic reticulum, where it is then cleaved. The resulting pro-ASM is glycosylated, which determines further cellular trafficking and later activity: High-mannose oligosaccharides yield lysosomal ASM (L-ASM); complex N-glycosylation yields secretory ASM (S-ASM) (Hurwitz et al. 1994; Schissel, Keesler, et al. 1998). Since S-ASM is secreted via the Golgi secretory pathway, this precursor depends on extracellular Zn^{2+} ions for activation, whereas L-ASM binds intracellular Zn^{2+} ions during trafficking to lysosomes (Schissel, Keesler, et al. 1998). The typical C-terminal cleavage of lysosomal hydrolases within the endolysosomal compartment is thought to promote the coordination of lysosomal Zn^{2+} ions by L-ASM: The C-terminal Cys631[1] residue of L-ASM is involved in the coordination of the active site Zn^{2+} ion, keeping the enzyme in the low activity form. C-terminal cleavage eliminates Cys631, thus enhancing activity (Qiu et al. 2003). Cleavage occurs at either a canonical-site or at a non-canonical site by Caspase-7 (Edelmann et al. 2011). S-ASM, on the other hand, still contains Cys631, enabling regulation by oxidation-driven dimerization for full activation (Qiu et al. 2003). Essentially, this cysteine-dependent regulatory mechanism is identical to the "cysteine switch" described for metalloproteinases. The recently identified crystallographic structure of ASM adds further support to this: The saposin-domain of ASM can interact with the C-terminal domain, thus adopting a closed conformation that keeps the enzyme inactive. In the active enzyme, the saposin-domain establishes an interface with the catalytic domain. The catalytic domain itself forms a calcineurin-like fold with two zinc ions, with the linker wrapping around the catalytic domain (Gorelik et al. 2016; Xiong et al. 2016).

[1] All amino acids are numbered according to the reference sequence NM_000543.4 throughout this work.

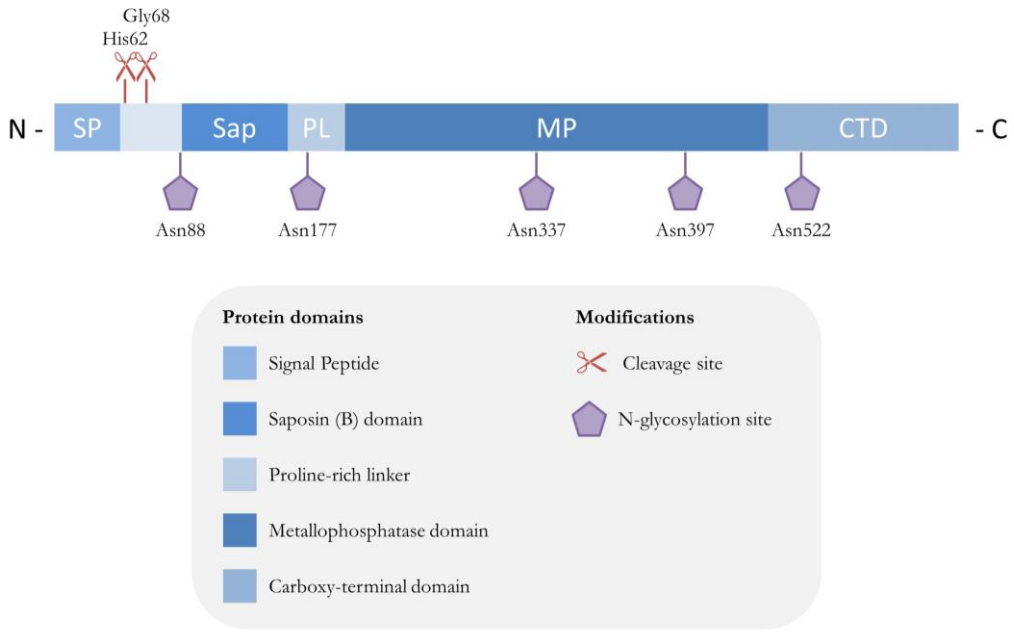

Figure 1: Protein domain structure of acid sphingomyelinase - Schematic representation of ASM-protein domains, including important posttranslational modifications. (Beckmann et al. 2017).

2.1.2. Signaling through ceramide-enriched platforms

Activation of ASM results in a reorganization of the plasma membrane. The "fluid mosaic model" by Singer and Nicolson was the first model to describe the organization of biological membranes, postulating a random distribution of lipids and free movement of proteins within the membrane (Singer and Nicolson 1972). This "fluid-disordered" model has since been overturned by a liquid-ordered model: Hydrophilic and hydrophobic interactions of lipids with each other promote the formation of ordered structures termed "lipid rafts" (Brown and London 1998; Simons and Ikonen 1997).

Biological membranes contain three main classes of lipids – glycerolipids, sterols and sphingolipids. Sphingolipids contain one of five sphingoid bases (unsaturated amino-alcohol) as a backbone, linked to one fatty acid through an amide bond. Variability is achieved both in the hydrophobic part – by different chain-length, saturation-status and degree of fatty-acid-hydroxylation – and the hydrophilic part, by addition of hydroxyl-groups, phosphates and/or sugar residues. Interactions between sphingolipids also occur in both parts: The hydrophobic tails of sphingolipids interact with each other and with cholesterol via van-der-Waal interactions, whereas the polar head-groups interact via hydrophilic forces.

These interactions can result in distinct membrane domains. Particularly, ceramide molecules, product of ASM-mediated sphingomyelin hydrolysis, self-associate by the abovementioned forces. Thereby, they separate themselves and other lipids within the membrane, resulting in the formation of small, ceramide-enriched domains. These, in turn, spontaneously fuse to even larger membrane domains, which are then termed platforms. Platform-formation reorganizes receptors and signaling molecules within the membrane, as proteins also associate with ceramide moieties (or are repelled) by the same biophysical and energetic forces. Protein reorganization does not only depend on the composition of a given protein's transmembrane domain, but also on its structure – e.g. ligand binding may induce a conformational change that alters the transmembrane domain in such a way that the ceramide-interacting moieties are exposed, enabling the sorting into ceramide-enriched platforms only after ligand binding. Additionally, attraction to- or repulsion from platforms can also be mediated by the lipid cofactors of a given protein.

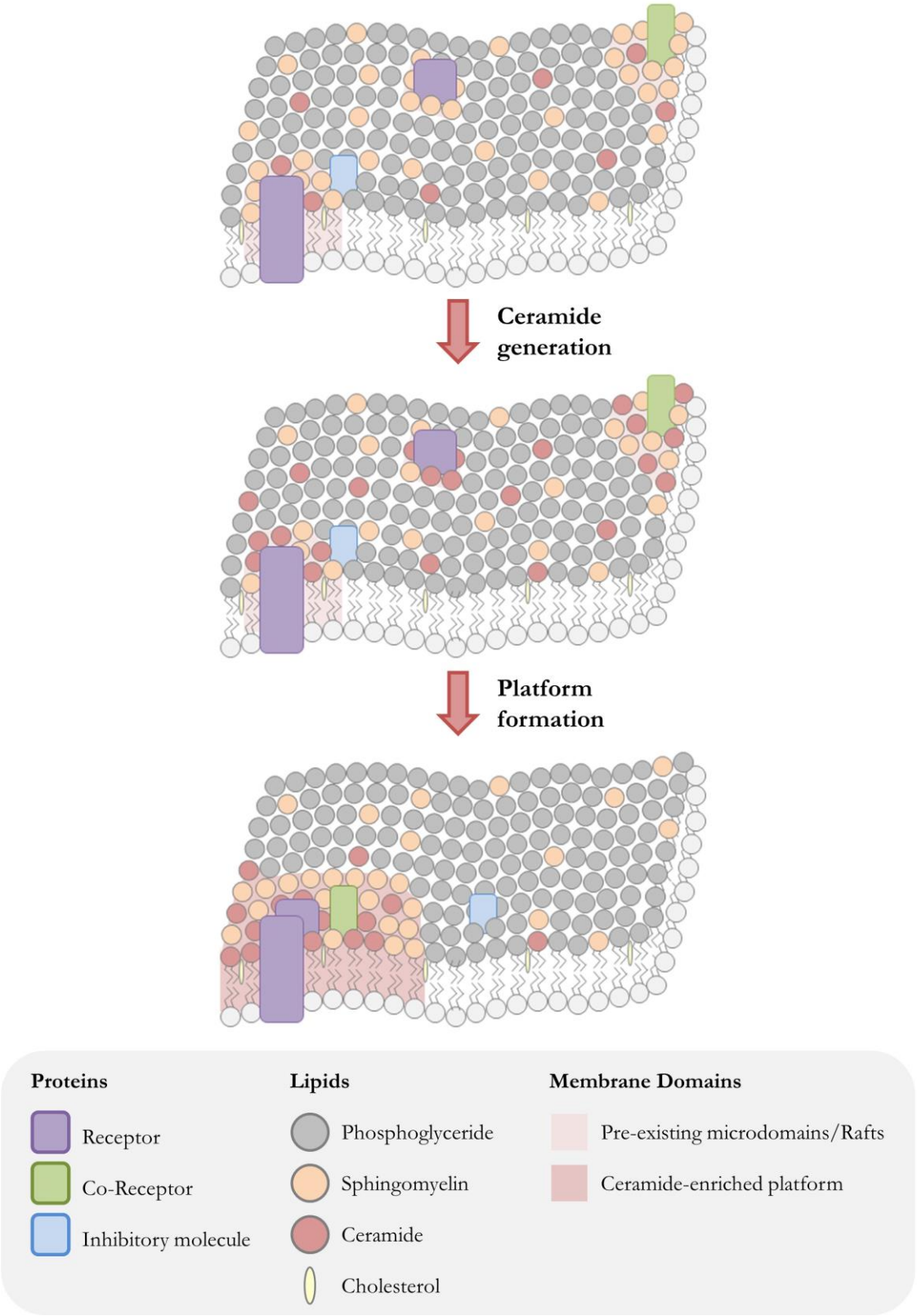

Figure 2: Ceramide-enriched platform formation – Upon activation and translocation of ASM to the plasma membrane, ceramide is generated from the abundant membrane lipid sphingomyelin. The resulting alteration to the biophysical properties of the membrane lead to the formation of small, ceramide-enriched microdomains. These fuse to form ceramide-enriched membrane platforms, which redistribute receptors and signaling molecules within the membrane, facilitating signal transmission. (Beckmann et al. 2017).

The reorganization of receptors and signaling molecules in ceramide-enriched platforms can act in several ways: By resulting in clustering of receptors, a high receptor density, spatial focusing of activated receptors with intracellular molecules, exclusion of inhibitory molecules and/or the transactivation of other enzymes. All this facilitates the transmission of a given signal across the membrane into the cell. Additionally, it enables generation of a strong, localized signal. Signaling via ceramide-enriched platforms is a unique mechanism and distinct from the stoichiometrical action of classical second messenger signaling. It also explains why various stimuli that activate ASM and induce platform formation can have so many different cellular effects.

ASM seems to typically signal via the formation of ceramide-enriched plasma-membrane platforms, while a signaling function of the intralysosomal protein is presently unknown. Given that these domains are formed in the plasma membrane, whereas ASM is present in the endolysosomal compartment (L-ASM) or secretory vesicles (S-ASM), ASM translocation is required in conjunction with ASM activation. L-ASM containing secretory lysosomes fuse with the plasma membrane in a syntaxin-4-dependent process (Perrotta et al. 2010), depositing L-ASM to the extracellular leaflet of the plasma membrane. Since the secretory lysosomes also include proton pumps, an acidic milieu is maintained locally in the subsequently formed ceramide-platforms, allowing optimal activity of ASM (Xu et al. 2012). It is important to note, however, that the lipid composition of the membrane alters the Michaelis-Menten constant (K_m) of ASM, thus also permitting ASM activity at higher pH (Schissel, Jiang, et al. 1998; Schissel, Keesler, et al. 1998). Since the generation of ceramide-enriched membrane platforms is a general mechanism reorganizing a given signalosome, not a specific signaling event, these platforms are able to play a role in the signaling of many receptors and cell stimuli. Thus, a large number of stimuli are known to trigger the formation of these membrane domains (an extensive list is provided in Table 1).

Table 1: ASM-activating stimuli – Overview of stimuli inducing ASM activation and/or ceramide-enriched platform formation (Beckmann et al. 2014).

Stimulus	References
Pathogens	
Listeria monocytogenes	Utermöhlen et al., 2003
Measles virus	Gassert et al., 2008; Avota et al., 2001
Mycobacterium avium	Utermöhlen et al., 2008
Neisseria gonorrhoeae	Grassme et al., 1997; Hauck et al., 2000
Pseudomonas aeruginosa	Grassme et al., 2003a; Zhang et al., 2008
Rhinoviruses	Grassme et al., 2005; Dreschers et al., 2007; Miller et al., 2012
Salmonella typhimurium	McCollister et al., 2007
Sindbis virus	Jan et al. 2000
Staphylococcus areus	Esen et al. 2001
Cluster of differentiation molecules	
CD5	Simarro et al., 1999
CD14	Pfeiffer et al., 2001
CD20	Bezombes et al., 2004
CD28	Boucher et al., 1995
CD32 (FCγRII)	Abdel-Shakor et al., 2004; Korzeniowski et al., 2007
CD38	Jia et al. 2008
CD40	Grassme et al. 2002
CD95	Cifone et al., 1994; Cremesti et al., 2001; Perrotta et al., 2010
CD95-DISC	Kirschneck et al., 2000; Grassme et al., 2001a,b, 2003b
CD253 (TRAIL)	Dumitru and Gulbins, 2006; Dumitru et al., 2007; Li et al., 2013
IL-1 receptor	Mathias et al., 1993

Table 1 (continued)	
Soluble molecules	
Platelet Activating Factor	Samapati et al., 2012; Predescu et al., 2013
Tumor necrosis factor	Schütze et al., 1992; Garcia-Ruiz et al., 2003; Edelmann et al., 2011; Adestani et al., 2013
Visfatin	Boini et al., 2010a
Drugs	
Cisplatin	Lacour et al., 2004; Zeidan et al., 2008
Cu2+-treatment	Lang et al., 2007
Doxorubicin	Dumitru et al., 2007
Heat damage	Chung et al., 2003
Ischemia-reperfusion injury	Yu et al., 2000
Oxidative stress	Zhang et al., 2007; Li et al., 2012
Oxygen radicals	Sheel-Toellner et al., 2004
UV-light	Zhang et al., 2001; Charruyer et al., 2005; Kashkar et al., 2005; Rotolo et al., 2005
γ-irradiation	Santana et al., 1996; Paris et al., 2001; Lee et al., 2011

2.1.3 Physiological Inhibition of ASM-mediated Signaling

Several innate ASM-inhibitory mechanisms have been described: Some of the alternative splice variants of ASM lack the catalytic and/or carboxy-terminal domains (transcripts 5, 6 and 7) and function as dominant-negative proteins (Rhein et al. 2012). Additionally, inositol-phosphates inhibit ASM. However, the physiological significance of their inhibitory interaction with ASM is not yet known (Kolzer et al. 2003).

The translocation of L-ASM can be inhibited by nitric oxide (NO), which induces phosphorylation of syntaxin-4 via activation of G-kinase, thus preventing the fusion of secretory lysosomes with the plasma membrane (Perrotta et al. 2010).

Pharmacologically, a number of functional inhibitors of ASM (FIASMAs) have been identified. These will be discussed in more detail in the next section (2.2 – Pharmacological inhibitors of ASM).

2.1.4 ASM in disease

ASM was originally identified as the cause of the lysosomal storage disorder Niemann-Pick disease type A and B (Brady et al. 1966). Patients exhibit varying degrees of lipid storage and foam cell infiltration in tissues and clinically present with hepatosplenomegaly (type A and B), CNS involvement (type A) and lung involvement (type B). Type A patients typically die in early childhood, whereas disease progression is more variable in type B patients, who often survive into adulthood (reviewed in (Schuchman and Desnick 2017)).

In addition to Niemann-Pick disease, the ASM/ceramide system has been reported to play a role in the pathophysiology of a number of different diseases, including cardiovascular-, metabolic-, hepatic-, inflammatory and infectious diseases, as well as in cancer and tumor metastasis (please see Table 2 for more specific examples).

Table 2: Acid sphingomyelinase-related diseases – Overview of diseases, which have been linked to ASM/ceramide signaling. To be published in Beckmann et al. 2017.

Autoimmunity	**Inflammatory Diseases**
Kawasaki disease	Graft-versus-host-disease
Multiple sclerosis	Hemophagocytic lymphohistiocytosis
Systemic sclerosis	Hepatic fibrosis
Cancer	Inflammatory bowel disease
Chemotherapeutics	Mast cell function/allergies
Irradiation and radiotherapy	**Metabolic Diseases**
Metastasis	Diabetes
Cardivoascular Diseases	Diabetic retinopathy
Atherosclerosis	Obesity-induced kidney damage
Cardiomyocyte apoptosis (cardioplegia/reperfusion)	Steatohepatitis
Thrombus formation	**Neurological Disorders**
Genetic Disorders	Alzheimer disease
Sickle-cell disease	Major depression
Niemann-Pick dsease A and B	Parkinson's disease
Wilson disease/liver cirrhosis	**Skin conditions**
Infectious Diseases	Atopic dermatitis
Bacterial infections	Scleroderma
L. monocytogenes	**Respiratory diseases**
M. avium	Acute lung injury
N. gonorrhoeae	Aspriation penumonia
P. aeruginosa	Cystic fibrosis
S. aureus	Hypoxemic respiratory failure
S. typhimurium	Lung fibrosis
Endotoxic shock syndrome	Tuberculosis
Malaria/plasmodia	
Virus infections	
Measles virus	
Rhinovirus	
Sindbis virus	

Currently, the role of ASM in major depression is the only one clinically exploited, as a number of long-standing antidepressant drugs are actually ASM inhibitors: Originally, these tricyclic antidepressants were thought to inhibit monoamine uptake, but the identification of their ASM inhibitory capacity (Hurwitz, Ferlinz, and Sandhoff 1994) has led to an investigation into the role of ASM in major depression (Grassmé et al. 2015; Gulbins et al. 2016; Gulbins et al. 2013). These studies have since revealed that these drugs exert their antidepressant effect by inhibiting ASM and thus reducing hippocampal ceramide concentrations as well as increasing neuronal proliferation, maturation and survival (Grassmé et al. 2015; Gulbins et al. 2016; Gulbins et al. 2013).

ASM inhibitors are also being tested in clinical studies to treat cystic fibrosis (CF): Ceramide has been shown to mediate inflammation, cell death and infection susceptibility in CF (Teichgräber et al. 2008). Targeting ceramide accumulation with the ASM inhibitor Amitriptyline has had favorable results in a recently reported phase II clinical study (Adams et al. 2016) and is currently under investigation in a phase III clinical trial.

2.2 Pharmacological inhibitors of ASM

2.2.1 Functional inhibitors of ASM

Antidepressant drugs like Amitriptyline functionally inhibit ASM. FIASMAs are weak bases and thus accumulate in the lysosomes due to acid trapping: In their neutral state, they can passively diffuse across membranes. In acidic compartments like the lysosome, however, they become protonated and thus lose their ability to cross the membrane (Daniel and Wojcikowski 1997; Ishizaki et al. 1996; Kornhuber, Retz, and Riederer 1995; Trapp et al. 2008). It is proposed that due to their high lipophilicity, they then interfere with ASM-membrane attachment. L-ASM attaches to the inner membrane leaflet of the lysosome by electrostatic forces. Without membrane attachment, there is no contact to its substrate sphingomyelin. Further, unbound L-ASM is a target for lysosomal proteases. Thus, FIASMAs result in abrogation of ASM activity and induce subsequent proteolytic degradation of L-ASM (Kolzer, Werth, and Sandhoff 2004). Weak basicity and high lipophilicity are the physicochemical properties required for ASM inhibition by these drugs – rather than a specific structural motive (Kornhuber et al. 2010; Kornhuber et al. 2008). The recent identification of the structure of ASM has not conflicted this model. It does, however, also allow for the possibility that these drugs bind to the hydrophobic surface of the saposin domain and thus prevent saposin-substrate interaction (Zhou et al. 2016).

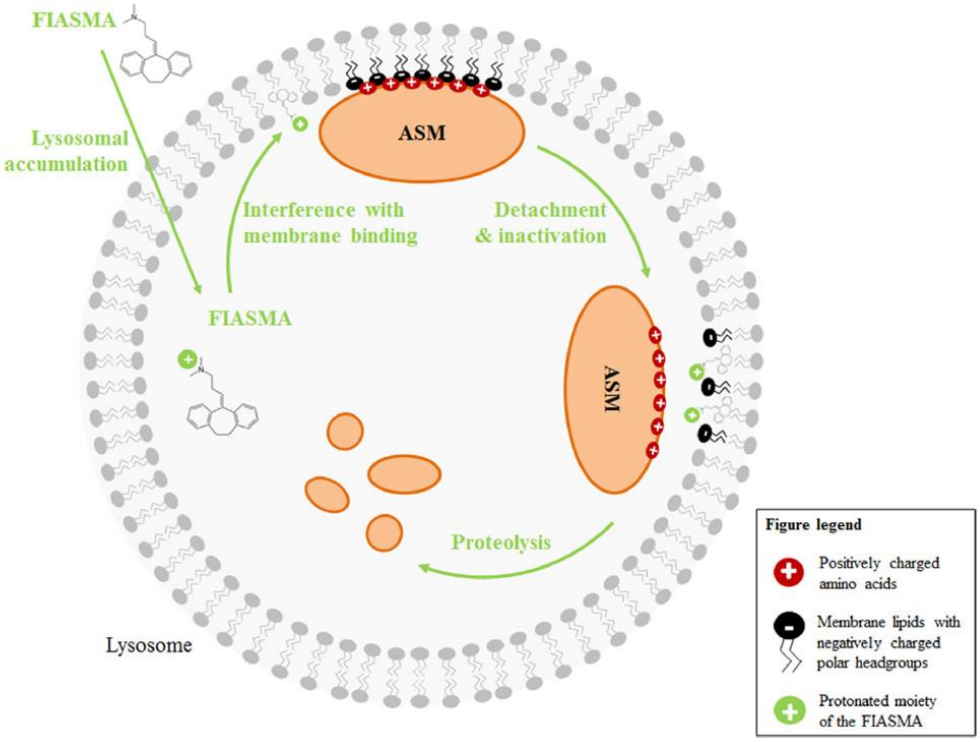

Figure 3: Mechanism of action of functional acid sphingomyelinase inhibitors – Due to acid trapping, FIASMAs accumulate in the lysosomes. Their lipophilic moieties anchor them in the membrane, exposing their protonated portion to the lumen. This alters the electrostatic dynamics of the inner lysosomal membrane and disrupts the electrostatic adherence of ASM, thereby inactivating the enzyme and targeting it for proteolytic degradation (Beckmann et al. 2014)

Extensive screening has identified a large number of substances as FIASMAs (Kornhuber et al. 2011; Kornhuber et al. 2008), most of them already in clinical use, e.g. the tricyclic antidepressants Amitriptyline, Desipramine, Imipramine and Fluoxetine. Favorable properties of FIASMAs include good absorption (all are orally active), distribution (extensive tissue binding, most can also cross the blood-brain barrier), metabolism and excretion, activity across different cell types, no habituation, reversible inhibition and no rebound effects (Kornhuber et al. 2010). Additionally, the inhibitory effects of FIASMAs are limited to the lysosomes, so neutral and alkaline sphingomyelinases are not affected. Concerning specificity, there also is no gross general inhibitory effect on other lysosomal hydrolases (Kornhuber et al. 2010). A few lysosomal enzymes, however, have been reported to be co-inhibited by cationic amphiphilic drugs, namely acid ceramidase (human AC, mouse Ac), lysosomal acid lipase and phospholipase A and C (Kornhuber et al. 2010). AC, for example, has been reported to be inhibited by Desipramine *in vitro* (Elojeimy et al. 2006).

2.2.2 Other inhibitors of ASM

Another option to inhibit ASM is by using sphingomyelin analogues which cannot be cleaved by ASM. Two such analogues ((3R,4S)-1,1-dufloro-4-hydroxy-3-palmitoylamino)-4-phenoylbutylphosphonic acid and AD2765) have been described, but both are clinically unsuitable because they are not selective: One also inhibited other sphingomyelinases (Yokomatsu et al. 2003) and the other (AD2764) also inhibited sphingomyelin synthase, thus even increasing ceramide concentrations (Darroch et al. 2005).

Some natural products isolated from the bark of *Garcinia speciosa* (α-mangostin, cowanin, cowanol) were also reported to inhibit ASM, however, they had greater selectivity for neutral sphingomyelinase (Okudaira et al. 2000) and subsequently synthesized substances (α-mangostin derivates) were less active overall (Hamada et al. 2003).

Phosphoinositides, such as phosphatidyl-myo-inositol-3,4,5-trisphosphate (Testai et al. 2004) and phosphatidyl-D-myoinositol-3,5-bisphosphate (Kolzer et al. 2003), are potent and selective physiological inhibitors of ASM. Unfortunately, they are ill suited for clinical application, as they are biologically active themselves, substrates for a variety of enzymes and unable to penetrate membranes and distribute intracellularly (Arenz 2010). The later feature, however, enables topical ASM inhibition in contexts where systemic ASM suppression is unneeded or unwanted. For instance, local administration of phosphatidyl-D-myoinositol-3,5-bisphosphate has been successfully used to improve oxygenation and pulmonary edema in an acute lung injury model (Preuss et al. 2012).

Several bisphophosphonates can also directly inhibit ASM (Roth et al. 2009). Zolendronic acid, for instance, is currently used for the treatment of osteoporosis. At present, however, it is unclear whether or not the bisphosphonates in current clinical use actually inhibit ASM *in vivo* and at therapeutic concentrations.

2.3. Acid ceramidase and Farber disease

2.3.1 Background, structure and maturation of acid ceramidase

Acid ceramidase (human AC, murine Ac; Enzyme Commission Classification number 3.5.1.23; also known as N-acylsphingosine deacylase) is the lipid hydrolase that acts downstream of ASM by deacetylating ceramide to sphingosine and free fatty acid. Importantly, however, AC can also catalyze the reverse reaction at a higher pH (Okino et al.

2003). Similar to ASM, AC also exists in a lysosomal and a secreted form (Ferlinz et al. 2001).

The AC gene (human *ASAH1*, murine *Asah1*) is located on the short arm of chromosome 8 (p21.3-22) and encompasses 14 exons and 13 introns (Li et al. 1999). The AC protein is synthesized as a precursor, which is glycosylated by Peptido-N-glycase and Endo-H and proteolytically processed into an α- and ß-subunit (Ferlinz et al. 2001). The later contains the catalytic domain. C-terminal processing also occurs (He et al. 2003). The processing enzymes and the precise subcellular localization of the precursors are presently unknown. The mature enzyme has been shown to form a multi-enzyme complex with ASM and a ß-galactosidase (putatively the one that uses galactosylceramide as a substrate) and requires Saposin D for activity (Azuma et al. 1994; He et al. 2003; Klein et al. 1994).

Deficiency of AC was identified as the cause of Farber Disease (FD) and has been linked to several cancers and Alzheimer's disease (reviewed in (Park and Schuchman 2006)).

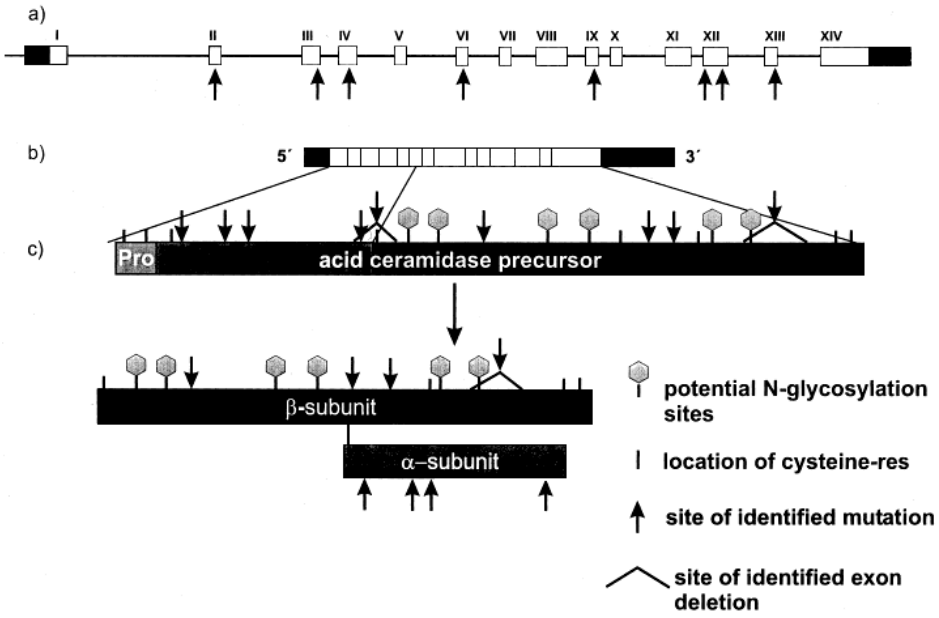

Figure 4: Structure of the *ASAH1* gene and the acid ceramidase protein – Illustration of the structure of the gene encoding AC (a), its cDNA structure (b) and protein domains (c). Sites of (putative) posttranslational modifications are indicated, as well as reported mutations. (Moser 2001).

2.3.2 Farber Disease

FD is a lysosomal storage disorder resulting from deficiency in AC, leading to an accumulation of lysosomal ceramide. The disease typically involves a triad of deformed

joints, subcutaneous nodules and progressive hoarseness. Histology shows granulomas and lipid-laden macrophages, which is why the disease is also known as Farber lipogranulomatosis. Since the first description by Sidney Farber in 1957 (Farber, Cohen, and Uzman 1957), 7 subtypes have been classified (Moser 2001). Subtype-I and IV patients have the most severe phenotype and most only survive for up to two years. Neurological involvement (type I) and/or hepatosplenomegaly (type IV) are common, as well as lung and heart involvement. The lungs have been reported to be involved in all severely affected patients and pulmonary disease is the most common cause of death in these patients. Some patients with a less severe phenotype survive into adulthood. The variability in disease severity and affected tissues cannot be explained so far – residual enzyme activity in *in vitro* assays does not appear to correlate with disease phenotype (Moser 2001).

FD is a very rare autosomal-recessive disease with a high frequency of consanguinity in the approximately 100 reported cases. Hence, the pathophysiology is only poorly described. FD in infancy can resemble juvenile idiopathic arthritis and a number of FD patients were originally diagnosed as having juvenile idiopathic arthritis (Sólyom et al. 2014; Torcoletti et al. 2014). Thus, it has been suggested that FD incidence may actually be higher, but that patients remain misdiagnosed as juvenile idiopathic arthritis. Diagnosis of FD is obtained by demonstration of reduced AC activity and/or abnormally high ceramide levels in cultured cells, biopsy samples or urine (Antonarakis et al. 1984; Ben-Yoseph et al. 1989; Dulaney et al. 1976; Fensom et al. 1979; Kudoh and Wenger 1982; Levade et al. 1995; Sugita et al. 1975). Prenatal diagnosis is possible with amniocytes or chorionic villus samples (Fensom et al. 1979).

Ceramide accumulation in FD occurs in the lysosomes (Levade et al. 1996; Sutrina and Chen 1982; van Echten-Deckert et al. 1997). Whereas this may influence ceramide levels in other compartments over time, it explains why the reported ceramide-mediated signaling pathways, i.e. apoptosis, do not appear to be aberrantly regulated in FD, as these are mediated by plasma membrane ceramide (Segui et al. 2000; Tohyama et al. 1999).

Currently, no cure for FD exists and treatment options are very limited. Some patients have been treated with allogenic haematopoetic stem cell transplantation with favorable results on joint manifestations (Ehlert et al. 2006; Torcoletti et al. 2014). However, this option is only suitable for patients without severe pulmonary disease and without neurological involvement (Yeager et al. 2000). The latter is also true for enzyme replacement therapy, which is currently being developed. Promising results from cell culture and mouse studies using the

recombinant human enzyme (rhAC) were recently reported (He et al. 2017). Still, the unsuitability of enzyme replacement therapy and hematopoietic stem cell transplantation for patients with neurological involvement means that there are essentially no treatment options for severely affected patients.

2.4 Rheumatoid arthritis

2.4.1 Background

Rheumatoid arthritis (RA) is a chronic autoimmune disorder with an intermittent course and the most common inflammatory arthropathy. It is characterized by an inflammation of synovial joints, which progresses chronically and continuously and results in joint swelling and deformation, cartilage loss and bone erosions (Landre-Beauvais 1800). Often, RA leads to disability as it progresses. Inflammation in RA is not limited to the joints, but can also develop into a systemic disease with cardiovascular, pulmonary and skeletal involvement (Cojocaru et al. 2010). Cardiovascular disease due to chronic inflammation is among the main causes of death among RA patients (Dhawan and Quyyumi 2008). Worldwide, approx. 1 % of adults are affected and women have an approximately 3 times higher risk of developing RA then men (Silman and Pearson 2002). Some risk factors for RA have been identified. The underlying mechanisms, however, remain incompletely understood.

2.4.2 Pathophysiology of rheumatoid arthritis

2.4.2.1 Genetic and environmental factors

Although the etiology is still unclear, both genetic and environmental risk factors have been identified in RA. One postulated mechanism is molecular mimicry, i.e. that sequence similarities between foreign and self-peptides result in a cross-activation of T lymphocytes or autoantibody production. An autoantibody commonly found in RA is anti-citrullinated protein antibody (ACPA). ACPA recognizes several citrullinated self-proteins, including α-enolase, keratin, fibrinogen, fibronectin, collagen and vimentin. ACPA production in patients has been associated with a common amino acid motif (QKRAA) in the human leucocyte antigen DR beta 1 (HLA-DRB1) gene region, the major genetic risk factor for RA (Gourraud et al. 2007). Additionally, ACPA seems to link genetic and environmental risk factors, since for instance smoking and HLA-DRB1 alleles synergistically increase one's risk of having ACPA (Lundstrom et al. 2009) and seropositivity for citrullinated α-enolase and vimentin yielded the strongest association of HLA-DRB1, protein tyrosine phosphatase non-receptor type 22 and smoking (Lundberg et al. 2013).

Viruses and bacteria, including Epstein-Barr virus, cytomegalovirus and *Escherichia coli* and their products have also been postulated to be linked to RA by molecular mimicry. During infection, the formation of immune complexes may also trigger the induction of rheumatoid factor (RF), a high-affinity autoantibody against the Fc portion of immunoglobulin and a diagnostic marker of RA. Periodontal disease increases the risk of RA through *Porphyromonas gingivalis* (*P. gingivalis*) peptidylarginine deiminase: The enzyme citrullinates bacterial proteins, but also host fibrinogen and α-enolase and thus provides a basis for autoantibody production (Rosenstein et al. 2004; Wegner et al. 2010). Additionally, specific bacterial signatures in the gut microbiome are emerging, that are also being associated with autoantibody production (Scher and Abramson 2011).

Environmental factors, such as smoking, may exert their effect through epigenetic modifications. Several such associations have been reported in RA: Alterations in DNA methylation, histone modifications and microRNA expression in immune and stromal cells influence key inflammatory and matrix-degrading pathways in RA (Messemaker, Huizinga, and Kurreeman 2015).

Despite all of these identified associations, critical issues remain unresolved: Autoantibodies such as RF and ACPA are not detected in all patients and the systemic loss of tolerance does not fit to the localized onset of inflammation in the joints.

2.4.2.2 Synovial inflammation

Synovial inflammation ("synovitis") results from leukocyte infiltration into the joint, rather than from local proliferation. Endothelial activation is thought to occur in synovial microvessels, resulting in an upregulation of adhesion molecules and chemokines and thus enabling cell recruitment into the joint (McMurray 1996). Platelets appear to help with this recruitment by adhering to the endothelium and releasing proinflammatory mediators and/or by providing a matrix for leukocyte adherence in a P-selectin dependent manner (Schmitt-Sody, Metz, Gottschalk, et al. 2007; Schmitt-Sody, Metz, Klose, et al. 2007).

Adaptive immunity appears to be at the center of early RA pathogenesis. The relationship between HLA-DRB1 and disease severity suggests an important role for T cells in RA. T cells are abundant in the synovial milieu and the RA synovium contains abundant myeloid cells, plasmacytoid dendritic cells, HLA class II molecules, stimulatory cytokines and other costimulatory molecules required for T-cell activation (Lebre et al. 2008; Schröder et al.

1996). After activation, T cells promote synovial inflammation through secretion of pro-inflammatory cytokines, but also through the support of B-cell activation and direct activation of innate immune cells, chondrocytes and osteoclasts. The later results in cartilage loss and bone erosion (McInnes, Buckley, and Isaacs 2016).

Although conventionally T_h1 helper cells are considered the key players in RA, the focus is now shifting towards the role of T_h17 cells: The cytokine milieu in RA (Transforming growth factor ß (TGFß), Tumor necrosis factor α (TNF-α) and Interleukins (IL)-1ß, -6, -21 and -23) shifts T cell hemostasis towards inflammation by supporting T_h17 differentiation and regulatory T cell suppression. Hence, the T_h17 cytokine IL-17 is currently being targeted in clinical trials (Genovese et al. 2014). Similar to the suppression of regulatory T cells, the differentiation into T_h2-like effector cells, which would produce anti-inflammatory cytokines, also appears to be suppressed in RA.

B cells are also integral to RA pathogenesis. The presence of T-cell-B-cell aggregates in the synovium and other observations suggest ongoing T-cell-promoted, local production of autoantibodies by plasma cells in the synovium and juxta-articular bone marrow (Ohata et al. 2005; Seyler et al. 2005). But the role of B cells in RA also goes beyond autoantibody production and includes autoantigen presentation and cytokine production (e.g. IL-6, TNF-α and lymphotoxin-ß) (Edwards et al. 2004).

The innate immune system is also represented in synovial inflammation. Macrophages, in particular, are central effectors in RA, by releasing cytokines (e.g. TNF-α, IL-1, IL-6, IL-12, IL-15, IL-18 and IL-23), reactive oxygen- and nitrogen species (ROS, RNS) and matrix-degrading enzymes, as well as by phagocytosis and antigen presentation (Haringman et al. 2005).

2.4.2.3 Key cytokines in rheumatoid arthritis

Cytokines play an important role in the pathogenesis of RA by mediating inflammation and joint destruction. Therefore, several anti-cytokine agents have been developed for the treatment of RA targeting TNF-α, IL-1, IL-6 and more recently also IL-17 (Cohen et al. 2002; Elliott et al. 1993; Hueber et al. 2010; Yoshizaki et al. 1998).

TNF-α is one of the main cytokines to result in inflammation during RA. It is released from activated macrophages, but also monocytes, fibroblasts, mast cells and natural killer (NK) cells. Locally, TNF-α stimulates the proliferation and differentiation of lymphocytes and NK

cells, promotes the production of other pro-inflammatory cytokines, e.g. IL-1 and IL-6, and induces the upregulation of adhesion molecules by fibroblasts. TNF-α is also elevated in the serum of RA patients, increasing the chances of cardiovascular disease through hypothalamic-pituitary-adrenal axis dysregulation (O'Connor, O'Halloran, and Shanahan 2000). Surprisingly, recent data also identified some anti-inflammatory effects of TNF-α (Masli and Turpie 2009; Yang et al. 1994).

IL-1ß is another pro-inflammatory and pro-erosive driver. It increases cytokine-, chemokine-, inducible NO synthase (iNOS)- and matrix metalloproteines (MMPs) secretion by synovial fibroblasts, as well as osteoclast activation and expression of adhesion molecules on the endothelium (McInnes, Buckley, and Isaacs 2016).

IL-6 contributes to inflammation and joint destruction through activation of neutrophils, which then secrete ROS and proteolytic enzymes, and stimulation of osteoclast differentiation. Synergistically with TNF-α and IL-1ß, it enhances the production of vascular endothelial growth factor (VEGF) to establish and maintain the pannus, i.e. the vascular fibrous tissue that expands over the joint surface in RA (Dayer and Choy 2010). Systemically, increased IL-6 levels in the blood of RA patients are associated with an increased risk of myocardial infarction (Yoshida and Tanaka 2014).

The main source of IL-17 are T_h17 cells, although some other cell types can also produce this cytokine. IL-17 increases the production of metalloproteinases, but also of pro-inflammatory cytokines, including again TNF-α, IL-1ß and IL-6 (McInnes, Buckley, and Isaacs 2016). Similarly to these, IL-17 also increases iNOS secretion and osteoclast stimulation. Moreover, IL-17 enhances the recruitment of further immune cells by stimulating chemokine production, e.g. C-X-C motif chemokine ligand 5 and 12 (CXCL5 and CXCL12) and by promoting neovascularization (Honorati et al. 2006; Kim et al. 2007). Suppression of IL-17 successfully reduced arthritis severity in experimental models (Gaffen 2009; Koenders et al. 2005; Sarkar et al. 2009).

In the experimental model of antigen-induced arthritis, which is employed as a model for inflammatory arthritis in this study, IL-6 and IL-1ß appear to be the driving cytokines, whereas TNF-α only increases mildly (Simon et al. 2001). Moreover, knock-out of TNF-α in mice conferred less protection from arthritis than IL-6 deficiency (Wong et al. 2006; Yokomatsu et al. 2003).

2.4.3 Treatment of rheumatoid arthritis

2.4.3.1 Disease modifying anti-rheumatic drugs

Historically, RA was treated with intramuscular (*i.m.*) injection of gold (Forestier 1932), because it was believed that RA had an infectious etiology and Koch had demonstrated the antimicrobial properties of gold cyanide in 1890. How gold salts actually reduce arthritis severity is unknown. *In vitro* studies suggested that gold works by interfering with lymphocyte and monocyte function, but *in vivo* studies do not support this. Thus, it is unclear how gold decreases the levels of immune complexes and RF (Klinefelter and Achurra 1973). Today, gold is no longer recommended for the treatment of RA due to high rate of adverse effects (approx. 33 %), potentially serious toxic effects (e.g. nephrotic syndrome, cytopenias, interstitial lung disease, peripheral neuropathies) and low response rates (only about 1/3 of patients achieve good clinical and radiographic responses) (Zampeli, Vlachoyiannopoulos, and Tzioufas 2015).

The first drug specifically synthesized for RA is Sulfasalazine (SSZ). Due to the idea that RA was caused by bacterial infections, which still prevailed at the time, the antibiotic sulfapyridine was linked to a complex saliacylic acid. SSZ effects T and B-cell populations and suppresses levels of IL-1 and TNF-α (Danis et al. 1992). Despite initially favorable results in open trials and a similar efficacy as *i.m.* gold and potentially also methotrexate, with less severe toxicity then both, SSZ therapy was discontinued.

The introduction of glucocorticoids (GCs) in the 1950 was originally hailed as the cure for RA. GCs do rapidly, reliably and effectively suppress synovitis and RA symptoms. Due to their devastating side effects at high and long-term doses, they are only used as a low-dose therapy today and even this is controversial (Saag 1997). The recommendation is to use GCs at the lowest possible dose for the shortest possible period of time to achieve the treatment goals (van der Goes et al. 2010).

Also in the 1950's, methotrexate (MTX) was shown to be effective in RA (Gubner, August, and Ginsberg 1951). It did not become the gold-standard of care until after the initial excitement over GCs had passed and the FDA approved treatment for RA in 1988. Originally developed as an anticancer drug, MTX is a folic acid analogue, that inhibits purine and pyrimidine synthesis and thus acts as a cytostatic agent. At the doses given for RA, however, MTX is minimally immunosuppressive. Thus, other mechanisms have been suggested, including inhibition of angiogenesis (Hirata et al. 1989). Mostly, adverse events due to MTX treatment are minor and can be managed without discontinuation of the drug. The potential

toxicity, however, is severe and may cause cytopenias, hepatotoxicity with subsequent fibrosis and cirrhosis, as well as pulmonary interstitial disease with subsequent fibrosis. For the later, the incidence may be up to 3-5 % (Zitnik and Cooper 1990). MTX is also abortifacient and teratogenic. Leflunomide, an inhibitor of *de novo* pyrimidine synthesis, is emerging as an alternative to MTX with similar efficacy but potentially better toxicity/tolerability profile (Xu et al. 1997).

Some more disease modifying anti-antirheumatic drugs (DMARDs) have been used clinically at some point. None have established themselves to a similar extent as MTX due to low efficacy (e.g. D-pencillamine and the antimalarials chloroquine and hydroxychloroquine) (Faarvang et al. 1993; Ferraz et al. 1994) or toxicity concerns (e.g. Cyclosporine A) (Case 2001). Thus, future advances are expected with biologic therapies rather than with classical DMARDs.

2.4.3.2 Novel therapeutic strategies in rheumatoid arthritis

Several new treatment options are in clinical development for the treatment of RA. Unsurprisingly, classical RA-cytokines were among the first new therapeutic targets. Anti-TNF biologics and anti-IL-6 receptor antibody have been shown to effectively control disease activity and prevent articular damage in RA, while anti-IL-17 antibodies, an anti-IL-21 and an anti-GM-CSF antibody are still being tested (Semerano et al. 2016).

The opposite route – delivering anti-inflammatory cytokines rather than blocking pro-inflammatory ones – is also being tried: Dekavil targets anti-inflammatory IL-10 to the joints by fusion with an anti-fibronectin antibody. IL-10 is an important suppressor of cytokine formation, including TNF-α, IL-1ß and IL-6. It also inhibits antigen-presentation by macrophages and MMP production (Mottonen et al. 1998). Dekavil obtained promising Phase 1b-trial results (Galeazzi et al. 2014).

The anti-CD20 antibody rituximab has already been approved for the treatment of RA. Next to depletion of all CD20-expressing B cells, rituximab has also been found to induce $CD4^+$ T cell depletion (Melet et al. 2013). Other antibodies against B-cell surface molecules, however, have been discontinued due to safety issues (Quattrocchi et al. 2016; Weinblatt et al. 1995).

Thus far, the targeting of cell-matrix interactions, ectopic lymphoid neogenesis, stromal cells, T_h17 differentiation, IL-17 receptor and the use of a non-depleting anti-CD4 antibody to induce tolerance have not yet achieved clinical efficacy (Semerano et al. 2016).

Targeting of intracellular signaling pathways in RA by small molecule kinase inhibitors are also being attempted: P38 mitogen-activated protein kinase (MAPK) inhibitors have already failed clinical development, probably due to redundant MAPK pathways (Genovese 2009). Similarly, the spleen-tyrosine kinase inhibitor Fostamatinib was also not pursued further (Kunwar, Devkota, and Ghimire 2016). A Bruton's tyrosine kinase inhibitor is currently undergoing a phase II study (Chang et al. 2011). One Janus kinase inhibitor, Tofacitinib, is already marketed in the US for RA, two (Decemotinib and Baricitinib) are currently in a Phase III study and two others (Filgotinib and ABT-494) have achieved significant clinical responses in phase IIb studies (Genovese et al. 2016; Kremer, Genovese, et al. 2016; Kremer, Emery, et al. 2016; Van Rompaey et al. 2013; Westhovens et al. 2016).

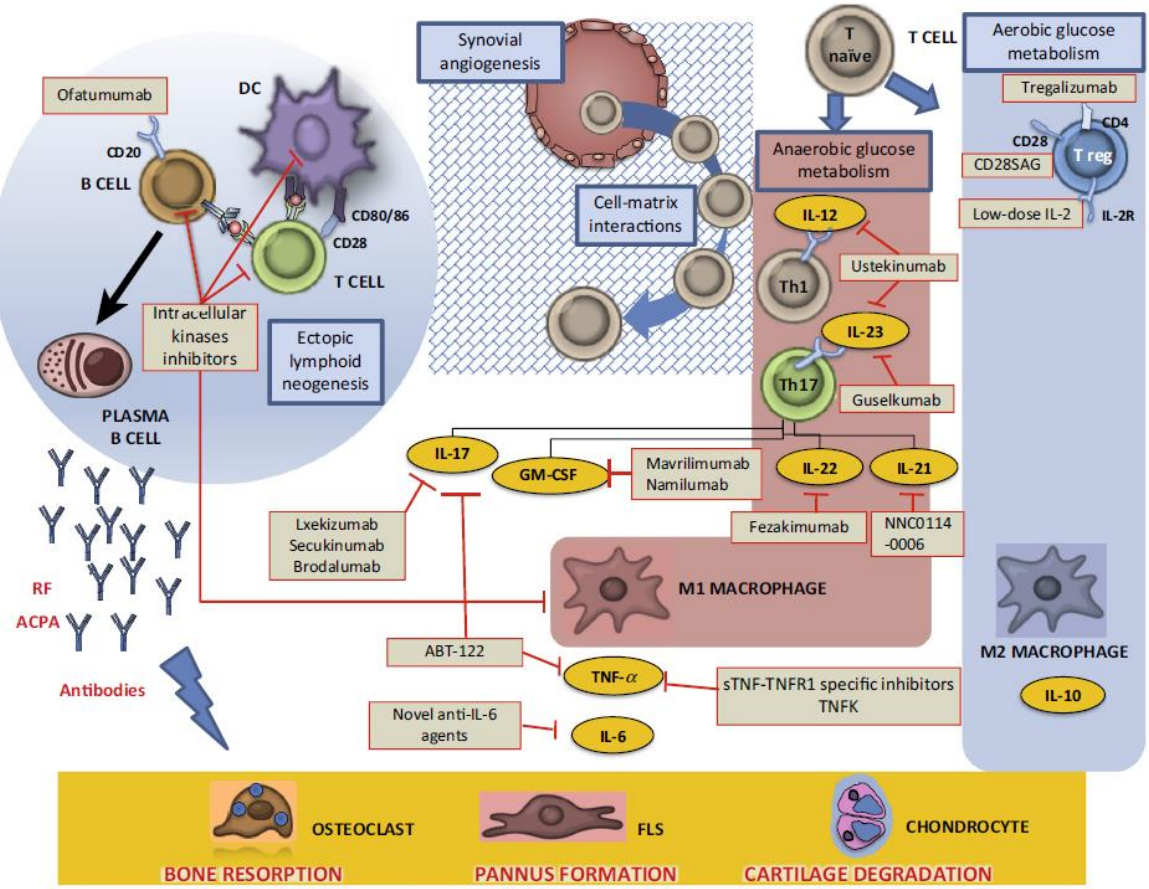

Figure 5: Novel therapeutic targets in rheumatoid arthritis – Monoclonal antibodies have been developed against T- and B- cell cytokines, the major new therapeutic targets. Small-molecule inhibitors of intracellular kinases are also being tested, as well as cell-directed treatments such as low dose IL-2 or T cell superagonists like CD28Sag. Current therapeutics are noted by red boxes, potential future therapeutic targets by blue boxes (Semerano et al. 2016).

2.5 Aim of the study

The overall goal of this study was to expand the existing applications of known ASM inhibitors to new ASM/ceramide-related diseases with a currently unmet clinical treatment need. FD and RA were chosen because of the potential implication of ASM/ceramide in the pathogenesis of these diseases and the high demand for new treatment strategies.

Concerning FD, the accumulation of lysosomal ceramide is the cause of the disease. Thus, the hypothesis arose that ceramide accumulation may be prevented by blocking lysosomal generation of ceramide with ASM inhibitors and the ceramide accumulation may thus redistribute upstream to less toxic lipids (Fig. 5). Indications that such an approach would be advantageous came from CF clinical trials, in which the pulmonary ceramide accumulation present in CF patients was successfully targeted with the ASM inhibitor Amitriptyline (Adams et al. 2016; Teichgräber et al. 2008).

An accurate assessment of the efficacy of such a treatment for FD cannot be obtained in *in vitro*-models alone and thus requires an experimental model of FD. Our group generated a viable Ac-KO mouse model for the study of FD – one of only two FD animal models worldwide. This study first characterizes the Ac-KO phenotype to assess its utility as a model for the human disease. Next, a double knock-out mouse was generated by co-ablation of Asm. The phenotype assessment of the double mutants serves as a proof-of-concept study to assess the efficacy of Asm inhibition as a treatment for FD. The FD part of this study concludes with the pharmacological treatment of Ac-KO mice with functional Asm inhibitor Amitriptyline.

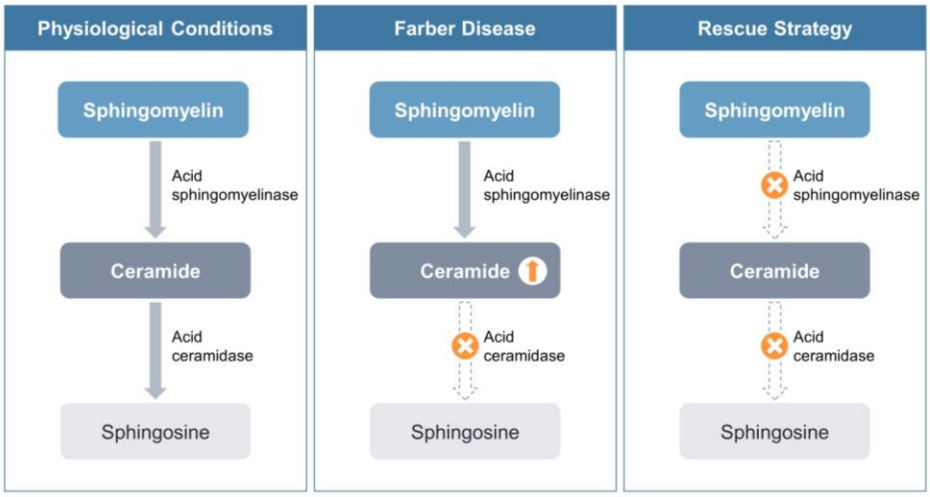

Figure 6: Rescue strategy – Under physiological conditions, ASM catalyzes the hydrolysis of sphingomyelin to ceramide and AC de-acetylates ceramide to sphingosine. In FD, deficiency in AC results in ceramide accumulation. The hypothesis tested in this study is that co-depletion of ASM may prevent ceramide accumulation and thus ameliorate FD symptoms.

The second part of this thesis addresses the role of ASM/ceramide in RA. A few reports already exist implicating ASM and/or ceramide in autoimmunity: Yang and coworkers demonstrated an important role for ASM in mast cell function (Yang et al. 2014). Studies on inflammatory bowel disease report an increase of ceramide combined with an induction of MMP-1 in a chronic colitis model, which could be blocked with the FIASMA Imipramine (Bauer et al. 2009). MMP1 has a rate-limiting role in RA as well, because it degrades articular collagen (Burrage, Mix, and Brinckerhoff 2006). In multiple sclerosis, Asm-KO mice were shown to be protected from a murine model of the disease (Verderio et al. 2012) and an *in vitro* study reported that endothelial ASM regulates T cell transmigration across brain endothelial cells via intracellular adhesion molecule-1 (Lopes Pinheiro et al. 2016). In RA itself, ceramide is increased in the synovial fluid of RA patients (Kosinska et al. 2014).

Due to these links between ASM/ceramide and autoimmunity, the susceptibility of Asm-KO mice was assessed in an experimental model of inflammatory arthritis – murine antigen-induced arthritis (AIA) – in the present study.

3. Materials and Methods

3.1 Materials

3.1.1 Chemicals

Acetic acid (100 %)	Merck KGaA, Darmstadt, Germany
Acrylamide	Carl-Roth GmbH & Co, Karlsruhe, Germany
Amitriptyline hydrochloride (≥ 98 %)	Sigma-Aldrich Chemie GmbH, Steinheim, Germany
Ammonium persulfate (APS)	Carl-Roth GmbH & Co, Karlsruhe, Germany
Aprotinin	Roche Deutschland Holding GmbH, Freiburg, Germany
BODIPY-sphingomyelin	Thermo Fisher Scientific, Waltham, MA, USA
Bovine serum albumin (BSA), fatty acid free	Sigma-Aldrich Chemie GmbH, Steinheim, Germany
Bradford Protein assay	Biorad Laboratories GmbH, München, Germany
Bromphenol blue	Sigma-Aldrich Chemie GmbH, Steinheim, Germany
Calcium chloride (≥ 99 %)	Carl-Roth GmbH & Co, Karlsruhe, Germany
Carbon dioxide (CO_2)	AIR LIQUIDE Medical GmbH, Düsseldorf, Germany
Chloroform	AppliChem GmbH, Darmstadt, Germany
Complete Freud's adjuvant (CFA)	Sigma-Aldrich Chemie GmbH, Steinheim, Germany
Complete protease inhibitor cocktail	Roche Deutschland Holding GmbH, Freiburg, Germany
Dabco	Sigma-Aldrich Chemie GmbH, Steinheim, Germany
Decalcifier soft	Carl-Roth GmbH & Co, Karlsruhe, Germany
Di-potassium hydrogen phosphate	Carl-Roth GmbH & Co, Karlsruhe, Germany
Di-sodium hydrogen phosphate	Merck KGaA, Darmstadt, Germany
Eosin	Carl-Roth GmbH & Co, Karlsruhe, Germany
Ethanol (absolute, anhydrous)	Diagonal GmbH & Co. KG, Münster, Germany
Ethyl acetate	Diagonal GmbH & Co. KG, Münster, Germany
FastGreen	Carl-Roth GmbH & Co, Karlsruhe, Germany
FITC-Phalloidin	Sigma-Aldrich Chemie GmbH, Steinheim, Germany
Glucose	Sigma-Aldrich Chemie GmbH, Steinheim, Germany
Glycerol (≥ 99 %)	Carl-Roth GmbH & Co, Karlsruhe, Germany

Hematoxylin	Carl-Roth GmbH & Co, Karlsruhe, Germany
HEPES	Carl-Roth GmbH & Co, Karlsruhe, Germany
Hydrochloric acid (fuming, 37 %)	Sigma-Aldrich Chemie GmbH, Steinheim, Germany
Isoflurane (Isothesia)	Henry Schein Vet GmbH, Hamburg, Germany
Leupeptin	Becton, Dickinson GmbH, Heidelberg, Germany
Liquid Nitrogen	AIR LIQUIDE Medical GmbH, Düsseldorf, Germany
Magnesium chloride hexyhydrate (≥ 99 % p.a.)	Carl-Roth GmbH & Co, Karlsruhe, Germany
Magnesium sulfate heptahydrate (≥ 99 %)	Sigma-Aldrich Chemie GmbH, Steinheim, Germany
Manganese chloride	Sigma-Aldrich Chemie GmbH, Steinheim, Germany
Methanol (≥ 99.8 %)	Diagonal GmbH & Co. KG, Münster, Germany
Methylated bovine serum albumin (mBSA)	Sigma-Aldrich Chemie GmbH, Steinheim, Germany
Mowiol-488	Hoechst GmbH, Frankfurt, Germany
NBD-ceramide	Thermo Fisher Scientific, Waltham, MA, USA
NP-40 (Igepal)	Sigma-Aldrich Chemie GmbH, Steinheim, Germany
Paraformaldehyde (powder, 95 %)	Sigma-Aldrich Chemie GmbH, Steinheim, Germany
Paraplast	Leica Mikrosysteme Vertrieb GmbH, Wetzlar, Germany
Perm/Wash buffer	Becton, Dickinson GmbH, Heidelberg, Germany
Polyoxyethyle glycol sorbitan monolaurate (Tween20)	Sigma-Aldrich Chemie GmbH, Steinheim, Germany
Potassium chloride (≥ 99 %)	Carl-Roth GmbH & Co KG, Karlsruhe, Germany
Propidium iodide (95-98 %)	Sigma-Aldrich Chemie GmbH, Steinheim, Germany
SafraninO	Carl-Roth GmbH & Co KG, Karlsruhe, Germany
Sodium chloride (≥ 99,5 %)	Carl-Roth GmbH & Co KG, Karlsruhe, Germany
Sodium citrate (tribasic, dehydrate)	Sigma-Aldrich Chemie GmbH, Steinheim, Germany
ß-Mercaptoethanol	Sigma-Aldrich Chemie GmbH, Steinheim, Germany
Starting Block TBS Blocking Solution	Thermo Fisher Scientific, Waltham, MA, USA
Xylene (mixture of isomers)	Diagonal GmbH & Co. KG, Münster, Germany

3.1.2 Antibodies

AC, ß-unit (goat-anti-mouse)	SantaCruz Biotechnology, Inc., Dallas, TX, USA
CD127 (IL-7Rα)-PE-Cy7 (anti-mouse)	Biolegend, San Diego, CA, USA
CD27-biotin (anti-mouse)	Biolegend, San Diego, CA, USA
CD44-APC (anti-mouse)	Becton, Dickinson GmbH, Heidelberg, Germany
CD45-PE (anti-mouse)	Thermo Fisher Scientific, Waltham, MA, USA
CD45R/B220-APCeFluor780 (anti-mouse)	Thermo Fisher Scientific, Waltham, MA, USA
CD4-PacificBlue (anti-mouse)	Becton, Dickinson GmbH, Heidelberg, Germany
CD62L-PE (anti-mouse)	Becton, Dickinson GmbH, Heidelberg, Germany
CD8-APCeF780 (anti-mouse)	Thermo Fisher Scientific, Waltham, MA, USA
CD95-PE-Cy7 (anti-mouse)	Becton, Dickinson GmbH, Heidelberg, Germany
GL7-AF488 (anti-mouse)	Thermo Fisher Scientific, Waltham, MA, USA
HRP-coupled anti-beta-actin	SantaCruz Biotechnology, Inc., Dallas, TX, USA
HRP-coupled secondary antibodies	Cell Signaling Technology, Danvers, MA, USA
IgG1-PE (anti-mouse)	Becton, Dickinson GmbH, Heidelberg, Germany
IgG-AF488 (goat anti-mouse)	Thermo Fisher Scientific, Waltham, MA, USA
IgG-AF647 (donkey-anti-rat)	Jackson ImmunoResearch Europe Ltd., Suffolk, UK
IgG-Cy3 (donkey-anti-goat)	Jackson ImmunoResearch Europe Ltd., Suffolk, UK
IgM-APC (anti-mouse)	Becton, Dickinson GmbH, Heidelberg, Germany
LAMP-1 (rat-anti-mouse)	Abcam PLC, Cambridge, UK
ß1-Integrin, activated (clone HUTS4, mouse anti-human)	Merck KGaA, Darmstadt, Deutschland
Steptavidin-FITC	Becton, Dickinson GmbH, Heidelberg, Germany
TCRb-PerCP-Cy5.5 (anti-mouse)	Thermo Fisher Scientific, Waltham, MA, USA

3.1.3 Kits, panels and enzymes

Bacterial Sphingomyelinase (from *Bacillus cereus*)	Sigma-Aldrich Chemie GmbH, Steinheim, Germany
BrdU cell proliferation ELISA (colorimetric) kit	Roche Deutschland Holding GmbH, Freiburg, Germany
Creatinine (serum) colorimetric assay kit	Biomol GmbH, Hamburg, Germany
ECL prime system	GE Healthcare Europe GmbH, Freiburg, Germany
Glucose (urinary) colorimetric assay kit	Biomol GmbH, Hamburg, Germany
IL-10 (mouse) Quantikine ELISA	R&D Systems Inc., Minneapolis, MN, USA
IL-17 (mouse) Quantikine ELISA	R&D Systems Inc., Minneapolis, MN, USA
IL-1ß (mouse) Quantikine ELISA	R&D Systems Inc., Minneapolis, MN, USA
IL-2 (mouse) Quantikine ELISA	R&D Systems Inc., Minneapolis, MN, USA
IL-4 (mouse) Quantikine ELISA	R&D Systems Inc., Minneapolis, MN, USA
IL-6 (mouse) Quantikine ELISA	R&D Systems Inc., Minneapolis, MN, USA
Insulin ELISA kit	Thermo Fisher Scientific, Waltham, MA, USA
Masson trichrome staining kit	Sigma-Aldrich Chemie GmbH, Steinheim, Germany
MCP-1 (mouse) Quantikine ELISA	R&D Systems Inc., Minneapolis, MN, USA
Mouse regulatory T cell staining kit #1	Thermo Fisher Scientific, Waltham, MA, USA
RotiLumin system	Carl-Roth GmbH & Co, Karlsruhe, Germany
Spotchem parameter strips	Scil animal care company GmbH, Viernheim, Deutschland
ß-hydroxybutyrate colorimetric assay kit	Biomol GmbH, Hamburg, Germany

3.1.4 Media and additives

DMEM	Thermo Fisher Scientific, Waltham, MA, USA
FBS	GE Healthcare Europe GmbH, Freiburg, Germany
Histopaque-1077	Sigma-Aldrich Chemie GmbH, Steinheim, Germany
Horse serum	Thermo Fisher Scientific, Waltham, MA, USA
IL-2 (human)	R&D Systems Inc., Minneapolis, MN, USA
IL-2, mouse	Thermo Fisher Scientific, Waltham, MA, USA
IMDM	Thermo Fisher Scientific, Waltham, MA, USA
L-Glutamine	Thermo Fisher Scientific, Waltham, MA, USA
Non-essential amino acids	Thermo Fisher Scientific, Waltham, MA, USA
PenStrep	Thermo Fisher Scientific, Waltham, MA, USA
Phytohaemagglutinin (PHA) P	Sigma-Aldrich Chemie GmbH, Steinheim, Germany
RPMI 1640 (1x, [+] L-Glutamine)	Thermo Fisher Scientific, Waltham, MA, USA
Sodium pyruvate	Thermo Fisher Scientific, Waltham, MA, USA
TNF-α, mouse recombinant	R&D Systems Inc., Minneapolis, MN, USA

3.1.5 Prepared buffers and solutions

Ac/Asm assay buffer	250 mM sodium acetate
	0.1 % NP-40
	pH 4,5 (Ac) or pH 5,0 (Asm)
Ac/Asm lysis buffer	250 mM sodium acetate
	1 % NP-40
	pH 4,5 (Ac) or pH 5,0 (Asm)
Ac/Asm substrate solution	1 µl NBD-Cer
	27.2 mL Ac assay buffer
Asm substrate solution	0,5 µl BODIPY-Sphingomyelin
	1 mL Asm assay buffer
HEPES/Saline (HS) (10x)	200 mM HEPES
	1.32 M NaCl
	10 M CaCl2
	7 mM MgCl2

	8 mM MgSO4
	54 mM KCl
Mowiol	20-25 % Mowiol-488
	2,5 % Dabco
Paraformaldehyde (PFA), 4 %	4 % PFA
	1 x PBS
	pH 7,2 – 7,4 adjusted with HCl and NaOH
Phosphate buffered saline (PBS)	137 mM NaCl
	2.7 mM KCl
	10 mM Na2HPO4 • 2 H_20
	2.0 mM KH2PO4
	pH adjusted with HCl and NaOH
Reducing SDS sample buffer (5x)	250 mM Tris pH 6.8
	20 % Glycerine
	4 % SDS
	8 % ß-mercaptoethanol
	0.2 % bromphenol blue
SDS lysis buffer, 0.1 %	25 mM HEPES, pH 7,3
	0.1 % sodium dodecyl sulfate
	0.5 % sodium deoxycholate
	1 % Triton-X-100
	125 mM NaCl
	10 mM NaF
	10 mM $Na_2P_2O_7$
	20 mM Na_3VO_4
	10 mM ethylenediaminetetraacetic acid
	10 µg/ml aprotinin
	10 µg/ml leupeptin
	1 x Roche Complete protease inhibitor cocktail
SDS Running buffer	25 mM Tris
	192 mM glycine
	0.1 % SDS
Tris/0.1 % Tween-20	20 mM Tris
	150 mM NaCl

	0.1 % Tween-20
Tyrode's buffer	134 mM NaCl 0.34 mM Na_2HPO_4 2,9 mM KCl 12 mM $NaHCO_3$ 20 mM HEPES 5 mM Glucose pH adjusted to pH 7,1

3.1.6 Consumables

Cathether (Vasofix Safety 18 G x 1 ¾'')	B. Braun Melsungen AG, Melsungen, Germany
Cell culture flasks	Sarstedt AG & Co, Nümbrecht, Germany
Cell strainer (70 µm)	Corning Inc., New York, NY, USA
Centrifuge tubes (15 mL, 50 mL)	Greiner Bio-One GmbH, Frickenhausen, Germany
Coverglass (18 x 18 mm)	Engelbrecht GmbH, Wien, Austria
Coverslips (Ø 12 mm)	Carl-Roth GmbH & Co, Karlsruhe, Germany
Cuvettes	Sarstedt AG & Co, Nümbrecht, Germany
EDTA collection tubes	Greiner Bio-One GmbH, Frickenhausen, Germany
Embedding cassettes	Carl-Roth GmbH & Co, Karlsruhe, Germany
Hybond ECL nitrocellulose membrane	GE Healthcare Europe GmbH, Freiburg, Germany
Hypodermic needle	Becton Dickinson GmbH, Heidelberg, Germany
Microscopic slides	Langenbringen Labor- und Medizintechnik, Emmendingen, Germany
Microtiter plates	Sarstedt AG & Co, Nümbrecht, Germany
Needles (different gauges)	Becton Dickinson GmbH, Heidelberg, Germany
NH4-Heparin collection tubes	Sarstedt AG & Co, Nümbrecht, Germany
Pipettes (5 mL, 10 mL, 25 mL)	Greiner Bio-One, Frickenhausen, Germany
Reaction tubes, 1.5 mL	Sarstedt AG & Co, Nümbrecht, Germany
Reaction tubes, 2 mL	Eppendorf AG, Hamburg, Germany
Stainless steel beads, 5 mm	Qiagen GmbH, Hilden, Germany

Syringes	
- Insulin syringe	Becton Dickinson GmbH, Heidelberg, Germany
- Luer-lock 1 mL syringe	Becton Dickinson GmbH, Heidelberg, Germany
- Rubber- and lubricant free	Sigma-Aldrich Chemie GmbH, Steinheim, Germany
Thin layer chromatography (TLC) Silica G60 plates	Merck KGaA, Darmstadt, Germany
X-Ray films	GE Healthcare Europe GmbH, Freiburg, Germany

3.1.7 Equipment

Centrifuges	
- 5417 R	Eppendorf AG, Hamburg, Germany
- Heraeus 3SR+ multifuge	Thermo Fisher Scientific, Waltham, MA, USA
Clean bench (biological safety cabinet class II)	NuArie, Plymouth, MN, USA
Microscopes	
- confocal fluorescence (TCS-SP5)	Leica Mikrosysteme Vertrieb GmbH, Wetzlar, Germany
- fluorescence (BIOREVO B2-9000)	Keyence Deutschland GmbH, Neu-Isenburg, Germany
Developer machine	Thermo Fisher Scientific, Waltham, MA, USA
Digital caliper	Mitutoyo UK Ltd., Andover, UK
Flow cytometer	
- Calibur	Becton, Dickinson GmbH, Heidelberg, Germany
- LSR III	Becton, Dickinson GmbH, Heidelberg, Germany
Freezers	
- 80 °C, ultra low MDF-U54V	Sanyo Electric Co, Osaka, Japan
- 20 °C, Premium NoFrost	Liebherr-International Deutschland GmbH, Biberach, Deuschland
Fridge (4 °C, Premium BioFresh)	Liebherr-International Deutschland GmbH, Biberach, Germany

Glasswares (beakers, cylinders, flasks)	DURAN Group GmbH, Wertheim, Germany
Incubator	Binder GmbH, Tuttlingen, Germany
Infrared lamp	Philips Consumer Lifestyle B.V., Drachten, The Netherlands
Magnetic stirrer (M21)	Intern. Laborat. App GmbH, Dottingen, Germany
Mass spectrometer (Q-TOF 6530)	Agilent Technologies, Waldbronn, Germany
Mechanical shaker (Rotamax120)	Heidolph Instruments GmbH & Co. KG, Schwabach, Germany
Microtome	Thermo Fisher Scientific, Waltham, MA, USA
pH Meter (HI9025)	Hanna instruments, Woonsocket, RI, USA
Pipettes (different sizes)	Nichiryo CO., Ltd., Saitama, Japan
Pipettus (pipetus-akku)	Hirschmann Laborgeräte GmbH und Co. KG, Eberstadt, Germany
Rotary microtome (Microm HM 3555)	Thermo Scientific, Waltham, MA, USA
Spectrophotometer	Eppendorf AG, Hamburg, Germany
SpeedVac	Thermo Fisher Scientific, Waltham, MA, USA
SpotChem EZ chemistry analyser	Scil animal care company GmbH, Viernheim, Deutschland
Thermomixer	Eppendorf AG, Hamburg, Germany
TissueLyser	Qiagen GmbH, Hilden, Germany
Typhoon FLA 9500	GE Healthcare Europe GmbH, Freiburg, Germany
Ultrasonic bath (sonorex RK 102 H)	BANDELIN electronic GmbH & Co. KG, Berlin, Germany
Vacuum concentrator (SpeedVac)	Bachofer GmbH, Reutlingen, Germany
VetABC	Scil animal care company GmbH, Viernheim, Deutschland
Vortexer (Reax 2000)	Heidolph Instruments GmbH & Co. KG, Schwabach, Germany
Water bath (1o12)	GFL Gesellschaft für Labortechnik mbH, Burgwedel, Germany

3.1.8 Software

GraphPad Prism (5.01)	GraphPad Software, La Jolla, CA, USA
ImageQuant	GE Healthcare Europe GmbH, Freiburg, Germany
Leica advanced Fluorescence – Application Suite (2.61)	Leica Mikrosysteme Vertrieb GmbH, Wetzlar, Germany
MassHunter Software	Agilent Technologies, Waldbronn, Germany
Microsoft Office (2016)	Microsoft Corporation, Redmond, WA, USA

3.2 Methods

3.2.1 Animal husbandry and animal procedures

3.2.1.1 Animal husbandry

All mice were maintained on the C57BL/6 Jackson background. Mice were bred and housed in the vivarium of the University Hospital Essen, Germany under pathogen-free conditions as defined by the Federations of European Laboratory Animal Science Associations (FELASA). The pathogen-free status was routinely assessed through a sentinel program. Mice had *ad libitum* access to food and water and were kept on a 12 h/12 h light/dark cycle. Genotypes were assessed by PCR. For antigen-induced arthritis experiments, only female mice were used. All procedures (subsequently described in detail) were approved by the State Agency for Nature, Environment and Consumer Protection (LANUV) NRW in Düsseldorf, Germany.

3.2.1.2 Generation of the *Asah1* knock-out mouse model

A conditional *Asah1* knock-out model was generated by GenOway (Lyon, France) through flanking Exon1 with loxP sites and removal of the neomycin selection cassette via crossing to Flp recombinase deleter mice. In detail, the *Asah1* exon/intron organization was established based on the cDNA sequence NM_019734. A targeting vector was then constructed containing two homology regions to the *Asah1* genomic sequence (one of 5.8 kb and one of 1.7 kb), two loxP sites flanking *Asah1* Exon1, a neomycin cassette flanked by FRT sites for positive selection and a diphtheria toxin A negative-selection marker to enhance the isolation of ES cell clones containing also the distal loxP site. This targeting vector was inserted into C57BL/6 embryonic stem cells by homologous recombination. The resulting chimeric mice were crossbred to C57BL/6 Flp deleter mice to remove the neomycin cassette and generate mice heterozygous for the Neo-excised conditional *Asah1* kock-out allele. These mice were

subsequently crossed to a C57BL/6 EIIa-cre transgenic strain and the resulting offspring with the heterozygous excised allele was mated among each other to obtain the constitutive knock-out model. Ac and Asm co-deficient mice were obtained by subsequent crossing of *Asah1*$^{+/-}$ mice to *Smpd1*$^{+/-}$ mice, which have been previously described in the literature (Horinouchi et al. 1995).

3.2.1.3 Induction and assessment of antigen-induced arthritis

mBSA was diluted at 10 mg/ml in 5 % Glucose, subsequently diluted further to 2 mg/ml in 5 % Glucose in PBS and emulsified 1:1 (v/v) with CFA (Sigma) using rubber- and lubricant free syringes (BD Bioscience). The emulsion was injected s.c. into the axillary and inguinal lymph node regions on day -21 and day -14 (4 x 50 µl/mouse) under anesthesia with isoflurane. Arthritis was induced on day 0 by injection of 10 µl 10 mg/ml mBSA in 5 % Glucose into one knee joint cavity through a 30 G needle. The contralateral joint was injected with the same volume 5 % Glucose. Intraarticular injections were also carried out under isoflurane-anesthesia. Knee joint diameter was assessed with a digital caliper immediately after induction and once daily on all subsequent days.

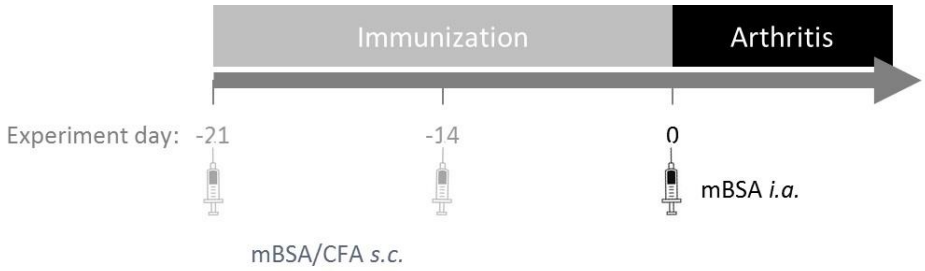

Figure 7: Timeline of the antigen-induced arthritis model – Mice are immunized with mBSA emulsified in CFA s.c. on experimental day -21 and -14. On day 0. mBSA is injected directly into the joint cavity to induce arthritis.

3.2.1.4 Platelet transplantation

Donor mice were placed under an infrared lamp for 5 min for vasodilatation in the tail. 400 µl of blood were freshly collected via a tail vein incision. Collection tubes contained 0.38 % sodium citrate for anti-coagulation. The blood was supplemented with 9 mL PBS (pH 7.2) + 3.5 % fatty acid free BSA (Sigma) and incubated for 15 min at 37 °C. Red blood cells and leukocytes were pelleted by centrifugation at 120 x g without brake for 20 min at room temperature. The platelet-rich supernatant was collected and the platelets were subsequently

pelleted by centrifugation at 1,340 x g for 10 min. Platelets were washed twice with Tyrode's buffer to remove BSA. After the final wash, platelets were resuspended in 200 µl Tyrode's buffer and injected via the tail vein into recipient mice 2 h prior to arthritis induction. Recipient mice were placed under infrared light for 5 min prior to the *i.v.* injection to help visualization of the tail vein.

3.2.1.5 Amitriptyline treatment

Arthritic mice were treated via *i.p.* injections: Amitriptyline was freshly diluted and injected at 9.375 mg/kg bodyweight in 50 µl 0.9 % sodium chloride every 6 h. Treatment commenced 2.5 days prior to arthritis induction and continued until the mice were sacrificed. The control group was injected with 50 µl 0.9 % sodium chloride.

Ac deficient mice were treated with Amitriptyline via the drinking water. In one group, treatment was started shortly after weaning, when FD symptoms were still relatively mild. In the second group, the treatment was already started *in utero* to prevent ceramide from accumulating. The parents were mated for 4 days. The male was then removed from the cage and the female received 180 mg/l Amitriptyline in 0.9 % sodium chloride as drinking water. Fresh amitriptyline was prepared every second day. After birth, treatment of the mother was continued and after weaning, the offspring received the same dose of Amitriptyline in the drinking water directly.

3.2.2 Biochemical and molecular methods

3.2.2.1 Intracellular localization of Ac and the mutant protein

Intracellular localization of Ac was assessed in mesenchymal stem cells isolated from wild-type or Ac deficient mice as previously described (Peister et al. 2004). These cells were maintained in IMDM K10 + 10 % horse serum. The cells were seeded on coverslips in a 12-well plate. Due to unequal proliferation rates, 2 x 10^4 wild-type cells/well were seeded and 3 x 10^4 Ac deficient cells/well and then grown for 48 h. Cells were washed with H/S and then fixed for 15 min with ice-cold methanol at 4 °C for 15 min. Cells were then washed 3 x 5 Min with BD Perm/Wash, followed by 20 Min blocking in Perm/Wash supplemented with 5 % FCS. Cells were subsequently stained with the first primary antibody directed against the ß-unit of AC diluted in Perm/Wash + 1 % FCS. The second primary antibody directed against the lysosomal marker protein LAMP-1 was added after 1 h for an additional 1 h incubation

period. The coverslips were washed 3 x 5 min with BD Perm/Wash to remove any unbound primary antibody molecules and then stained with the corresponding secondary antibodies for 1 h at room temperature. The coverslips were washed three times again and then mounted with Mowiol.

3.2.2.2 Determination of Ac and Asm activity

Ac and Asm activities were determined as recently described (Mühle and Kornhuber 2017). Mice were sacrificed by CO_2 exposure and blood was drawn from the *V. cava inferior* into reaction tubes containing 50 µl 3.8 % sodium citrate to prevent coagulation. Plasma was collected after centrifugation for 10 min with 2,500 x g and snap-frozen in 2 mL reaction tubes with a 5-mm stainless steel bead (hereafter called TissueLyser tube). Bone marrow was flushed from both femurs and tibias into a 2 mL reaction tube using a syringe and large gauge needle filled with 1 ml PBS. Cells were pelleted by 5 min centrifugation at 300 x g and the supernatant was removed. A 5-mm stainless steel bead was added and samples were snap-frozen. Lymph nodes and thymus were dissected and snap-frozen in TissueLyser tubes. The other organs were dissected, snap-frozen and pulverized using a mortar and pestle filled with liquid nitrogen. A generous scoop of the organ powder was transferred to pre-cooled TissueLyser tube on dry ice. Samples were incubated at room temperature for 2 min prior to addition of Ac- or Asm lysis buffer. Samples were then homogenized in a TissueLyser for 5 Min at 50 Hz. An aliquot was removed for protein determination and another aliquot was dispensed on ice for determination of Ac- or Asm activity. Ac- or Asm lysis buffer was added to a final volume of 20 µl. Samples and the NBD-ceramide or BODIPY-sphingomyelin substrate solutions were sonicated in an ultrasonic bath for 10 min to induce micelle formation, before 100 pmol/sample NBD-ceramide or 100 pmol/sample BODIPY-sphingomyelin were added to the samples. The reaction was carried out for 2 h (Ac) or for 1 h (Asm) at 37 °C. The reaction was terminated by lipid extraction through addition of chloroform:methanol (2:1, v/v), vortexing and centrifugation for 5 min at 15 000 x g. The lower phase was collected and dried in a SpeedVac at 37 °C. Dried lipids were resuspended in 20 µl chloroform:methanol (2:1, v/v) and spotted onto a thin layer chromatography (TLC) plate. The TLC run was conducted with ethyl acetate:acetic acid (100:1, v/v, Ac) or chloroform:methanol (80:20, v/v, Asm) as the running buffer. The plate was then dried and imaged using a Typhoon FLA 9500. Spots were quantified with ImageQuant software.

3.2.2.3 Ceramide and sphingomyelin quantification

Ceramides and sphingomyelins were quantified by Dr. Fabian Schumacher (University Duisburg-Essen und University Potsdam) by rapid resolution liquid chromatography/mass spectrometry as recently described (Huston et al. 2016): Lipids were extracted from spleen tissues with C17-ceramide and C16-d31-sphingomyelin as internal standards. Sample analysis was conducted by rapid-resolution liquid chromatography-MS/MS using a Q-TOF 6530 mass spectrometer operating in the positive ESI mode. Ceramide precursor ions (C16-ceramide (*m/z* 520.508), C17-ceramide (*m/z* 534.524), C18-ceramide (*m/z* 548.540), C20-ceramide (*m/z* 576.571), C22-ceramide (*m/z* 604.602), C24-ceramide (*m/z* 632.634) and C24:1-ceramide (*m/z* 630.618)) were cleaved into the fragment ion m/z 264.270 and sphingomyelin precursor ions (C16-sphingomyelin (*m/z* 703.575), C16-d31-sphingomyelin (*m/z* 734.762), C18-sphingomyelin (*m/z* 731.606), C20-sphingomyelin (*m/z* 759.638), C22-sphingomyelin (*m/z* 787.669), C24-sphingomyelin (*m/z* 815.700) and C24:1-sphingomyelin (*m/z* 813.684)) were cleaved into the fragment ion *m/z* 184.074. Quantification was performed with MassHunter Software.

3.2.2.4 Histopathological assessment

Mice were sacrificed by CO_2 exposure and perfused with 0.9 % sodium chloride via the right ventricle to remove red blood cells, followed by perfusion with 4 % PFA. Organs were dissected and fixed further in 4 % PFA, de-calcified with Decalcifier soft (Roth) if necessary, dehydrated with ethanol, embedded in paraffin and trimmed to 6 µm thin sections. These were stained with hematoxylin and eosin, Masson trichrome staining kit or SafraninO/FastGreen as indicated. Samples were analyzed on a Leica SP5.

3.2.2.5 Blood, serum and urine analysis

Blood was drawn from the tail vein and serum was collected by centrifugation as previously described (please refer to section 3.2.1.4). Insulin levels were quantified by enzyme-linked immunosorbent assay (ELISA) and creatinine levels using a colorimetric assay kit according to the respective manufacturer's instructions. All other serum parameters were analyzed using a SpotChem EZ chemistry analyzer and the corresponding parameter strips from Scil. When necessary, samples were diluted in Aqua dest to enable measurement of small sample volumes or to obtain an accurate measurement when sample contents exceeded the maximum

detection limit of a given parameter. The differential blood count was obtained from EDTA-anti-coagulated full blood using a VetABC.

Urine was caught into a collection tube when mice urinated prompted by removal from their cages. Levels of ß-hydroxybutyrate and glucose were quantified using colorimetric assay kits (Cayman) and protein levels by Bradford protein assay.

3.2.2.6 MCP-1 quantification

Monocyte chemoattractant protein-1 (MCP-1) levels were measured by enzyme-linked immunosorbent assay. Mice were sacrificed by CO_2 exposure, blood was drawn from the *V. cava inferior* and serum was obtained by centrifugation at 2,500 x g for 20 min. The spleen, liver and brain were dissected, snap-frozen and homogenized in PBS + 10 µg/ml Aprotinin + 10 µg/ml Leupeptin + 1 x Complete Protease Inhibitor Cocktail using a TissueLyser as described above (please refer to section 3.2.1.7). Samples were centrifuged for 5 min at 15 000 x g to remove debris and MCP-1 levels were analyzed using the R&D Quantikine ELISA according to manufacturer's instructions. Serum samples were directly analyzed without any further treatment.

3.2.2.7 Joint cytokine measurements

Arthritis was induced as described in section 3.2.1.3 and mice were sacrificed on day 2 or on day 4 after arthritis induction as indicated. Joint homogenates were prepared as described by Rioja and colleagues with slight alterations (Rioja et al. 2004): Whole knee joints (synovium, adjacent tissues and bone) were removed, snap-frozen and pulverized using a mortar and pestle under liquid nitrogen. The organ powder was transferred to pre-cooled 15 mL reaction tubes on dry ice. Samples were resuspended in 1 mL cold PBS containing 10 µg/ml each of Aprotinin and Leupeptin and 1 x Complete Protease Inhibitor Cocktail. Samples were vortexed, spun down at 300 x g for 5 Min at 4 °C and then sonicated three times for 10 sec each. Homogenates were centrifuged at 400 x g for 10 Min at 4 °C. The supernatants were transferred to 1.5 mL tubes and centrifuged again at 15,000 x g to remove insoluble components. The supernatants were collected, protein content was quantified by Bradford protein assay and cytokine levels were assessed using R&D Quantikine ELISA kits according to the manufacturer's instructions. For IL-1ß and IL-6 analyses, samples were routinely

diluted with the respective calibrator diluent to prevent samples from exceeding the linear range of the respective ELISA.

3.2.2.8 Analysis of lymphocyte subsets

Immunized mice were sacrificed on experimental day 0 (21 days after the initial immunization) and inguinal lymph nodes were resected. Single cell suspensions were prepared by carefully pushing cells through a 70 µm filter. Follicular B cells were stained using labelled antibodies against B220, CD95, GL7, IgM and IgG. T cell subsets were stained using anti-CD4, anti-CD8, anti-TCRb, anti-CD62L and anti-CD44 labelled antibodies. Cells were analyzed by flow cytometry using a BD LSR II. Regulatory T cells were stained using the Mouse Regulatory T Cell Staining Kit # 1 (Affymetrix) according to the manufacturer's instructions and analyzed on a BD FACS Calibur.

3.2.2.9 *In vitro* antigen-restimulation of lymphocytes

Immunized mice were sacrificed on experimental day 0 (21 days after the initial immunization) and single cell lymphocyte suspensions were prepared as described above. Cells were seeded at 5 x 10^6 cells/ml in 96-well plates in serum-free RPMI K10. Stimulation media were added at a ratio of 1:1 (v/v) to achieve a final concentration of 5 % Asm-free mouse serum and 0.5 % Glucose in all samples. Asm-free mouse serum was obtained by drawing blood via tail vein incision from Asm-KO mice and subsequent centrifugation at 2 500 x g for 20 Min. When indicated, stimulation media also contained a final concentration of either 1 or 2 mg/ml mBSA or 10 µg/ml PHA-P (Sigma) and 10 U/ml mouse recombinant IL-2 (eBioscience). Cell proliferation was assessed after 48 h using the BrdU Cell Proliferation ELISA (colorimetric) kit (Roche) according to the manufacturer's instructions. The BrdU labeling reagent was added for the final 24 h of incubation. The supernatants from these cultures were collected and the levels of IL-2, IL-4, IL-6, IL-10 and IL-17 were assessed using R&D Quantikine ELISA kits according to the manufacturer's instructions.

3.2.2.10 ß1-Integrin activation

Blood was drawn from healthy volunteers into NH4-Heparin collection tubes. PBMCs were isolated by Ficoll gradient centrifugation. Cells were then washed and allowed to rest for 8 Min at 37 °C. Subsequently, anti-human ß1-Integrin-ß1 antibody (Merck Millipore, clone HUTS4) was added to a final concentration of 1 µg/sample and cells were stimulated with

either 1mM Mn^{2+} or 2 U/ml bacterial sphingomyelinase (bSM) for 10 Min at 37 °C. The ß1-Integrin staining was continued for 20 min on ice after the stimulation, cells were then washed and incubated with the respective, labelled secondary antibody (Alexa Fluor 488 goat anti-mouse; Jackson Immuno) and analyzed by flow cytometry on a BD FACS Calibur.

3.2.2.11 Statistical analyses

Data are presented as arithmetic mean ± standard deviation. For multiple comparisons, normal distribution of data was first confirmed with D'Agostino & Pearson omnibus normality test. Analysis of variance (ANOVA) was then employed with Bonferroni posttests to assess significant differences between selected pairs. Ordinal data (histopathological scores) were compared using the non-parametric Wilcoxon-signed rank test. Survival curves were compared using log-rank/Mantel-Cox test.

4. Results

4.1 Asm inhibition for the treatment of FD

4.1.1 Molecular characterization of the *Asah1* knock-out mouse

4.1.1.1 Knock-out strategy

A conditional *Asah1* knock-out model was generated through flanking Exon1 with loxP sites and removal of the neomycin selection cassette via crossing to Flp recombinase deleter mice. To generate the constitutive knock-out model, the floxed mice were mated with EIIa-cre deleter mice and heterozygous mice were subsequently mated among each other.

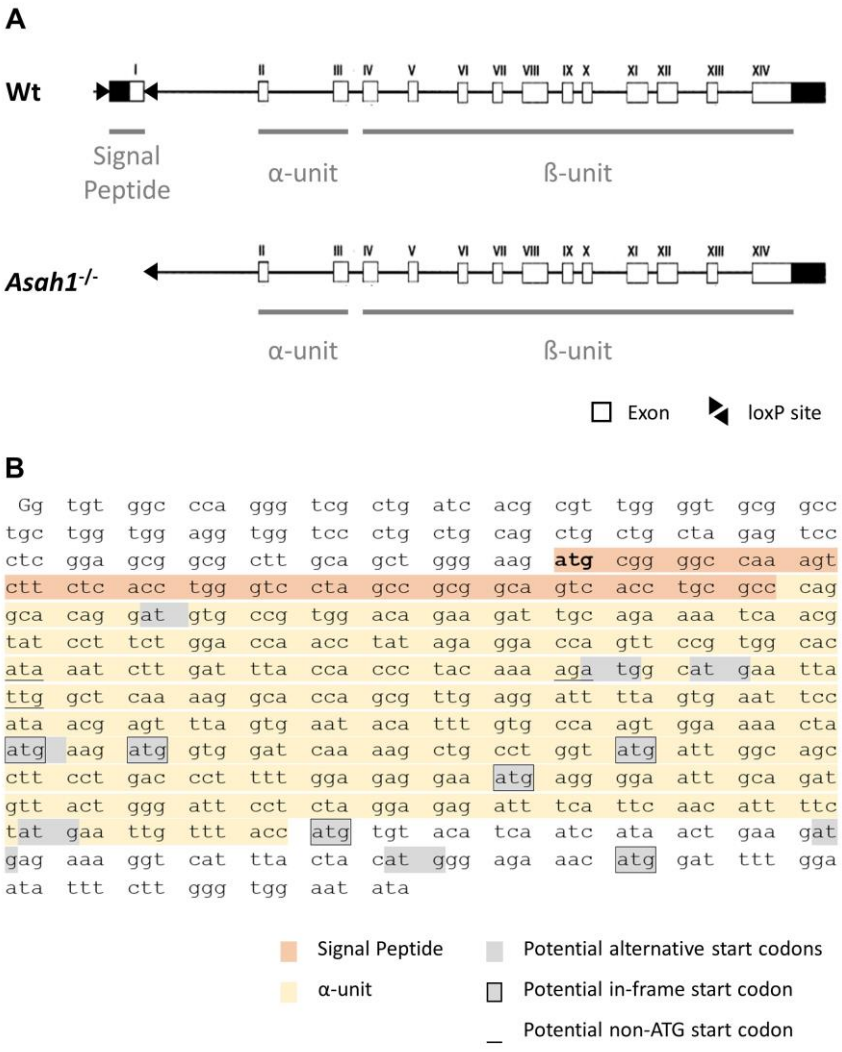

Figure 8: Knock-out strategy – (**A**) The structure of the murine *Asah1* gene in the *Asah1*$^{fl/fl}$ EIIa-cre^{tg} constitutive knock-out line is schematically shown. LoxP sites were added flanking Exon 1. Upon EIIa-cre mediated excision, Exon1 is thus deleted in the *Asah1*$^{-/-}$ mice. Image adapted from (Moser 2001). (**B**) The beginning of the *Asah1* mRNA sequence is shown (NCBI Reference Sequence: NM_019734.2) in open-reading frame. The sequences encoding the signal peptide and the α-unit are highlighted in color. Grey boxes indicate potential alternative start codons, an additional black frame indicates that these fit the open reading frame. Underlined codons are putative non-ATG start codons.

Figure 8A schematically shows the target genotypes resulting from heterozygous mating after crossing to EIIa-Cre mice. Exon1 includes the sequence for the start codon to initiate translation. Figure 8B shows part of the *Asah1* mRNA sequence in open-reading frame. Several potential alternative start codons are highlighted (grey boxes), as well as some putative non-ATG start codons (underlined). Some of these fit the open-reading-frame (black frame). However, no alternative start sequence is present in front of the signal peptide. It has not been investigated which of the potential alternative start codons is used in our model.

4.1.1.2 Knock-out of Ac signal peptide disrupts lysosomal targeting

Since knock-out of Exon1 deletes the signal peptide sequence, the protein expressed in *Asah1*$^{-/-}$ mice should display disrupted lysosomal targeting. Intracellular localization of Ac was therefore assessed by confocal microscopy in mesenchymal stem cells isolated from either Wt- or Ac-deficient mice. Cells were stained with an anti-Ac antibody in parallel with an antibody directed against the lysosomal marker protein LAMP1 to visualize the lysosomes and determine colocalization.

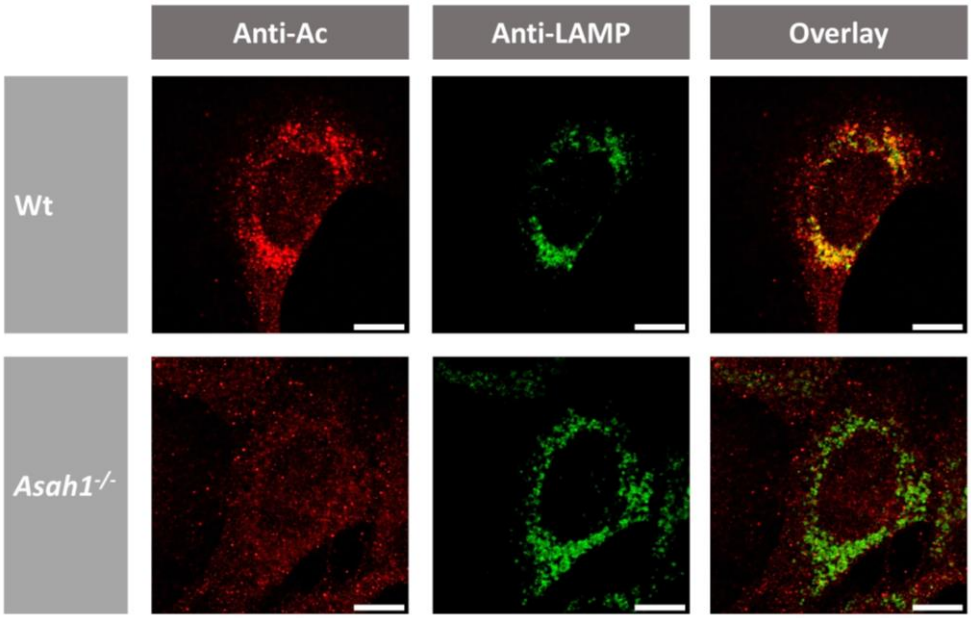

Figure 9: Deletion of acid ceramidase-signal peptide disrupts lysosomal targeting – Immunofluorescence staining of mesenchymal stem cells with antibodies directed against Acid ceramidase (Ac, red) and the lysosomal marker LAMP1 (green). Scale bar: 10 µm. Representative images are shown.

Immunofluorescence analysis showed colocalization of Ac with the lysosomal marker in Wt cells (Fig. 9). No such colocalization was observed in the Ac-deficient cells. Instead, Ac-staining in the *Asah1*$^{-/-}$ cells followed a diffuse, cytosolic pattern.

4.1.1.3 Reduction of Ac activity in *Asah1* knock-out mice

To assess the effect of the KO-model on Ac activity, an enzyme activity assay using NBD-labeled ceramide as a substrate was established. Organs were lysed, micelles were induced by sonication, the labelled ceramide substrate was added and incubated at 37 °C. The reaction was terminated by lipid extraction and the non-deacetylated substrate was separated from the liberated fatty acid through TLC. Spots were scanned with a Typoon FLA 9500 and quantified using ImageQuant software. The linearity of the assay was confirmed for each organ in the respective protein range by control reactions (data not shown).

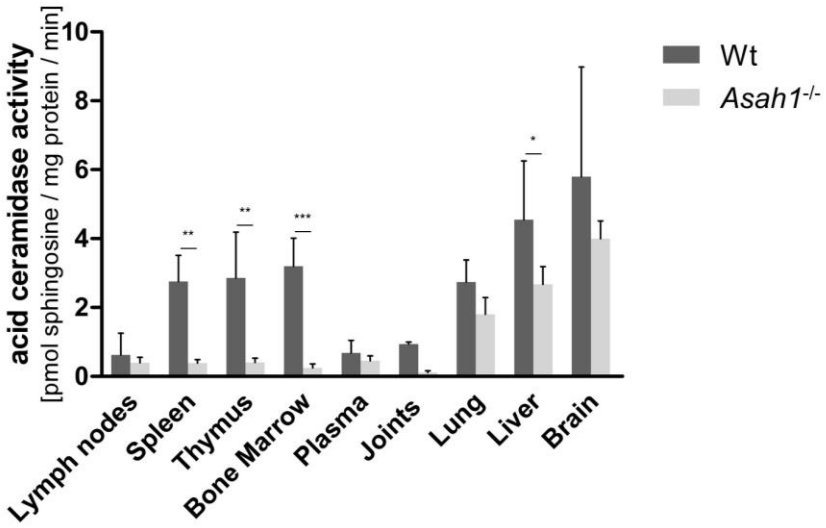

Figure 10: Acid ceramidase activity & ceramide accumulation – Assessment of acid ceramidase (Ac) activity upon knock-out of the signal peptide. Organ lysates were prepared and incubated in the presence of NBD-labeled ceramide. Means ± SD from n = 4-7 mice are depicted. Data passed the D'Agostino & Pearson omnibus normality test. Asterisks indicate significant differences as assessed by 2-way ANOVA with Bonferroni posttests: * $p < 0.05$; ** $p < 0.01$; *** $p < 0.001$.

Ac activity is reduced in Ac-KO mice in a tissue-specific manner (Fig. 10). Significant reduction in activity was observed for most of the lymphoid organs with the lymph nodes as the sole exception. Ac activity was also significantly reduced in the liver. Residual activity was present in all tested organs.

4.1.2 Pathological assessment of FD manifestations and effect of Asm ablation

4.1.2.1 Ceramide accumulation in Ac-deficient mice is blunted by Asm-deficiency

To assess if ASM inhibition would be therapeutically beneficial for FD, a preliminary rescue study was conducted in mice by crossing the Ac-deficient line to an Asm-deficient line. Ceramide and sphingomyelin levels were assessed by mass spectrometry.

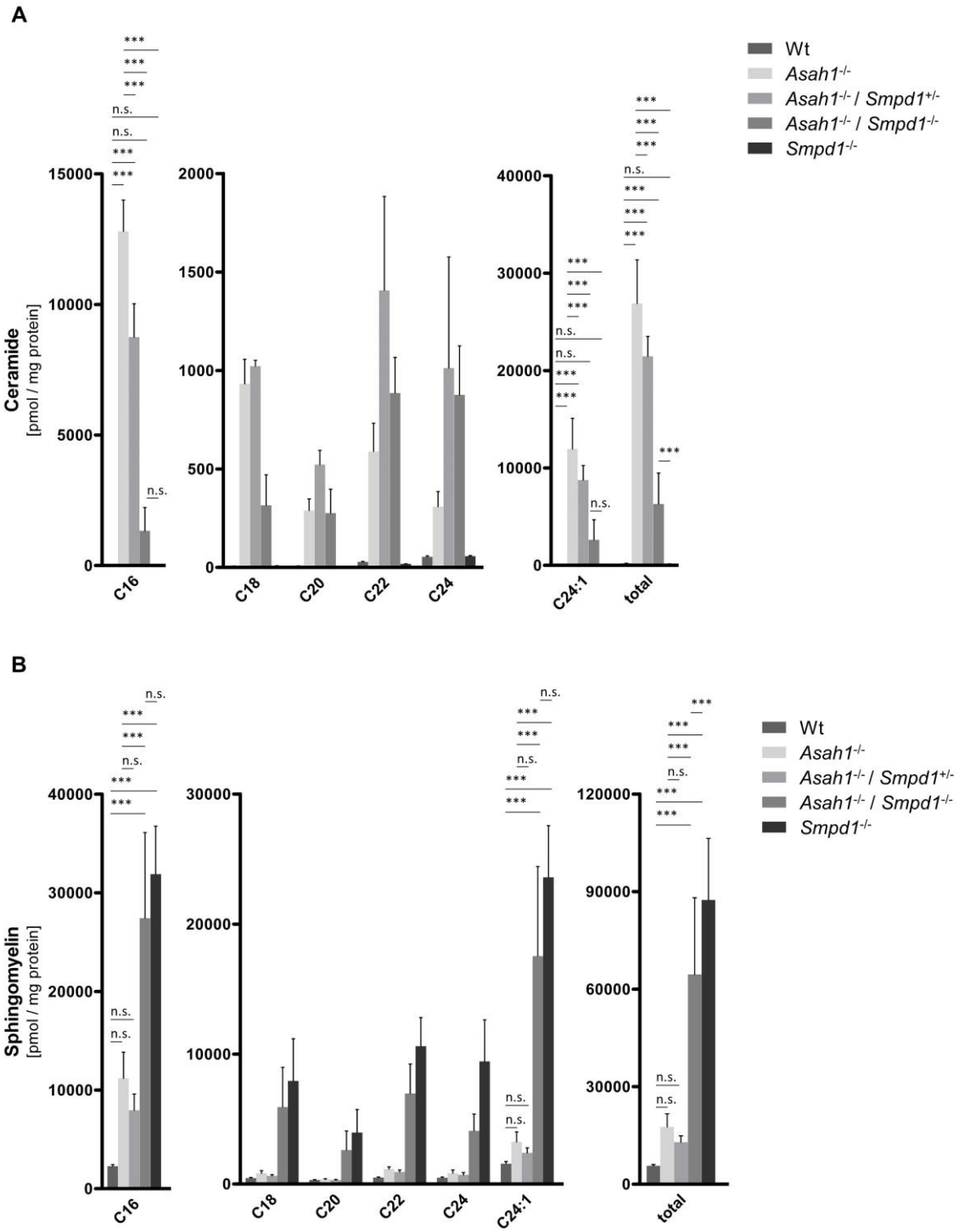

Figure 11: Ceramide and sphingomyelin quantification – The effect of acid ceramidase and acid sphingomyelinase knock-out on ceramide (**A**) and sphingomyelin (**B**) levels were analyzed by rapid resolution liquid chromatography/mass spectrometry of homogenates of snap-frozen spleen samples. Means ± SD from n = 5 mice are depicted. Data passed the D'Agostino & Pearson omnibus normality test. Asterisks indicate significant differences as assessed by ANOVA with Bonferroni posttests (* $p < 0.05$; ** $p < 0.01$; *** $p < 0.001$). No significant differences were detected for C18-, C20-, C22- and C24-ceramides and sphingomyelins.

Total ceramide was approximately 130-fold elevated compared to Wt mice upon Ac-deficiency. All individual ceramide species were also elevated irrespective of chain length, but only the increase in C16- and C24:1 ceramide was statistically significant (Fig. 11A). Total sphingomyelin and C16-sphingomyelin levels also increased upon Ac-deficiency, but not significantly. Crossing of Ac-deficient mice to Asm-deficient mice blunted ceramide accumulation in FD mice both in heterozygous and homozygous *Smpd1* mice. Whereas C16- and C24:1-ceramides were normalized, total ceramide levels were still significantly higher than in Wt mice. On the other hand, the double mutants had comparable sphingomyelin levels to Asm-mono-deficient mice, but the increase in total sphingomyelin was blunted.

4.1.2.2 Body weight and survival

To analyze the biological effects of reduced Ac activity and ceramide accumulation and the therapeutic relevance of the partially reduced ceramide levels in *Asah1*$^{-/-}$ / *Smpd1*$^{-/-}$ double mutants, mice were monitored with regard to their body weight and survival.

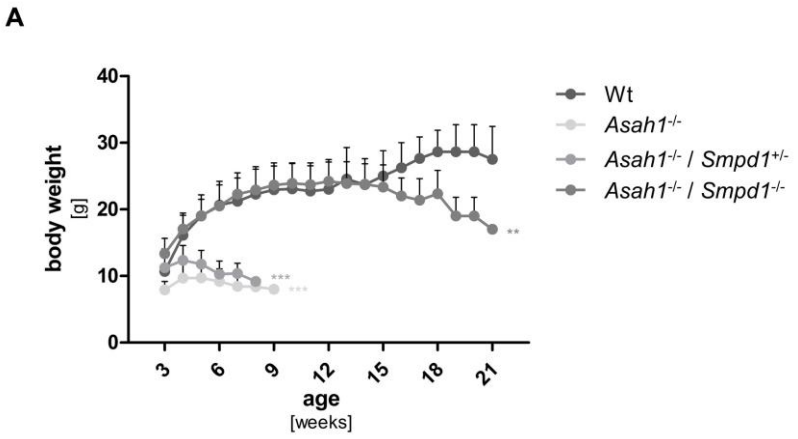

Figure 12: Body weight and survival of *Asah1*-/- and *Asah1*-/- / *Smpd1*-/- double-deficient mice - (**A**) Body weight of different genotypes. Mice were weighted once a week starting after weaning. Given are means ± SD from n = 3-33 mice per group and time-point. Data passed the D'Agostino & Pearson omnibus normality test and were compared by ANOVA with Bonferroni posttests. Asterisks indicate significant differences to Wt mice: ** $p < 0.01$; *** $p < 0.001$

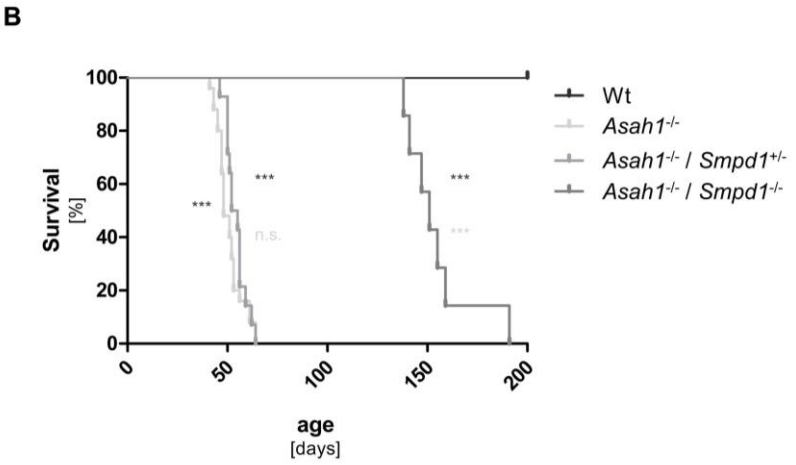

Figure 12 (continued): Body weight and survival of *Asah1*$^{-/-}$ and *Asah1*$^{-/-}$ / *Smpd1*$^{-/-}$ double-deficient mice - (**B**) Survival curve of different genotypes. Mice were monitored daily. Survival of n = 7-25 mice was compared using log-rank (Mantel-Cox) test. Dark grey asterisks indicate significant differences to Wt mice, light grey asterisks indicate significant differences to *Asah1*$^{-/-}$ mice. *** $p < 0.001$.

Ac-deficient mice already weight significantly less than their Wt littermates at weaning. After weaning, they barely gained weight and body weight started to decline at 5-6 weeks (Fig. 12A). Survival was markedly shortened in the *Asah1*$^{-/-}$ group: The earliest death occurred on day 41 and no Ac-deficient mouse survived for more than 64 days. The mean survival time was 51 days. No Wt mice died during the entire observation period (Fig. 12B).

Asah1$^{-/-}$ / *Smpd1*$^{-/-}$ double-deficient mice appeared to develop normally until 13 weeks of age, when body weight slowly started to decline (Fig. 12A). Survival of Ac-KO mice was markedly enhanced by Asm-deficiency: The average survival time of the double knock-out mice was 151 days and thus approximately 3 times longer than that of regular Ac-deficient mice (Fig. 12B). Heterozygous depletion of *Smpd1* was less beneficial – both in terms of weight gain and survival (Fig12. A+B) and failed to yield statistically relevant differences.

4.1.2.3 Histiocytic infiltration in lymphoid tissues

A key feature of FD is granuloma formation. To investigate if any such changes are present in the *Asah1*-KO model and possibly ameliorated by Asm co-ablation, a histopathological analysis was conducted on perfused, PFA-fixed and paraffin-embedded tissue samples. Additionally, MCP-1 levels were quantified by ELISA in the spleen and serum, because a recent cytokine profile of FD patients has suggested MCP-1 to be the driver of macrophage

infiltration and further inflammatory cytokine production in FD (Alayoubi et al. 2013; Dworski et al. 2017)

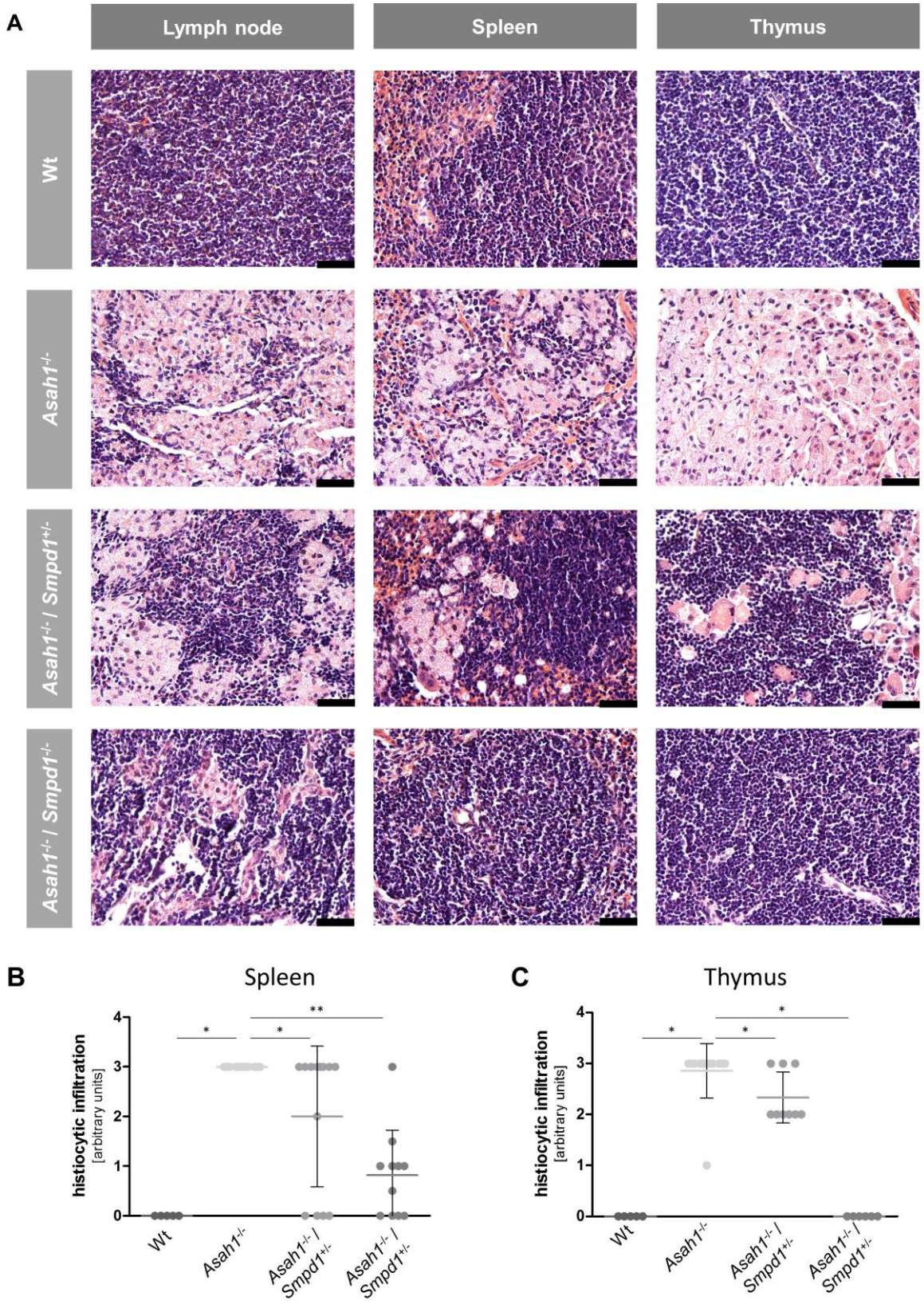

Figure 13: Histiocytic infiltration in lymphoid tissues – (**A)** HE staining of perfused, PFA-fixed and paraffin-embedded tissue sections. Scale bar: 50 µm. Representative images are shown. (**B+C**) Histiocytic

infiltration with foamy macrophages were exemplary scored on a scale of 0 (no signs) to 4 (very severe) in spleen (**B**) and thymus (**C**) by a blinded investigator. Graphs depict each replicate and the mean ± SD. Indicated p-values are the result of Wilcoxon signed-rank test.

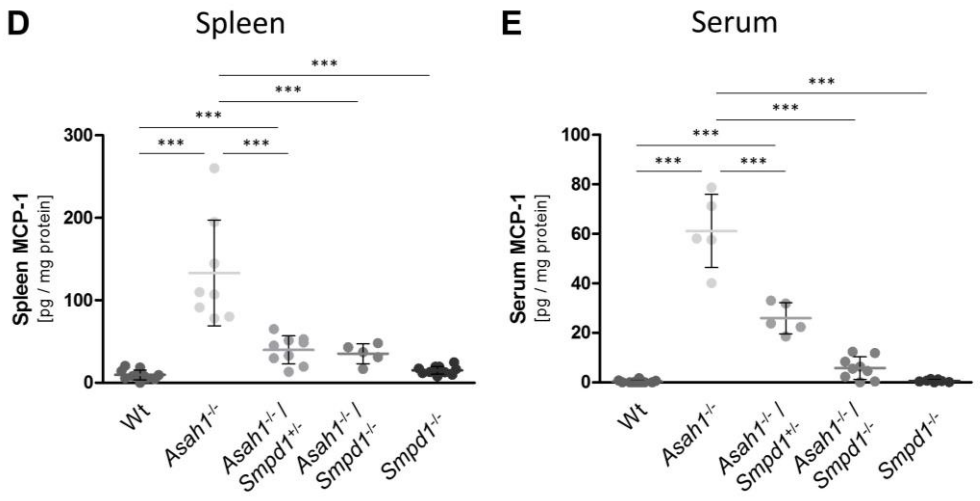

Figure 13 (continued): Histiocytic infiltration in lymphoid tissues – (**D**-**E**) MCP-1 levels in spleen (**D**) and serum (**E**) were quantified by ELISA. Given are means ± SD of n = 5-12 mice per group. Data passed the D'Agostino & Pearson omnibus normality test. Asterisks indicate significant differences as assessed by ANOVA with Bonferroni posttests: *** $p < 0.001$.

Ac-deficient mice showed massive histiocytic infiltrations in all lymphoid tissues with a concomitant disturbance of the underlying tissue architecture (Fig. 13A). The infiltrates have the appearance of foamy macrophages and were confirmed as such by a pathologist (PD Dr. Jan Becker, University Hospital Cologne, personal communication). Foamy macrophages were also present in the gut associated lymphoid tissues (not shown).

Heterozygous depletion of Asm in Ac-deficient mice reduced histiocytic infiltration in a subset of mice in the thymus and spleen (Fig13. A-C). Complete genetic ablation of Asm in Ac-deficient mice had even better and more uniform outcomes: Reduction of histiocytic infiltrates were seen in all lymphoid tissues and in all mice except for one (Fig. 13A-C). Histiocytic infiltration was also reduced in the lymph nodes (Fig. 13A).

MCP-1 quantification showed elevated levels of this chemokine in the spleen (Fig. 13D) and serum (Fig. 13E) upon *Asah1* knock-out. Both heterozygous and homozygous co-deficiency of Asm blunted the MCP-1 elevation in FD mice significantly (Fig. 13D-E).

4.1.2.4 Joint pathology

Joint manifestations are one of the key features of FD. To investigate if the *Asah1* knock-out model mimics this feature of the disease, knee joints were dissected and analyzed histologically.

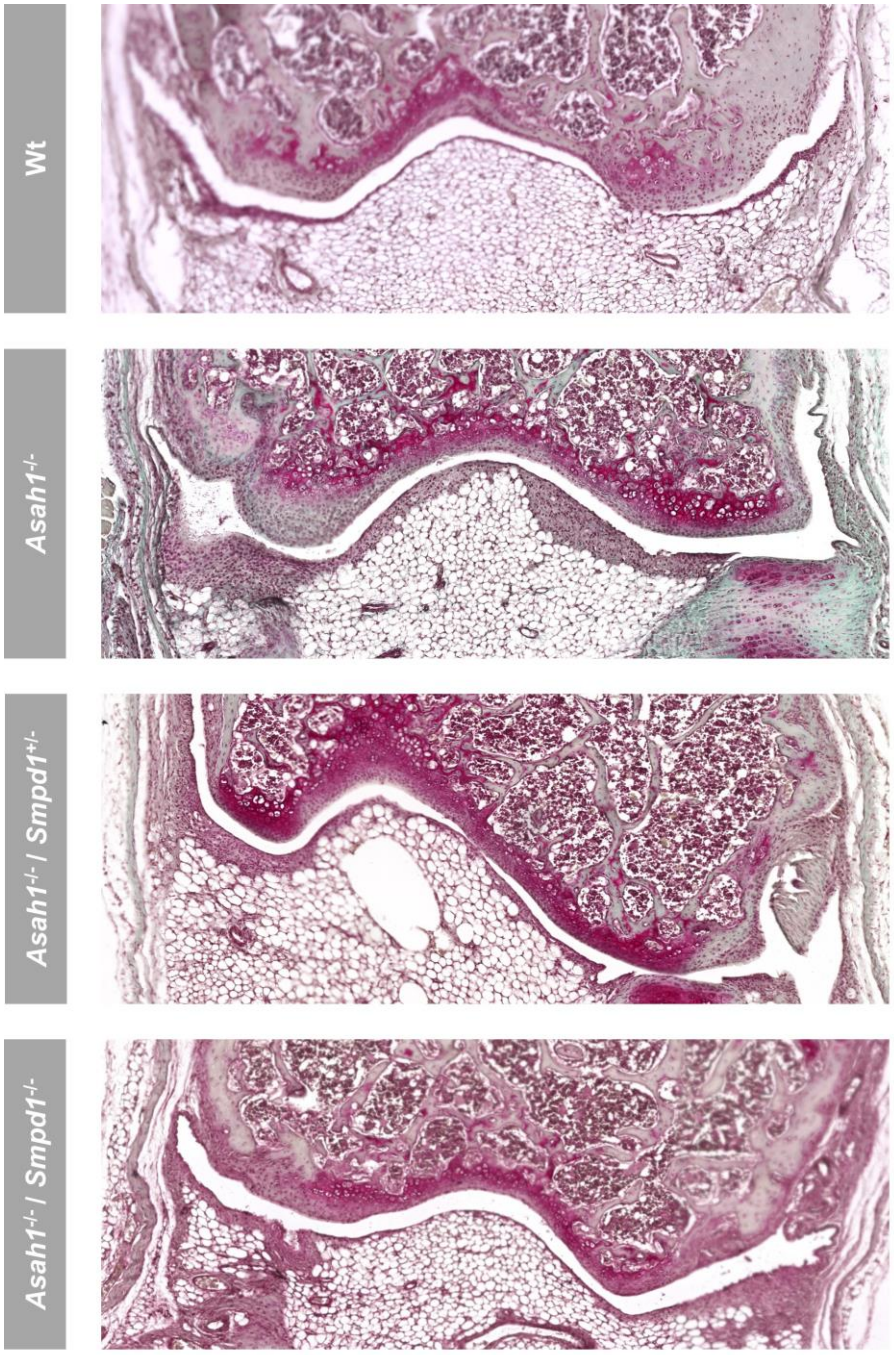

Figure 14: Synovial hyperplasia in knee joints – SafraninO/FastGreen staining of PFA-fixed, de-calcified and paraffin-embedded knee joint sections. Representative images from 5 mice per group are shown.

Knee joints of Ac-deficient mice exhibited pronounced synovial hyperplasia. The hyperplastic tissue appeared to consist mostly of cells with the same foamy-macrophage-like appearance

as the histiocytic infiltrates in the lymphoid tissues. No pannus formation, cartilage loss or bone erosions were observed, as well as no other signs of inflammation including no exudation into the joint cavity (Fig. 14). Synovial hyperplasia was partially reduced upon Asm co-deficiency.

4.1.2.5 Lung inflammation

Pulmonary involvement has been reported for all severely affected FD patients. The lungs of *Asah1*-KO mice therefore were also evaluated histologically.

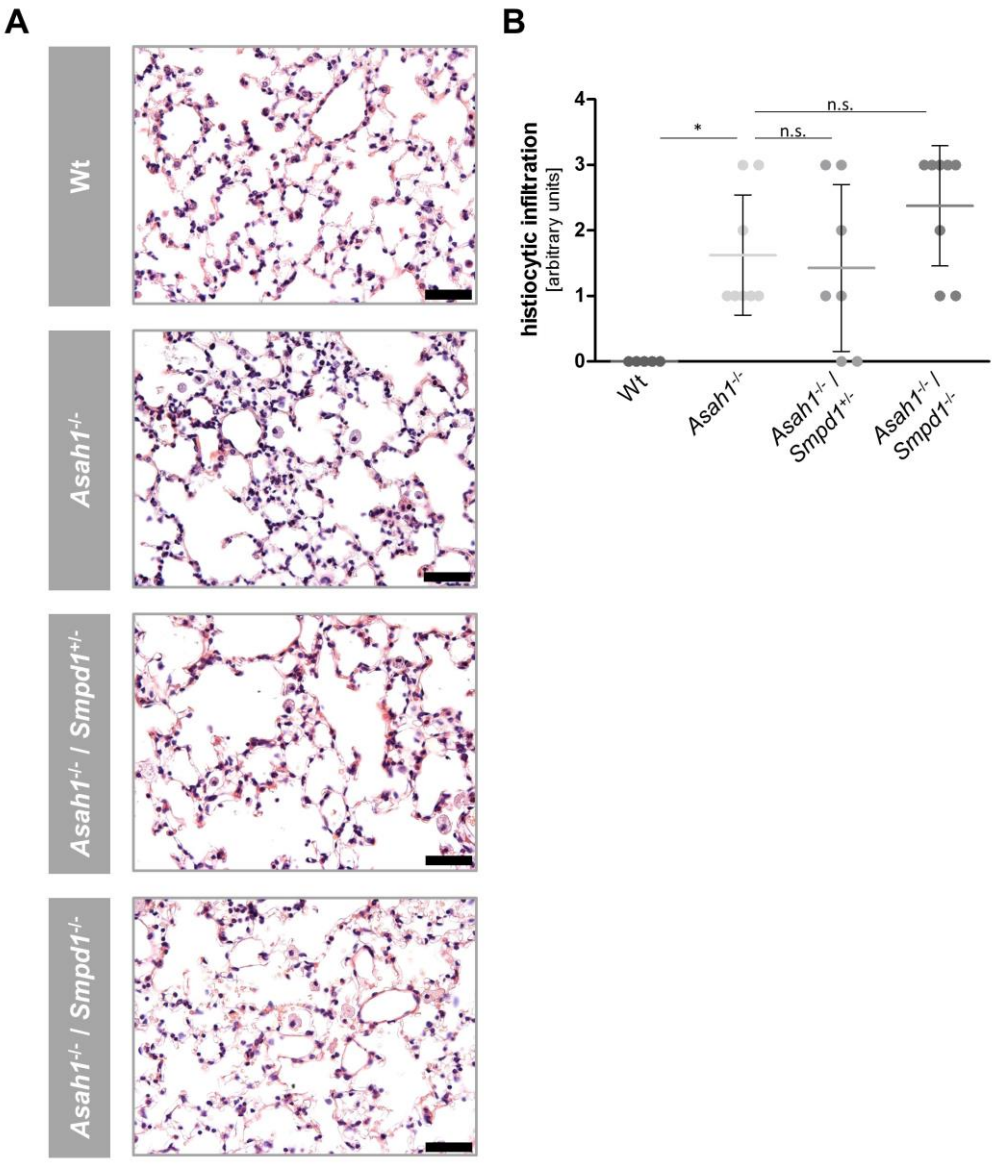

Figure 15: Increased cell numbers in acid ceramidase deficient lungs – (**A**) HE staining of perfused, PFA-fixed and paraffin-embedded lung sections. Scale bar: 50 µm. Representative images are shown. (**B**) Lung infiltration was scored on a scale of 0 (no signs) to 4 (very severe) by a blinded investigator. Graphs depict each replicate and the mean ± SD. Indicated p-values are the result of Wilcoxon signed-rank test of the respective genotype compared to *Asah1*$^{-/-}$ mice.

Ac-deficient mice showed an increased number of cells in the lung, including foamy macrophages. Additionally, there was also an increased number of smaller cells, which have the appearance of neutrophils (Fig. 15).

The lung phenotype of Ac-deficient mice was also analyzed further and compared to the CF phenotype, since ceramide accumulation was also reported in CF lungs. Since these further studies constitute an independent project and were conducted in co-operation with a postdoctoral fellow at our institute, they are not included in this thesis. Briefly, we confirmed the significant increase of total cell number/lung in *Asah1*$^{-/-}$ mice by flow cytometry. Whereas dendritic cells were significantly decreased upon Ac-deficiency, neutrophils were significantly increased. Preliminary data also shows an increase in macrophages, myeloid-derived suppressor cells and $CD4^+$ $CD8^+$ double positive T cells, whereas all other T cell subsets were unaltered or reduced. Preliminary cytokine analysis also shows showed an increase in various cytokines, including for instance MCP-1 and IL-8 (Beckmann & Kadow, unpublished data).

The lungs of *Asah1*$^{-/-}$ / *Smpd1*$^{-/-}$ double mutant mice show a slight, but not significant tendency toward more macrophage infiltration (Fig. 15A), which matches the reported lung phenotype of *Smpd1* knock-out mice (Kuemmel et al. 1997).

4.1.2.6 Liver pathology

Hepatic involvement has been reported for the more severe forms of FD and up to 25 % of FD patients exhibit liver failure (Bao et al. 2017). An initial insight into liver manifestations of FD in the *Asah1*-KO mice and potential amelioration by Asm-deficiency was therefore obtained by histology.

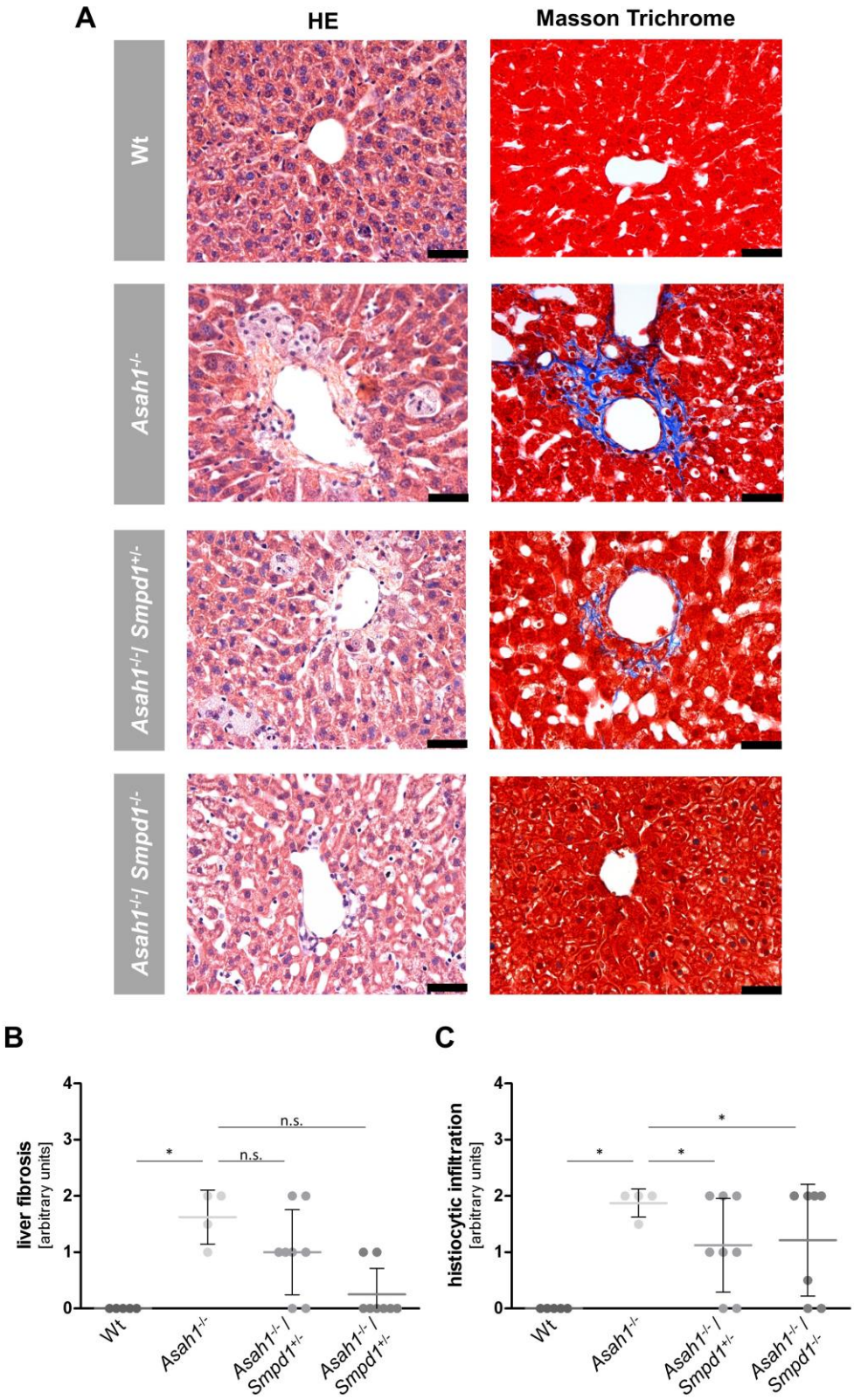

Figure 16: Liver histopathology – (**A**) HE and Masson Trichrome staining of perfused, PFA-fixed and paraffin-embedded liver sections. Scale bar: 50 µm. 4-6 mice were analyzed per group. Representative images are shown. (**B**-**C**) Macrophage infiltration (**B**) and liver fibrosis (**C**) were scored on a scale of 0 (no signs) to 4 (very severe) by a hepato-pathologist. The graphs depict each replicate and the mean ± SD. Indicated p-values were determined by Wilcoxon-signed rank test.

Analysis of the liver revealed conspicuous patches in *Asah1*-KO mice, which were mostly located around the central veins. These were subsequently confirmed to be fibrous by Masson-Trichrome staining and staged by a blinded pathologist (Jiang Wang, MD, PhD, University of Cincinnati, personal communication) as early stages of pericentral and pericellular hepatic fibrosis (Fig. 16A+C). Some foamy macrophages were also present - both within the fibrotic areas and isolated outside of them (Fig. 16A+B). Whereas macrophage infiltration in the liver was not significantly affected by Asm-depletion (Fig. 16A+B), liver fibrosis was almost completely absent (Fig16. A+C).

Given these findings, a more detailed analysis of liver function was conducted. Clinical liver parameters were assessed in the serum using a dry chemistry system (Scil Spotchem^{TM}).

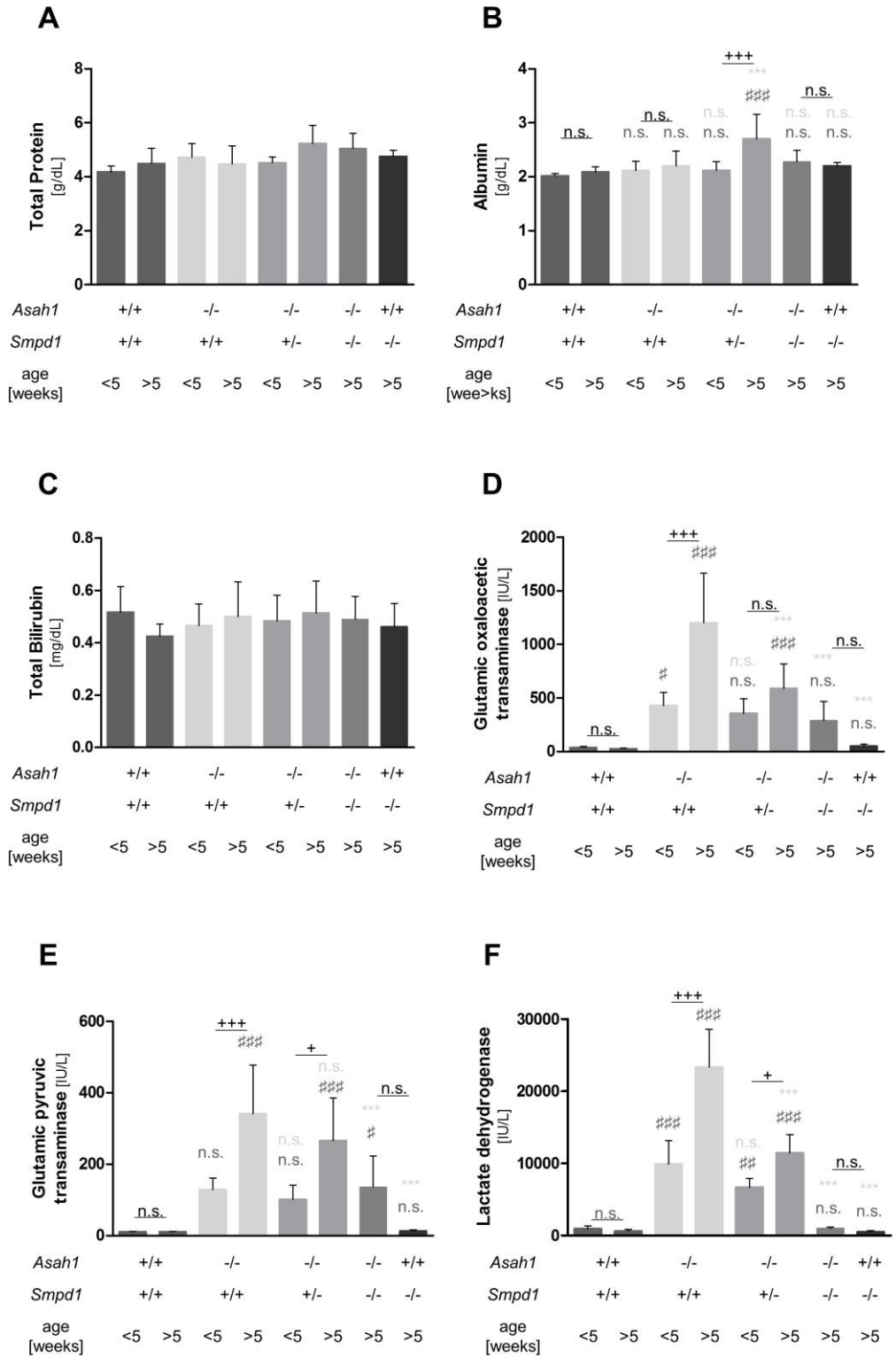

Figure 17: Serum analysis of liver parameters – (**A-F**) Liver parameters were analyzed in serum using a Scil Spotchem™. Graphs depict the mean ± SD of n = 6-11 mice per group. Data passed the D'Agostino & Pearson omnibus normality test and asterisks indicate multiplicity adjusted p-values as determined by ANOVA with Bonferroni posttests: * $p < 0.05$; ** $p < 0.01$; *** $p < 0.001$. ♯ indicates significant differences compared to the age matched Wt group, * to the age-matched *Asah1*$^{-/-}$ group and + the comparison of the different ages within the given genotype or the comparison of *Smpd1*$^{-/-}$ with *Asah1*$^{-/-}$ / *Smpd1*$^{-/-}$ double

deficient mice respectively. No significant differences were detected for total protein (**A**) and total bilirubin (**C**).

Whereas total serum protein, albumin and total bilirubin (Fig. 17A-C) were not altered, liver transaminases and LDH were significantly increased (Fig. 17D-F) in Ac-deficient mice. We also analyzed Gamma-glutamyl-transferase, but all samples were below the detection limit (data not shown). Hepatic damage worsened with age, but could be improved significantly already by heterozygous depletion of Asm, and even more so by homozygous depletion of Asm (Fig. 17 D-F).

4.1.2.7 Hematological manifestations

Hematological manifestations of FD were indicated in some case reports (Antonarakis et al. 1984; Fujiwaki et al. 1992; Mondal et al. 2009), but have not been reported with any clear consistency. To gain further insights, blood counts were prepared.

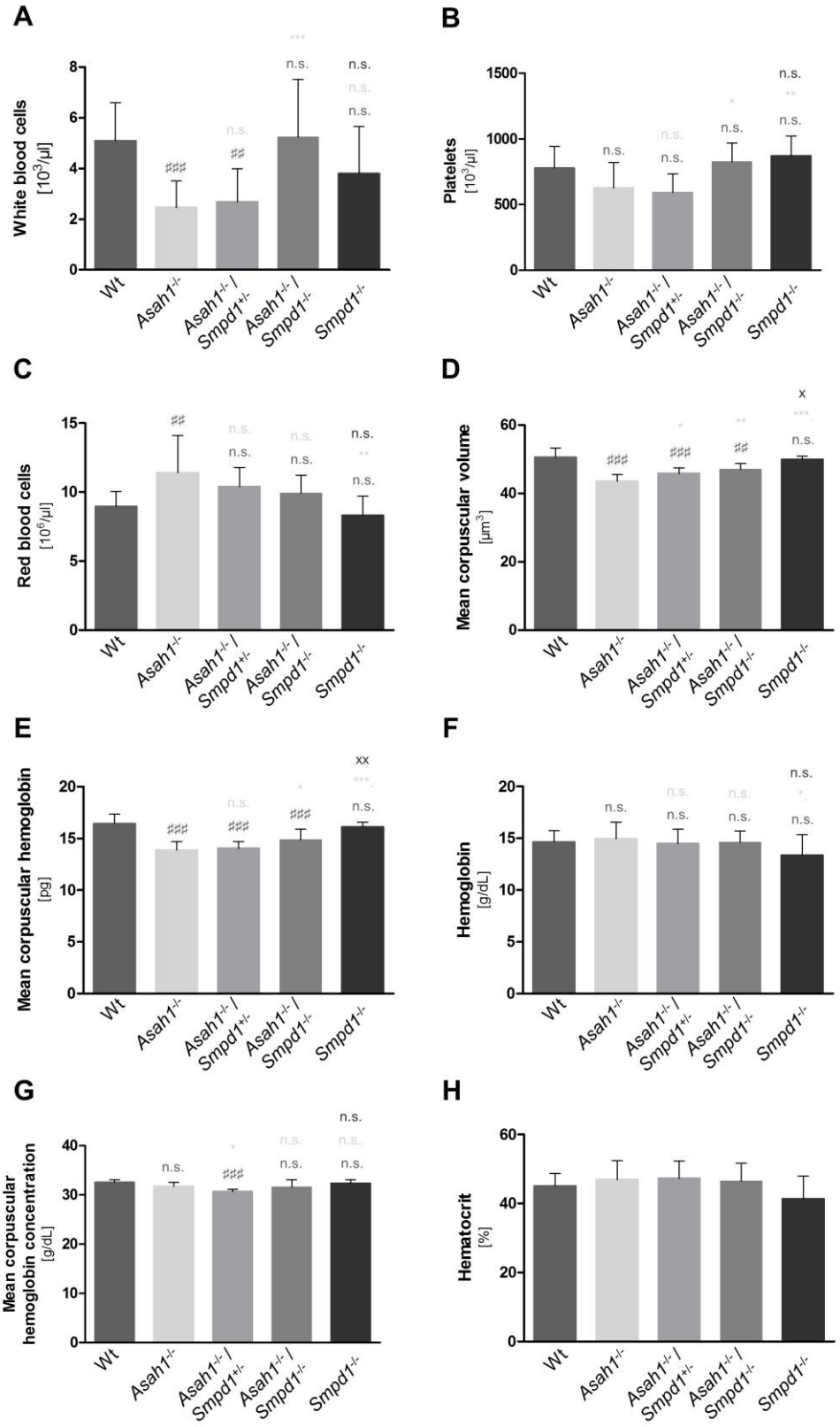

Figure 18: Blood count – Blood counts were obtained using Scil VetABC™. Given are means ± SD of n = 5-17 mice per group. Data passed the D'Agostino & Pearson omnibus normality test and asterisks indicate multiplicity adjusted p-values as determined by ANOVA with Bonferroni posttests: * $p < 0.05$; ** $p < 0.01$; *** $p < 0.001$. ♯ indicates significant differences compared to the age matched Wt group, * to the age-matched *Asah1*$^{-/-}$ group and x the comparison of *Smpd1*$^{-/-}$ with *Asah1*$^{-/-}$ / *Smpd1*$^{-/-}$ double deficient mice. No significant differences were detected for hematocrit (**H**).

Ac-deficient mice showed significantly decreased white blood cell counts (Fig. 18A), whereas the red blood cell count (Fig. 18B) was slightly increased. Ac-deficient erythrocytes had reduced mean corpuscular hemoglobin (Fig. 18G), but the total amount of hemoglobin was not changed (Fig. 18C). Other erythrocyte indices and hematocrit were normal (Fig. 18D, F, H). Platelet number was reduced, albeit not significantly (Fig. 18E). Heterozygous depletion of Asm showed no or only mild improvements, whereas homozygous knock-out of *Smpd1* normalized all parameters (Fig. 18A-G).

4.1.2.8 Muscular manifestations

Creatinine phosphokinase (CPK) indicates damage of tissues that rapidly consume ATP (i.e. muscle tissue, brain) and is thus used as a marker for myocardial infarction, rhabdomyolysis, muscular dystrophy, acute kidney injury and some other conditions. It was included in the test panel because Ac-deficient mice showed some indicators of muscular dystrophy upon observation (progressive wasting, scoliosis, waddling gate). Additionally, mutations in the *ASAH1* gene have been reported in a subset of spinal muscular atrophy patients (Dyment et al. 2014; Filosto et al. 2016; Gan et al. 2015; Zhou et al. 2012) and some patients have even been reported to suffer from both FD and spinal muscular atrophy (Teoh et al. 2016). Elevated CPK activity is frequently reported in spinal muscular atrophy patients (Rudnik-Schoneborn et al. 1998).

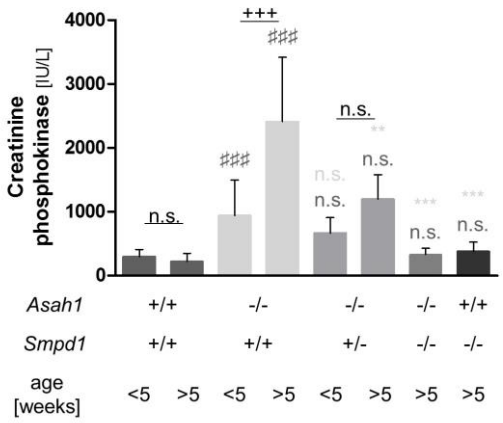

Figure 19: Creatinine phosphokinase quantification – Creatinine phosphokinase levels were quantified in serum using a Scil Spotchem^{TM}. Given are means ± SD from n = 5-10 mice per group. Data passed the D'Agostino & Pearson omnibus normality test and asterisks indicate multiplicity adjusted p-values as determined by ANOVA with Bonferroni posttests: * $p < 0.05$; ** $p < 0.01$; *** $p < 0.001$. ♯ indicates significant differences compared to the age matched Wt group, * to the age-matched *Asah1*$^{-/-}$ group and + the comparison of the different ages within the given genotype or the comparison of *Smpd1*$^{-/-}$ with *Asah1*$^{-/-}$ / *Smpd1*$^{-/-}$ double deficient mice respectively.

CPK levels were significantly elevated even in young Ac-deficient mice and increased further with age (Fig. 19). Co-deficiency of Asm significantly blunted CK elevation and even normalized them upon complete Asm depletion (Fig. 19).

4.1.2.9 Metabolism

The reduced body weight and size of Ac-deficient mice prompted an investigation into their metabolism. We analyzed glucose levels in the serum, as well as the ketone body ß-hydroxybutyrate in the urine. Ketonuria occurs when alternative sources of energy are being used, e.g. during starvation or in type I diabetes mellitus.

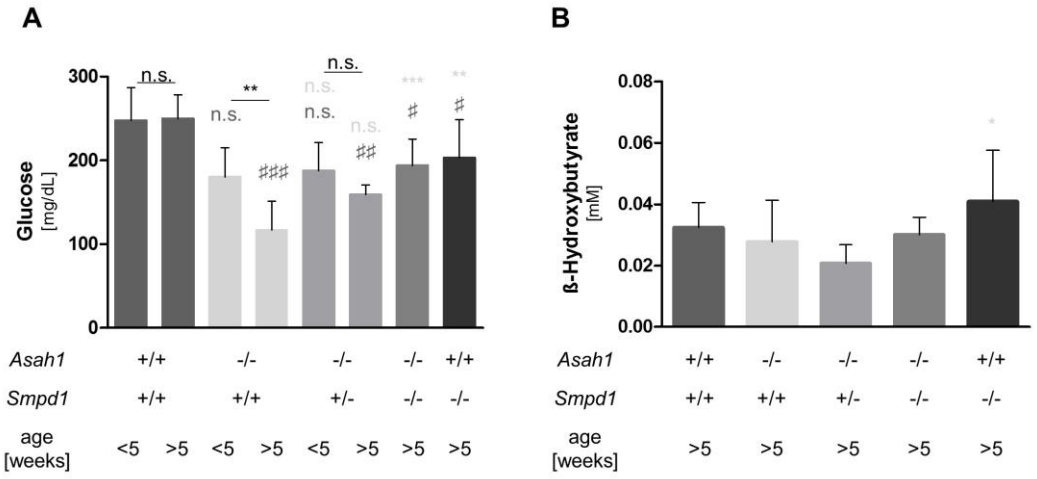

Figure 20: Metabolic analysis – (**A**) Serum analysis of glucose levels of n = 6-11 mice per group. (**B**) Levels of ß-hydroxybutyrate were quantified in urine of n = 7-14 mice per group using a colorimetric assay. (**A-B**) Given are means ± SD. Data passed the D'Agostino & Pearson omnibus normality test and was subsequently compared by ANOVA with Bonferroni posttests: * $p < 0.05$; ** $p < 0.01$; *** $p < 0.001$. (**A**) ♯ indicates significant differences compared to the age matched Wt group, * to the age-matched Ac-KO group and + the comparison of the different ages within the given genotype.

Serum glucose levels were decreased in Ac-deficient mice and declined progressively. Hypoglycemia reached statistical significance in the older Ac-deficient mice (Fig. 20A). Heterozygous depletion of Asm did not sufficiently improve glucose levels (Fig. 20A). Complete depletion of Asm in *Asah1*$^{-/-}$ mice ameliorated hypoglycemia significantly, but could not restore it to Wt levels (Fig. 20A). Given the observed hypoglycemia, insulin levels were also analyzed. However, insulin levels remained below the detection limit of the assay in almost all samples (not shown).

Ketonuria was also assessed. The levels of the ketone body ß-hydroxybutyrate in the urine were slightly decreased in Ac-deficient mice, but not significantly when compared to Wt littermates (Fig. 20B).

4.1.2.10 Kidneys

Although kidneys have high AC expression (Li et al. 1999) and ceramide was reported to accumulate in the kidneys of FD patients as well (Fujiwaki et al. 1995), little is known about FD manifestations in the kidney. Renal FD manifestations were therefore investigated by histological analysis and by determination of different functional kidney parameters.

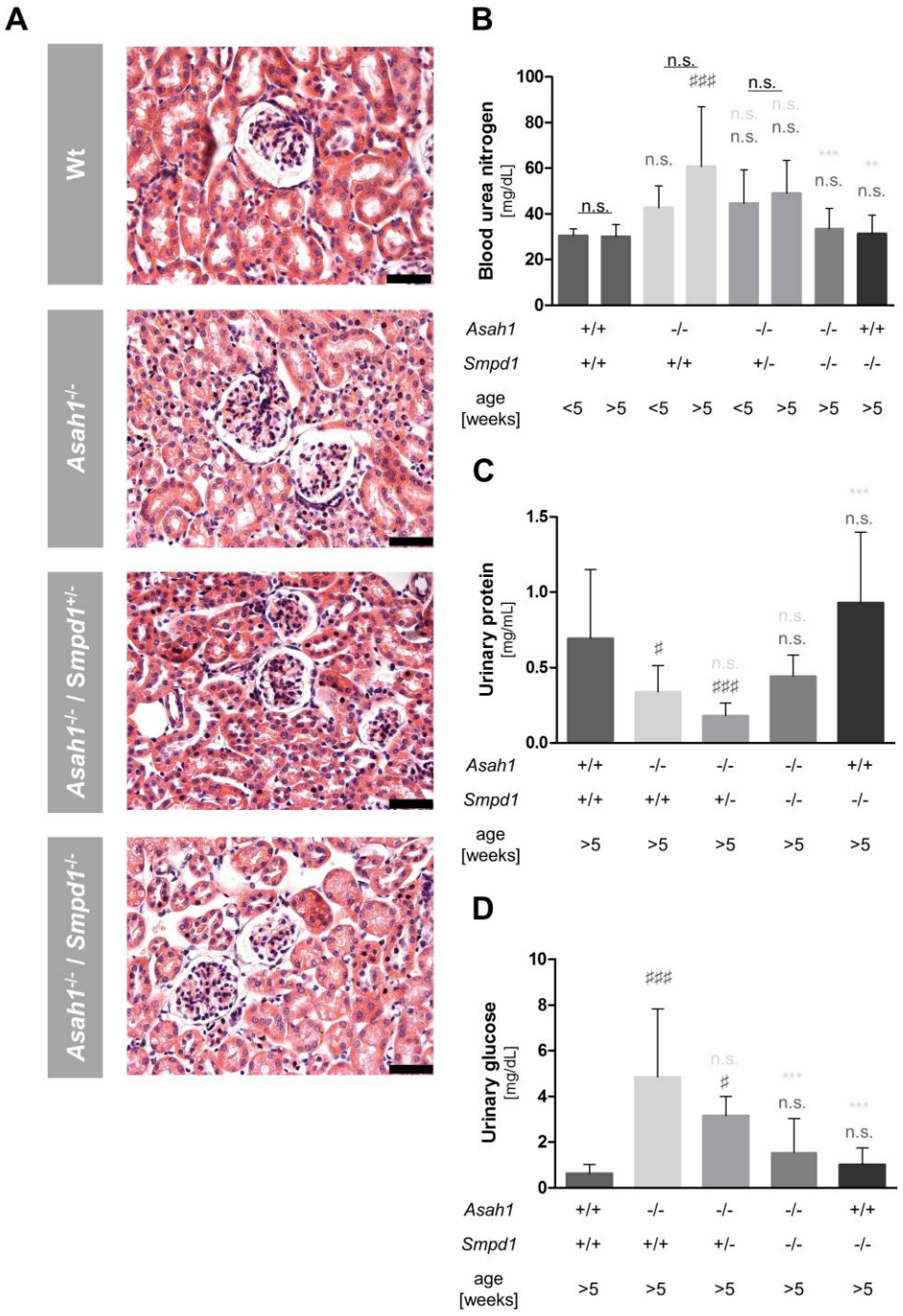

Figure 21: Analysis of kidney function – (**A**) HE staining of perfused, PFA-fixed and paraffin-embedded kidney sections. Scale bar: 50 µm. Representative images of n = 4-6 mice per group are shown. (**B-E**) Blood urea nitrogen (**B**), urinary protein (**C**) and urinary glucose (**D**) were quantified. Given are means ± SD of n = 6-15 mice per group. Data passed the D'Agostino & Pearson omnibus normality test and was subsequently compared by ANOVA with Bonferroni posttests: * $p < 0.05$; ** $p < 0.01$; *** $p < 0.001$. ♯ indicates significant differences compared to the age matched Wt group, * to the age-matched Ac-KO group and + the comparison of the different ages within the given genotype.

Histologic analysis showed no pathologies in the kidney upon Ac-deficiency (Fig. 21A). A seasoned nephrotic pathologist confirmed this finding (PD Dr. Jan Becker, University Hospital Cologne, personal communication). However, blood urea nitrogen (BUN) levels

were significantly increased in Ac-deficient mice above 5 weeks of age (Fig. 21B). Additional markers of kidney function and damage were therefore assessed only in the older mice. Serum creatinine remained below the detection limit of 0.2 mg/dl (not shown). Urinary protein levels decreased in Ac-deficient mice (Fig. 21C) and a significant loss of glucose via the urine was detected (Fig. 21D). Homozygous depletion of Asm normalized all parameters, whereas heterozygous depletion of Asm did not improve urinary protein and glucose excretion.

4.1.3 Pharmacological inhibition of Asm in *Asah1* knock-out mice

4.1.3.1 Treatment of juvenile *Asah1* knock-out mice with Amitriptyline

Given the beneficial effects of genetic Asm-depletion on FD manifestations and survival, Asm was targeted pharmacologically with the functional Asm inhibitor Amitriptyline to translate the findings to a setting with clinical applicability. In a first study, Ac-deficient mice were treated with Amitriptyline via the drinking water from week 4 onwards and survival was monitored.

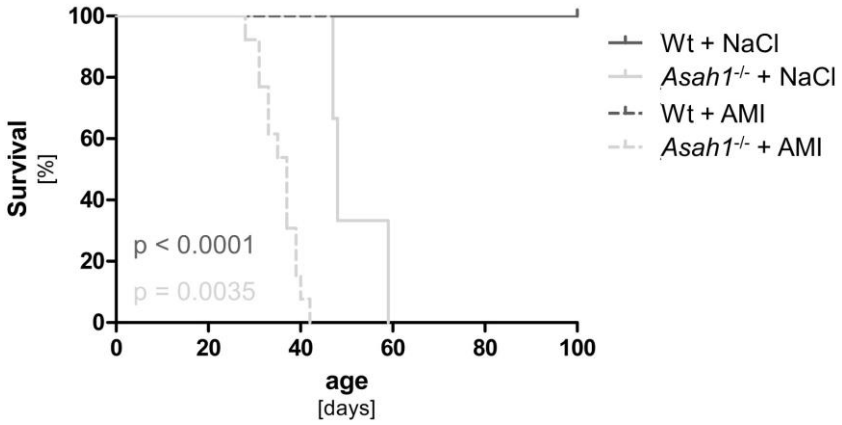

Figure 22: Survival of juvenile acid ceramidase deficient mice upon Amitriptyline treatment – *Asah1*$^{-/-}$ mice received 180 mg/L Amitriptyline hydrochloride (AMI) in 0.9 % saline solution as their drinking water with *ad libitum* access or only saline solution (NaCl). Treatment commenced 4 weeks after birth. Survival was monitored by daily visitation. Indicated p-values are the result of log-rank (Mantel-Cox) test: Light gray indicates the comparison between Amitriptyline and placebo-treated *Asah1*$^{-/-}$ mice and dark grey the comparison between Amitriptyline treated groups.

Treatment with Amitriptyline severely shortened the survival time of *Asah1*$^{-/-}$ mice compared to their untreated counterparts. Death typically occurred within days of treatment and the median survival time was only 37 days. Amitriptyline treatment had no adverse effects on age-matched Wt mice – all Wt mice survived for the entire observation period and showed no signs of health impairment (Fig. 22).

4.1.3.2 Amitriptyline treatment throughout development

4.1.3.2.1 Survival upon Amitriptyline treatment

Given the apparent contrast of prolonged survival of *Asah1*$^{-/-}$ mice upon genetic co-ablation of *Smpd1* and shortened survival upon pharmacological Asm inhibition, a second pharmacological study with Amitriptyline was employed. In the second study, Amitriptyline treatment was already started *in utero* through treatment of the *Asah1*$^{+/-}$ mothers. After birth, treatment of the offspring was continued through breast milk via treatment of the mothers until the offspring was weaned. Then, treatment of the juvenile mice was continued directly via the drinking water. The aim of the second study was to commence Amitriptyline early enough to prevent significant ceramide accumulation. Survival of treated mice was monitored daily.

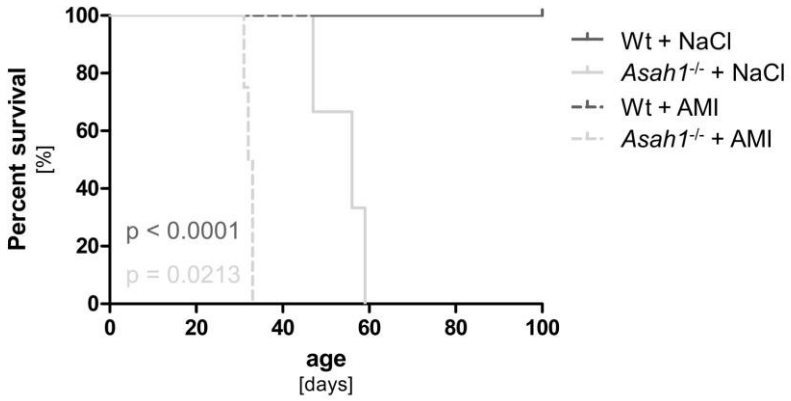

Figure 23: Survival upon Amitriptyline treatment throughout development – *Asah1*-heterozygous mice were mated for four days. Pregnant females then received either 180 mg/L Amitriptyline hydrochloride (AMI) in 0.9 % saline solution or only saline solution (NaCl) as their drinking water with *ad libitum* access. Treatment was continued after birth. After weaning, the offspring received Amitriptyline or placebo as drinking water in the same dose. Survival was monitored by daily visitation and compared using log-rank (Mantel-Cox) test.

Amitriptyline treatment throughout development did not improve the survival of Ac-deficient mice. Instead, they died shortly after weaning and thus at a similar age to the mice that received Amitriptyline at an age of 4 weeks. No adverse effects of Amitriptyline treatment were observed in Wt mice and the vehicle alone also had no effect (Fig. 23).

4.1.3.2.2 Asm and Ac activity upon Amitriptyline treatment

Since no differences in survival were observed whether *Asah1*$^{-/-}$ mice were treated with Amitriptyline throughout development or starting from an age of 4 weeks, the efficacy

of Amitriptyline treatment via the mothers was assessed by with an enzyme activity assay using BODIPY-labeled sphingomyelin as a substrate.

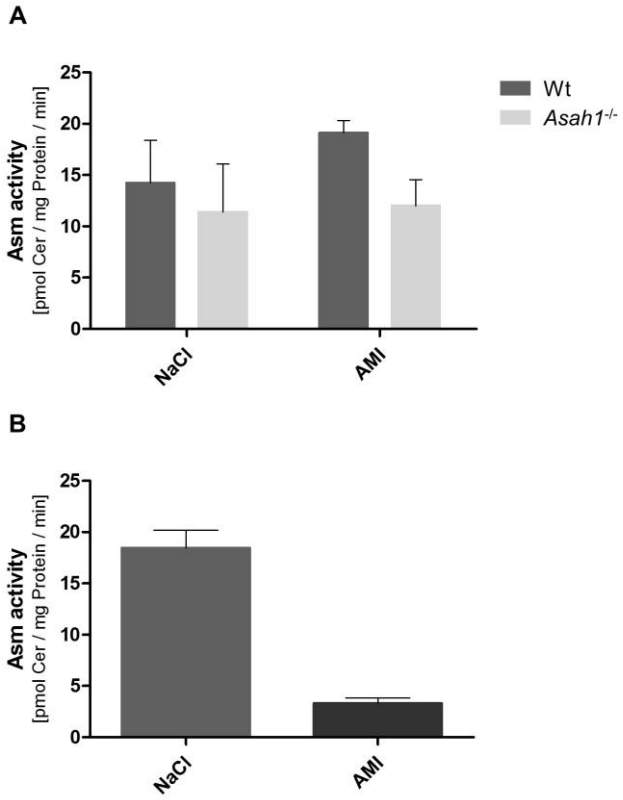

Figure 24: Acid sphingomyelinase activity upon Amitriptyline treatment – (**A**) Pregnant females received either 180 mg/L Amitriptyline hydrochloride (AMI) in 0.9 % saline solution, or only saline solution (NaCl) as their drinking water with *ad libitum* access. Treatment was continued after birth. After weaning, offspring was sacrificed and spleens were dissected. (**B**) Adult Wt mice were treated with either Amitriptyline or saline solution as described above and sacrificed after 4 weeks. Spleens were dissected. (**A+B**) Acid sphingomyelinase (Asm) activity was assessed using BODIPY-labeled sphingomyelin as a substrate. Given are means ± SD of n = 3-6 mice per group.

The results show that Amitriptyline treatment via the mothers was insufficient to cause a reduction of Asm activity in the offspring (Fig. 24A). Direct treatment of adult Wt mice with the same dose, however, resulted in an almost 80 % reduction of Asm activity (Fig. 24B).

4.2. Asm inhibition for the treatment of RA

4.2.1 Susceptibility of *Smpd1* knock-out mice to experimental arthritis

To define the role of ASM in RA, we utilized a murine antigen-induced arthritis model that mimics some features of the human disease. Asm-deficient mice and wild-type littermates were compared in this model. Joint swelling and joint histopathology were assessed during the acute phase of inflammation.

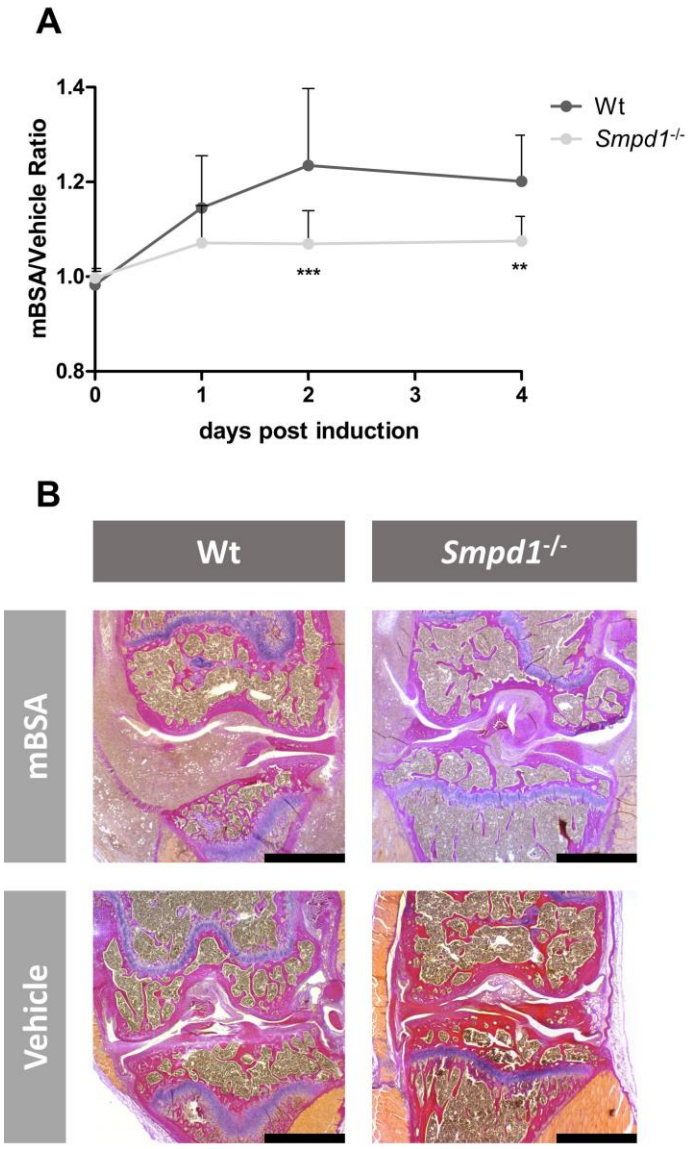

Figure 25: Acid sphingomyelinase-deficiency ameliorates experimental arthritis severity – (**A+B**) AIA was induced in *Smpd1*$^{-/-}$ mice and Wt littermates. (**A**) Joint swelling was monitored over 5 days by measuring joint diameter with a digital caliper. Data are presented as the ratio of the arthritic joint to the vehicle-injected control joint as mean ± SD of n = 9-11 mice per group. Data passed the D'Agostino & Pearson omnibus normality test and was subsequently compared by repeated measures 2-way ANOVA with Bonferroni posttests: ** $p < 0.01$; *** $p < 0.001$. (**B**) On day 4 after arthritis induction, knee joints were dissected and Masson-Goldner stained sections were prepared. Representative images of n = 4-5 mice per group are shown. Scale bar: 1 mm.

Joint swelling was monitored over a period of 5 days and was markedly reduced upon Asm-deficiency (Fig. 25A). On experimental day 4 after arthritis induction, joints were dissected and analyzed histologically. Asm-deficient mice showed reduced histopathological signs of arthritis (Fig. 28B).

Given the observed differences, the severity of arthritis in *Smpd1*$^{-/-}$ mice was analyzed further by quantification of articular pro- and anti-inflammatory cytokine levels with commercially available ELISA kits.

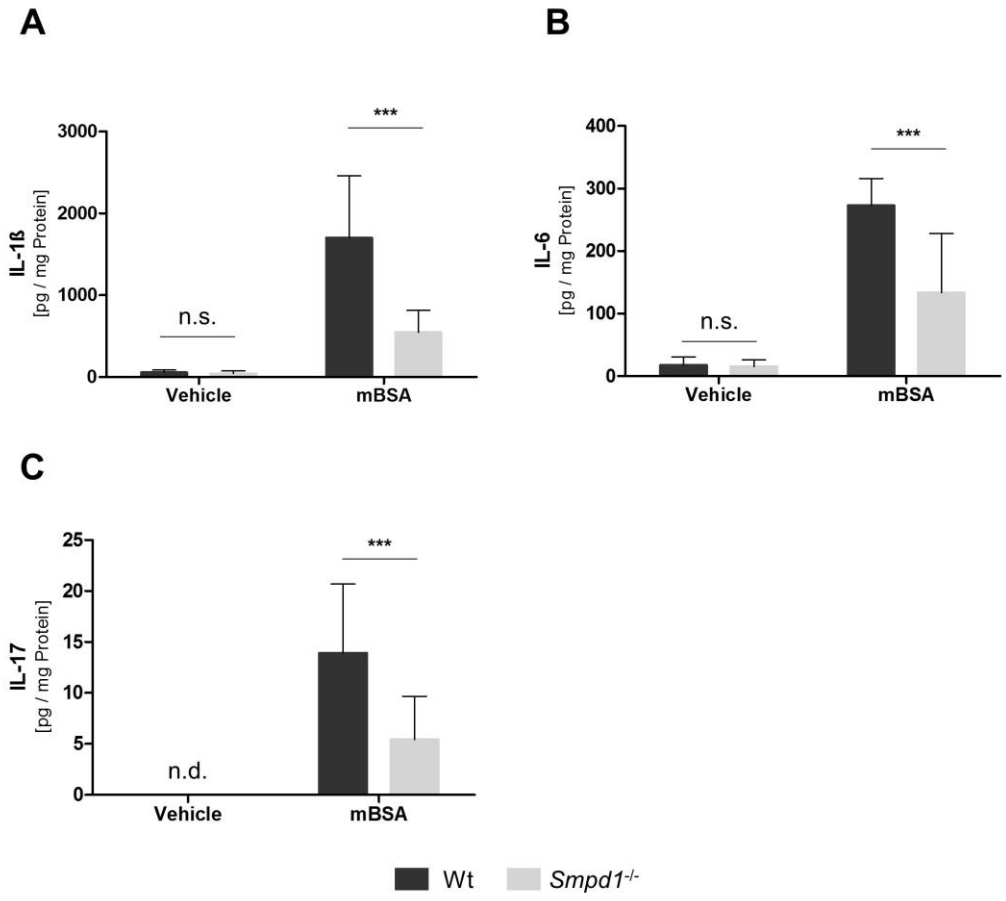

Figure 26: Reduced levels of articular pro-inflammatory cytokines upon *Smpd1* kock-out – (**A-C**) AIA was induced and on day 4 (A-C) after arthritis induction knee joints were dissected and levels of IL-1ß (**A**), IL-6 (**B**), IL-17 (**C**) were quantified by ELISA. Data are presented as the amount of the respective cytokine per mg protein ± SD of n = 9-10 mice per group. Data passed the D'Agostino & Pearson omnibus normality test and asterisks indicate significant differences as assessed by 2-way ANOVA with Bonferroni posttests: *** $p < 0.001$.

Concurrently to the histological reduction of arthritis severity, levels of the pro-inflammatory cytokines IL-1ß, IL-6 and IL-17, which mark synovial inflammation, were also significantly reduced in the arthritic joint of *Smpd1*$^{-/-}$ mice (Fig. 26A-C).

4.2.2 B- and T-Cell numbers and *in vitro* responses upon immunization are unaffected by Asm-deficiency

Reduced arthritis severity in *Smpd1*$^{-/-}$ mice could potentially result from an insufficient response to the immunization. Different lymphocyte subsets were analyzed in immunized mice to assess the efficacy of immunization in Asm-deficient mice.

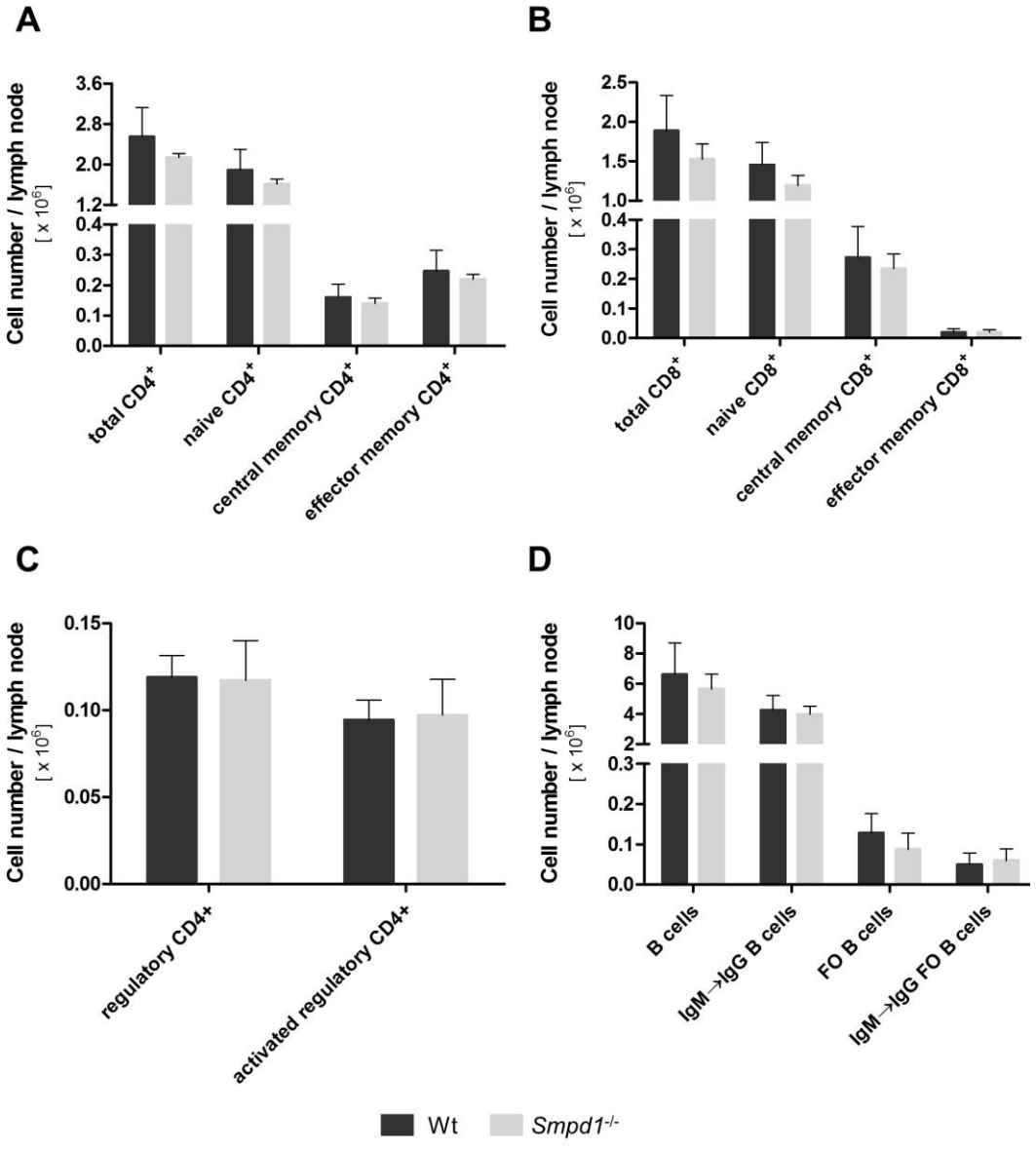

Figure 27: *Smpd1* knock-out has no effect on B- and T-Cell numbers after immunization – (**A-D**) Mice were immunized with mBSA and lymphocytes were isolated from inguinal lymph nodes on experimental day 0. Different lymphocyte subsets were analyzed by flow cytometry. Data are presented as the mean of the absolute cell numbers per lymph node of n = 4-8 mice ± SD. Significant differences were assessed by 2-way ANOVA with Bonferroni posttests, but no significant differences were detected. T-helper (**A**) and cytotoxic T-Cells (**B**) cells: Naiv: TCRbeta^{+}, CD62L^{+}, CD44^{-}; central memory: TCRbeta^{+}, CD62L^{+}, CD44^{+}; effector memory: TCRb^{+}, CD62L^{-}, CD44^{+}. Regulatory T-Cells (**C**): CD4^{+}, FoxP3^{+}; activated regulatory T-Cells: CD4^{+}, FoxP3^{+}, CD25^{+}. B cells (**D**): B220^{+}, follicular (FO) B cells: B220^{+}, CD95^{+}, Gl7^{+}; class-switched (IgM→IgG) B cells: IgM^{-}, IgG^{+}.

No differences in T helper (Fig. 27A) or T effector cell subsets (Fig. 27B) were detected in *Smpd1*$^{-/-}$ mice, including no differences in the number or activation status of regulatory T cells (Fig. 27C). Additionally, there was also no difference in the number of B cells, including follicular B cells, with a similar percentage of IgM→IgG class-switched cells (Fig. 27D).

Additionally, lymphocytes from immunized mice were isolated and re-stimulated with the mBSA-antigen *in vitro* to monitor the functional capacity of Asm-deficient lymphocytes to respond to antigen re-stimulation.

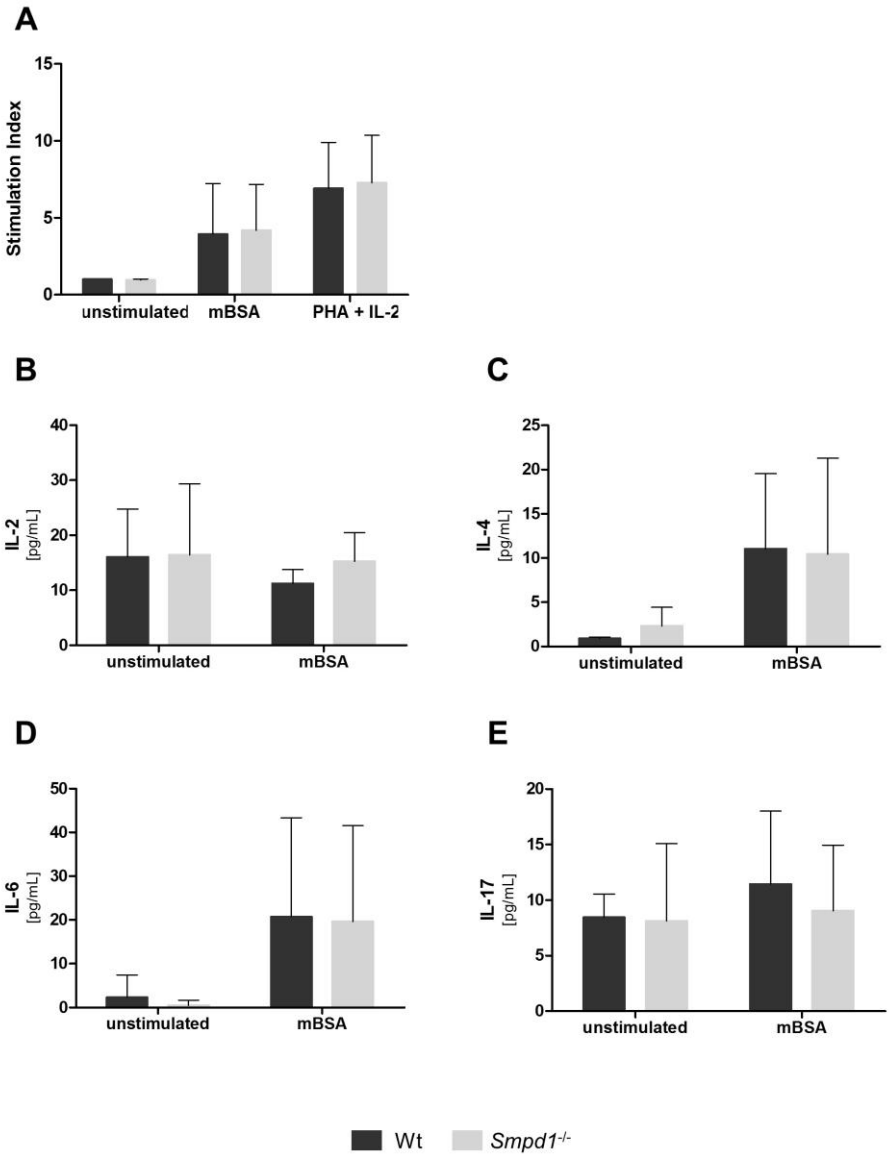

Figure 28: Functional B- and T-Cell responses to immunization are unaffected by *Smpd1* knock-out – (**A-E**) Mice were immunized with mBSA and lymphocytes were isolated from inguinal lymph nodes on experimental day 0. Lymphocyte were left untreated, re-stimulated with 1 mg/mL mBSA or stimulated with 10 µg/mL PHA and 10 U/mL IL-2 *in vitro* and proliferation (**A**) was monitored or release of IL-2 (**B**), IL-4 (**C**), IL-6 (**D**) or IL-17 (**E**) was quantified by ELISA. Given are means ± SD of n = 4-8 mice per group. No significant differences were detected by repeated measures 2-way ANOVA with Bonferroni posttests.

Concurrently to the unaltered lymphocyte distribution *in vivo* in Asm-deficient mice, the proliferation of lymphocytes in response to antigen-restimulation *in vitro* was not affected by Asm-deficiency and neither was the release of pro-inflammatory cytokines, including markers of T Cell activation, i.e. IL-2, IL-4, IL-6 and IL-17 (Fig. 28C-F).

4.2.3 Transfusion of wild-type platelets reverses protection in Asm-deficient mice

Platelets have been attributed a significant role in autoimmune inflammation. In the context of tumor metastasis, our group has previously shown that platelet-derived Asm mediates tumor cell extravasation via P-selectin, p38 MAPK and ß1-Integrin (Becker et al. 2017; Carpinteiro et al. 2015; Carpinteiro et al. 2016). All of these molecules have also been implicated in RA (Grober et al. 1993; Han et al. 1999; Laffon et al. 1991; Schett et al. 2000; Schmitt-Sody, Metz, Gottschalk, et al. 2007). Thus, any upstream effect that impacts on adhesion and extravasation of lymphocytes into the joint would be bypassed by a direct infusion of platelets, while a direct defect in platelets would not reconstitute arthritis in Asm-deficient mice. To test these hypotheses, platelets were isolated from untreated donor mice and transfused to immunized recipients two hours prior to arthritis induction. Arthritis severity was subsequently assessed by monitoring joint swelling and quantifying the levels of pro-inflammatory cytokines in the joints.

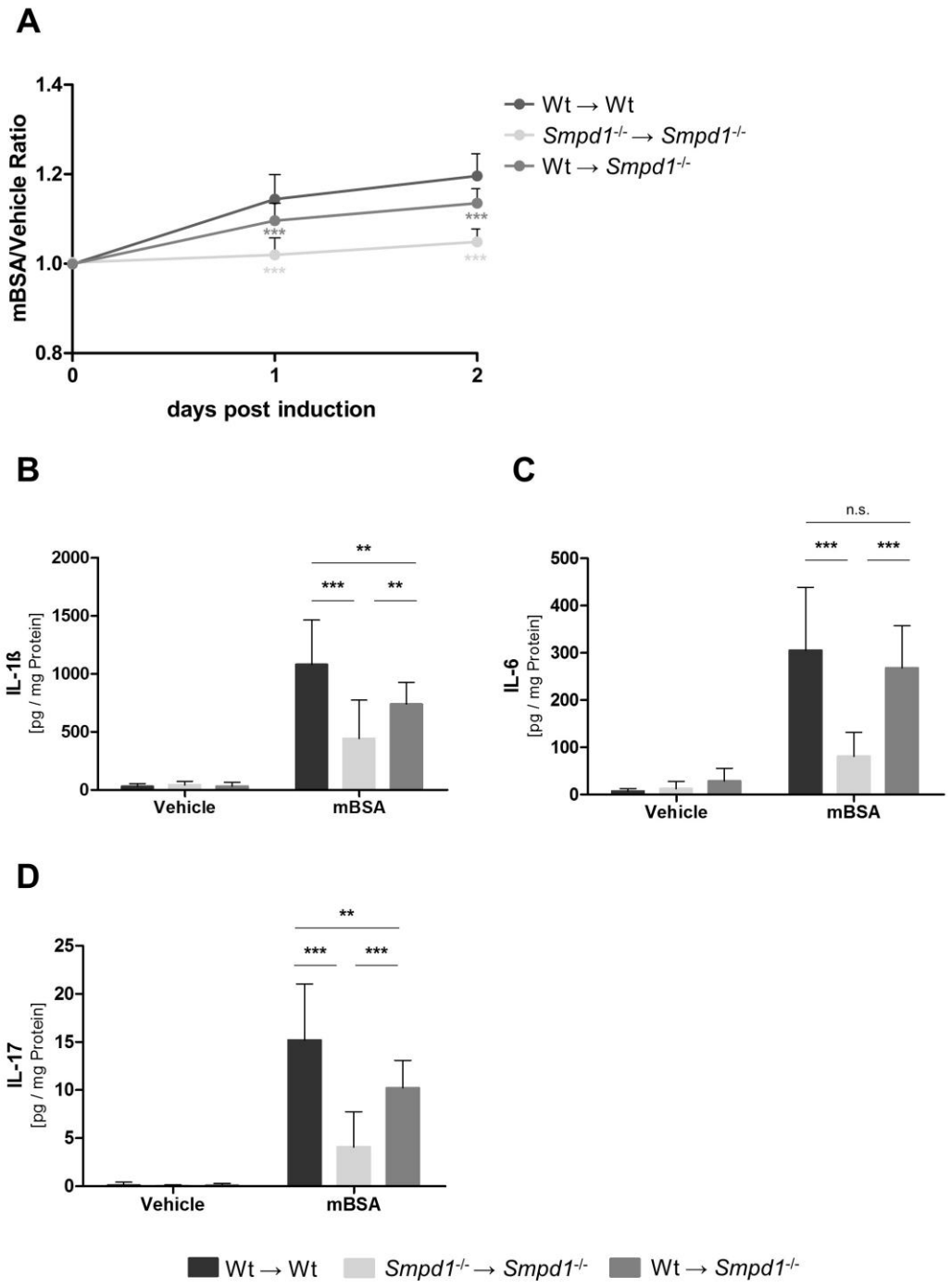

Figure 29: Transfusion of wild-type platelets reversed protection in *Smpd1* knock-out mice – (**A-D**) Immunized mice were transfused with either wild-type or *Smpd1* knock-out platelets two hours prior to arthritis induction. (**A**) Joint swelling was monitored over 3 days by measuring joint diameter with a digital caliper. Data are presented as the ratio of the arthritic joint to the vehicle-injected control joint as mean ± SD of n = 18 mice. (**B-D**) On day 2 after arthritis induction, knee joints were dissected and analyzed by ELISA for the levels of IL-1ß (**B**), IL-6 (**C**) and IL-17 (**D**). Data are presented as the amount of the respective cytokine per mg protein ± SD of n =9-11 mice after elimination of statistical outliers through Grubb's test. Asterisks indicate significant differences as assessed by 2-way ANOVA with Bonferroni posttests: ** $p < 0.01$; *** $p < 0.001$.

Transfusion of Asm-deficient platelets to *Smpd1*$^{-/-}$ mice did not alter the previously observed reduction of arthritis severity. Upon transfusion of wild-type platelets to Asm-deficient recipients, however, the protective effect of Asm-deficiency was partially lost, as seen by significantly more joint swelling (Fig. 29A) and higher levels of pro-inflammatory cytokines in the joint (Fig.29 B-D). Except for IL-6, however, joint swelling and pro-inflammatory cytokine levels were not completely reconstituted, as they still differed significantly from wild-type in wild-type transfused controls.

4.2.4 Sphingomyelinase stimulation activates ß1-Integrin

Platelet-derived Asm was shown to regulate the adhesion of melanoma cells through clustering and activation of ß1-Integrin (Carpinteiro et al. 2015). To test if this is also the case in lymphocytes, we isolated PBMCs from healthy volunteers and stimulated them with commercially available bacterial sphingomyelinase *in vitro* to induce the formation of ceramide-enriched plasma membrane platforms. The stimulation was done in the presence of the HUTS-4 anti-ß1-Integrin antibody. This clone exclusively detects ß1-Integrin molecules in the active conformation. Activation of ß1-Integrin was monitored by flow cytometry.

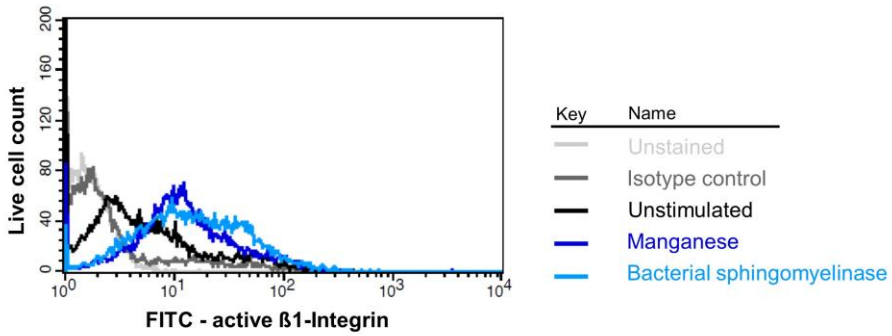

Figure 30: Sphingomyelinase-stimulation activates ß1-Integrin – PBMCs from healthy volunteers were isolated by Ficoll gradient centrifugation and were stimulated either with 10 mM Mn^{2+} or 2 U/mL bSM in the presence of an anti-active-ß1-Integrin antibody. Only live cells were considered for the analysis. A representative flow cytometrical analysis of four independent experiments is shown.

Stimulation of human PBMCs with bacterial sphingomyelinase to induce the formation of ceramide-enriched platforms, resulted in activation of ß1-Integrin to a similar extend as the known Integrin activator Mn^{2+} (Fig. 30A).

4.2.5 Pharmacological inhibition of Asm ameliorates arthritis severity

To test if the identified mechanism of platelet-Asm mediated joint inflammation could be exploited clinically, the efficacy of Amitriptyline treatment on suppressing arthritis severity in AIA was tested. For this, immunized mice were treated 4 times daily with either Amitriptyline or placebo starting two days prior to arthritis induction and continuing treatment throughout the arthritic phase. Arthritis severity was then assessed by joint swelling and articular levels of pro-inflammatory cytokines.

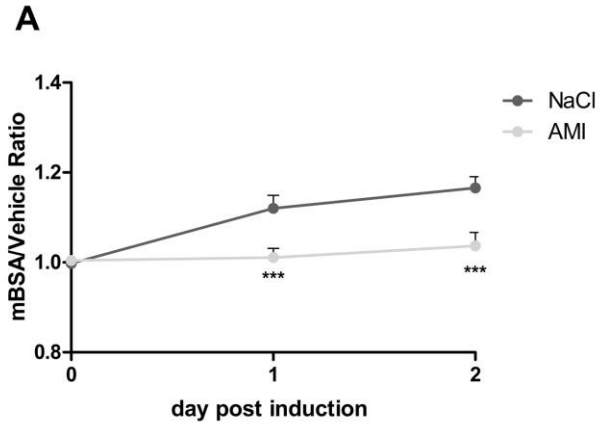

Figure 31: Pharmacological acid sphingomyelinase-inhibition ameliorates arthritis severity - (**A-D**) Immunized mice were treated with 9.375 mg/kg bodyweight Amitriptyline hydrochloride (AMI) *i.p.* every 6 hours or received placebo (NaCl). Treatment commenced two days prior to arthritis induction and was continued until the mice were sacrificed. (**A**) Joint swelling was monitored over 3 days by measuring joint diameter with a digital caliper. Data are presented as the ratio of the arthritic joint to the vehicle-injected control joint as mean ± SEM of n = 9-11 mice. Asterisks indicate significant differences as assessed by 2-way ANOVA with Bonferroni posttests: *** $p < 0.001$.

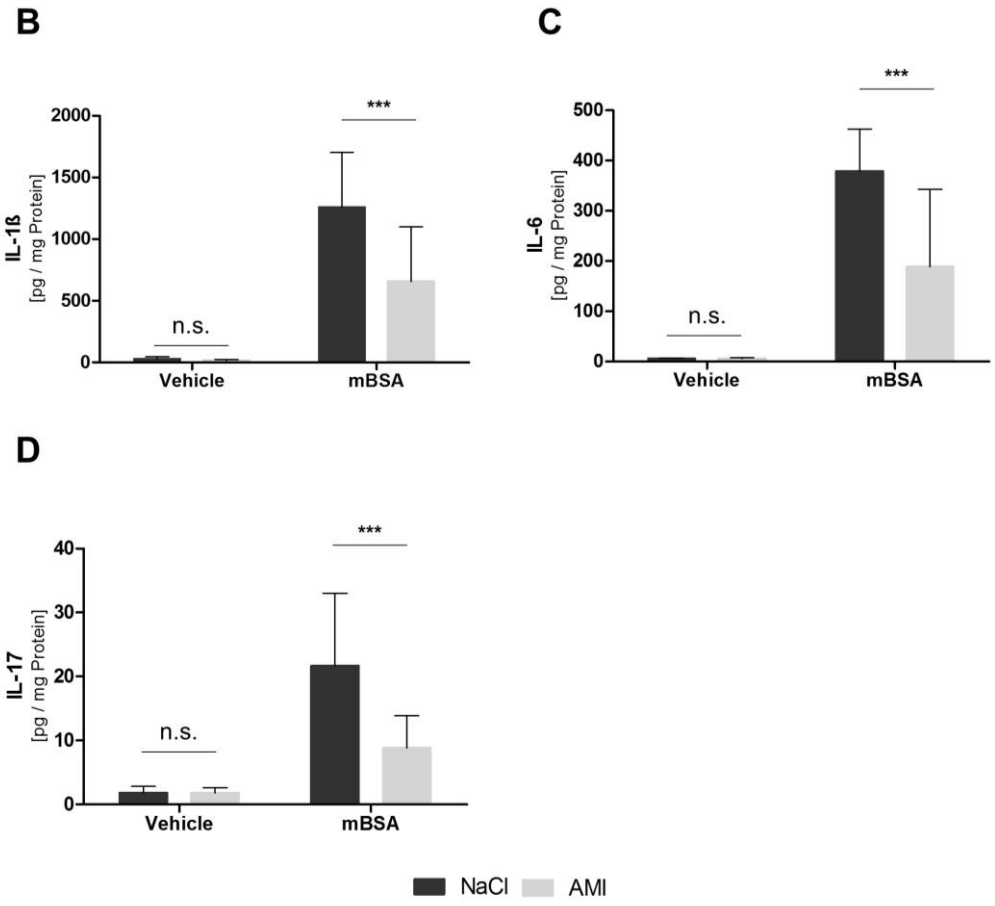

Figure 31 (continued): Pharmacological acid sphingomyelinase-inhibition ameliorates arthritis severity - (**B-D**) On day 2 after arthritis induction, knee joints were dissected and analyzed by ELISA for the levels of IL-1ß (**B**), IL-6 (**C**) and IL-17 (**D**). Data are presented as the amount of the respective cytokine per mg protein ± SEM of n = 8-11 mice. Asterisks indicate significant differences as assessed by 2-way ANOVA with Bonferroni posttests: *** $p < 0.001$.

Pharmacological inhibition of Asm resulted in a similar reduction of arthritis severity to genetic ablation of Asm, as seen both by a reduction of joint swelling (Fig. 31A) and reduced levels of pro-inflammatory cytokines in the joint (Fig. 31B-D).

4.2.6 Further studies on platelet-Asm mediated cell adhesion

As mentioned previously, my colleagues and I first identified the role of platelet-derived Asm in melanoma cell metastasis. In the melanoma model, we have analyzed the mechanism further. Through experiments with P-Selectin-deficient mice and *in vitro* experiments with P-selectin glycoprotein ligand, we could show that tumor cells interact with platelets via P-

Selectin (Becker et al. 2017). This interaction results in phosphorylation and activation of p38 MAPK in platelets, followed by secretion of Asm (Carpinteiro et al. 2016; Becker et al. 2017). Either genetic deficiency of P-Selectin or pharmacological inhibition of p38 MAPK thus resulted in a similar reduction of hematogenous metastasis as Asm-deficiency (Carpinteiro et al. 2016; Becker et al. 2017) and metastasis could be restored in P-Selectin-deficient mice by pre-incubation of the tumor cells with recombinant ASM (Becker et al. 2017). As these results are already published and were obtained in cooperation with my colleagues, they are not included in more detail in this thesis.

The identified platelet-Asm mediated cell adhesion mechanism could also play a role in other diseases. Sickle-cell disease, for instance, is a hereditary disorder caused by mutations in the beta globin gene (Ingram 1957). Polymerization of mutated hemoglobin leads to red blood cell remodeling, triggering vaso-occlusive crises prompted by adhesion of blood cells to the vascular wall (reviewed in (Conran, Franco-Penteado, and Costa 2009)). P-selectin has been implicated in this process (Ataga et al. 2017) and ASM has been suggested to be involved as well (Awojoodu et al. 2014). Therefore, we want to investigate the role of ASM in Sickle-cell disease further in the future. To gain a preliminary insight into the relevance of ASM, serum was collected from Sickle-cell disease patients and healthy volunteers and the levels of ASM activity were compared.

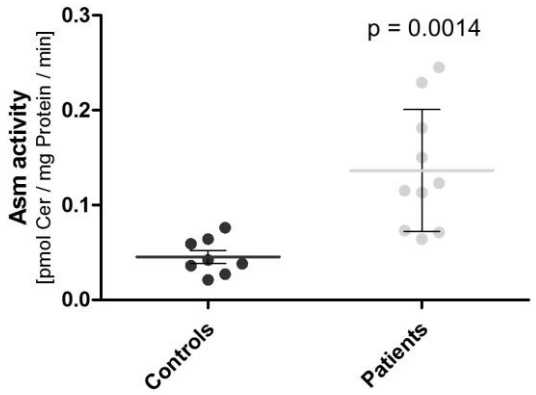

Figure 32: Serum acid sphingomyelinase activity in Sickle-cell disease – Blood was drawn and serum collected from Sickle-cell disease patients and age-matched healthy volunteers. Acid sphingomyelinase (ASM) activity in the serum was quantified using BODIPY-sphingoymelin as a substrate. The graph shows reach replicate ± SD. Data passed the D'Agostino & Pearson omnibus normality test. The indicated p-value is the result of unpaired, two-tailed Student's t-test.

Serum ASM activity was significantly higher in Sickle-cell disease patients than in healthy controls. Controls were age-matched to the Sickle-cell disease patients to avoid any potential age-dependent differences.

5. Discussion

5.1 Asm inhibition for the treatment of FD

5.1.1 Phenotypic characterization of the *Asah1* knock-out mouse

FD is a severe, genetic disorder with no cure so far. Little is known about the underlying pathologies, except that ceramide accumulates due to mutations in the *ASAH1* gene. To enable further insights into the disease and, in particular, to facilitate research into new therapies, a constitutional *Asah1* knock-out model was generated by deletion of Exon1, which encodes the signal peptide (Fig. 8A). Two single base pair mutations (Gln22His and His23Asp) in the signal peptide sequence have been previously described in FD patients (Zhang et al. 2000). This was shown to abrogate lysosomal targeting of Ac (Fig. 9). Ac has been suggested to undergo autocatalytic cleavage at acidic pH and that this maturation step is required for later activity (Shtraizent et al. 2008). Concurrently, reduced Ac activities were detected in all tested organs, with a significant reduction in the lymphoid organs and the liver (Fig. 10) and an accompanying accumulation of ceramide (Fig. 11A).

Next to the biochemical similarities between FD and our *Asah1* knock-out model, the Ac-deficient mouse line also matched the clinical phenotype of FD patients: Survival was shortened (Fig. 12B), the characteristic histiocytic infiltrates were found in several tissues (Fig. 13-16), MCP-1 levels – the putative driver of macrophage infiltration (Dworski et al. 2017) – were elevated (Fig13D-E) and synovial hyperplasia without other signs of inflammatory arthritis was observed in the joints (Fig. 14). Additionally, lung- and liver involvement – typically present in the more severe human cases – were also detected (Fig. 15-17).

The *Asah1* knock-out model thus closely mirrors the human disease. It also matches the only other mammalian model of FD – a mouse line with a point-mutation in the *Asah1* gene (Alayoubi et al. 2013). Another previously reported knock-out-model resulted in early embryonic lethality already at the four-cell stage (Eliyahu et al. 2007). In contrast to the model reported here, this model targeted the catalytic domain of Ac and thus abolished Ac activity completely. Through the deletion of Exon1, only lysosomal targeting of Ac is blocked (Fig. 9) and residual enzyme activity (Fig. 10) is apparently sufficient during embryogenesis. Residual ceramide turnover has also been reported for FD patients (Levade, Tempesta, and Salvayre 1993). The residual enzyme activity

measured with the NBD-ceramide assay may be the result of ceramide deacetylation by other enzymes: Neutral- and alkaline ceramidases 1-3 may have low activity at acidic pH. Recently, adiponectin receptors have also been suggested to have ceramidase activity (Vasiliauskaite-Brooks et al. 2017). The most likely candidate, given the acidic pH of the assay, is N-Acylethanolamine acid amidase, which has been reported to exhibit ceramidase-like activity and high sequence similarity to AC (Tsuboi et al. 2005).

Next to research into FD, the *Asah1* knock-out model also enables studies into other diseases which have been associated with increased ceramide. For instance, a similar lung inflammation as in the *Asah1*$^{-/-}$ mice has been previously reported in cystic fibrosis mice that also accumulate pulmonary ceramide (Teichgräber et al. 2008). The hepatic pathologies, such as the elevations of liver transaminases and LDH reported here, have already been linked to ceramide accumulation and even led to noninvasive hepatocellular carcinoma in a ceramide synthase 2 knock-out model (Pewzner-Jung et al. 2010). Thus, the *Asah1* knock-out model is also very relevant outside the context of FD and the assessment of Asm inhibition to target pathological ceramide accumulation potentially also has broader clinical implications (please refer to table 2 for a list of ASM/ceramide-mediated diseases).

5.1.2 New insights into the pathophysiology of Farber Disease

Next to assessing the known indicators of FD in the *Asah1* knock-out model, other parameters were also assessed to garner further insights into the pathophysiology of FD and ceramide accumulation.

Next to ceramide, total sphingomyelin and C16-sphignomyelin also accumulated, although not significantly. Nevertheless, this 3-5 fold increase is a new finding, since sphingomyelin levels have not yet been investigated in detail in FD. So far, only one report has suggested an increase in d18:2 and 24:1 sphingomyelin (Jones et al. 2014). Increased sphingomyelin levels may contribute to FD manifestations: Niemann-Pick disease type A+B are caused by sphingomyelin accumulation due to ASM deficiency and share some features with FD, including foam cell infiltration and pulmonary, hepatic and central nervous system involvement (reviewed in (Schuchman and Desnick 2017)).

Hematological manifestations of FD have been suggested in some case reports (Antonarakis et al. 1984; Fujiwaki et al. 1992; Mondal et al. 2009), but where not reported with any clear

consistency. Differential blood counts of Ac-deficient mice showed a reduction in white blood cells, a trend toward reduced platelet numbers and increased red blood cell number with reduced mean corpuscular hemoglobin concentration (Fig. 18). The reduction of white blood cells both matches and contrasts reports from the *Asah1* point mutation model: Initially, significant elevations of peripheral blood leukocytes were reported (Alayoubi et al. 2013), but a later study detailed perturbed hematopoiesis in Ac-deficient mice due to damage to the stem cell niche by foam cells (Dworski et al. 2015). The changes to the red blood cell count and erythrocyte indices observed in our model require further studies. Despite the normal hemoglobin levels, these changes may reflect an imbalance of cellular iron distribution as the result of chronic disease.

The observed elevation of CPK levels (Fig. 19) fits well with reports of CPK elevation in spinal muscular atrophy patients (Rudnik-Schoneborn et al. 1998) as mutations in the *ASAH1* gene have not only been reported in FD, but also in spinal muscular atrophy (Dyment et al. 2014; Filosto et al. 2016; Gan et al. 2015; Zhou et al. 2012) and a subset of patients suffer from both FD and spinal muscular atrophy (Teoh et al. 2016). Ac-deficient mice also showed some indicators of muscular dystrophy (progressive waisting, scoliosis, waddling gate). The data indicates that determination of CPK levels in FD patients may be a useful biomarker for the disease in order to help to distinguish FD from juvenile idiopathic arthritis, for which FD is commonly misdiagnosed (Sólyom et al. 2014; Torcoletti et al. 2014).

The failure of Ac-deficient mice to thrive and their progressive waisting (Fig. 11A) match reports that FD patients also have poor weight gain (Moser 2001). To gain further insight, a metabolic analysis was conducted. Serum glucose levels were significantly decreased in *Asah1*$^{-/-}$ mice and seemed to decline progressively (Fig. 20A). Insulin levels could not be reported, because they remained below the detection limit of the assay. Thus, while an over-production of Insulin cannot be excluded as the cause of the observed hypoglycemia in FD mice, it seems unlikely. As decreased glucose levels might also be the result of reduced food intake and starvation, levels of the ketone body ß-hydroxybutyrate were analyzed in the urine. Ketonuria occurs when the body uses fat as an energy source rather than carbohydrates, e.g. during starvation or in type I diabetes mellitus. Ac-deficient mice, however, showed no signs of ketonuria (Fig. 20B), arguing against that.

Interestingly, we found that Ac-deficient mice loose significantly more glucose in the urine than their Wt littermates (Fig. 21D). This did not appear to be the result of a general filtration

defect, since *Asah1*$^{-/-}$ mice showed no histopathological signs of renal disease (Fig. 21A) and urinary protein excretion was reduced rather than elevated (Fig. 21C).

A plausible scenario for the reduction of blood glucose in combination with the loss of glucose through the urine in the absence of a general filtration defect would be a specific impairment of intestinal glucose uptake and renal glucose reabsorption. Both are mediated by sodium-glucose linked transporters (SGLT). These are secondary active transporters, meaning that they are dependent on the sodium-potassium adenosine triphosphatase (Na^+/K^+-ATPase) driven sodium gradient. Increased ceramide levels could interfere either with the function of SGLT proteins or with the function of Na^+/K^+-ATPase through alteration of their lipid environment, in a similar mechanism to the previously reported ceramide-mediated inhibition of the potassium channel Kv1.3 (Bock et al. 2003). This would inhibit glucose uptake and reabsorption. Alternatively, or in combination to this, ceramide might also downregulate the expression of nutrient transporters, as has been suggested by a previous *in vitro* study (Guenther et al. 2008).

We plan to investigate the role of ceramide in glucose uptake and reabsorption further in the future. If ceramide accumulation indeed impairs glucose uptake, patients might benefit from a diet with a high content of membrane-permeant energy sources, e.g. methyl pyruvate, by improving their general constitution and resistance.

Given that indicators of kidney function were altered upon Ac-deficiency (Fig. 21A), however, further studies into the effects of ceramide accumulation in the kidneys are also necessary. For instance, it is currently unclear whether BUN levels are increased due to renal dysfunction or as the result of the reported liver disease (Fig. 16-17).

5.1.3 Effects of Asm-inhibition on Farber Disease manifestations

Having established the usefulness of the *Asah1* knock-out mouse line as a model of FD, a rescue study was conducted to assess the suitability of Asm depletion as a new treatment strategy for FD. For this, the Ac-deficient line was cross-bred to an Asm-deficient mouse line. Genetic ablation of Asm significantly blunted ceramide accumulation in Ac-deficient mice (Fig. 11), resulting in improved weight gain and survival (Fig. 12). Histiocytic infiltrations were also significantly reduced or completely absent in the double-deficient mice in all organs except for the lung and liver (Fig. 13-16). Liver fibrosis, however, was successfully reduced by Asm-deficiency (Fig. 16). Clinical chemistry analysis also showed marked improvements

in liver parameters (Fig. 17), blood count (Fig. 18), CPK levels (Fig. 19), serum glucose (Fig. 20A) and kidney indices (Fig. 21). Heterozygous depletion had only limited success: Most parameters improved somewhat, e.g. particularly liver transaminases (Fig. 17) and CPK levels (Fig. 19), but the median survival time could only be improved by a few days (Fig. 12B).

Despite the significantly enhanced survival time of Ac- and Asm-double deficient mice and the beneficial effect on most FD manifestations, pharmacological inhibition of Asm was unsuccessful: Juvenile Ac-deficient mice died within a few days of Amitriptyline treatment, thus even significantly shortening the survival time of Ac-deficient mice (Fig. 22). Treatment with Amitritpyline throughout development had similar outcomes (Fig. 23). Amitriptyline seems to have a toxic effect specifically in Ac-deficient mice, as vehicle treatment or treatment of wild-type littermates had no adverse effects (Fig. 22-23). Potentially, this toxicity arises from suppression of residual Ac activity in Ac-deficient mice: Amitriptyline functionally inhibits Asm by interfering with Asm-membrane binding (Kornhuber et al. 2008). Ac also has to attach to the inner lysosomal membrane and even exists in a complex with Asm (He et al. 2003). It could thus be displaced from the lysosomal membrane by Amitriptyline in the same fashion as Asm. Another tricyclic antidepressant and functional inhibitor of ASM – Desipramine – has already been reported to co-inhibit AC in this manner (Elojeimy et al. 2006). Given that lysosomal targeting of Ac is disrupted Ac-deficient mice, however, the open question is how such a co-inhibition would be possible. Putatively, small amounts of the mislocated enzyme could be secreted and taken up by endocytosis, thus being delivered to the lysosomes. Cell culture experiments with conditioned medium support such a cross-correction effect (data not shown), as well as the residual Ac activity detected in organs of Ac-deficient mice (Fig. 10) and the reported successes of allogenic stem cell transplantation on FD manifestations (Ehlert et al. 2006; Torcoletti et al. 2014). A cross-correction effect would also help to explain why our knock-out model is not embryonic lethal, whereas a previously reported model lacking the catalytic domain could not survive past the four-cell stage (Eliyahu et al. 2007).

Another possible explanation is that the existing damage from FD manifestations, particularly in the liver (Fig. 16-17) and putatively also in the heart (Fig. 19), sensitize Ac-deficient mice to the toxic side effects of Amitriptyline. Adverse effects of Amitriptyline are known to include liver injury (Voican et al. 2014) and cardiotoxicity (Sari et al. 2011). Thus, Ac-deficient mice may be more susceptible to Amitriptyline poisoning.

Alternatively, altering sphingolipid metabolism after immense amounts of ceramide have already accumulated might trigger a toxic surge of redistribution to other sphingolipids. This was the rationale for treating one group with Amitriptyline throughout development, since this should have prevented ceramide accumulation in the first place. As Amitriptyline has been reported to cross the placenta (Heikkinen, Ekblad, and Laine 2001) and to be present in breast milk (Yoshida et al. 1997) upon treatment of the mothers, such an approach should have been feasible. As FD diagnosis is possible prenatally (Fensom et al. 1979), such a treatment regimen could at least potentially also be translated clinically. However, treatment throughout development had a similar effect to the treatment of juvenile Ac-deficient mice: Both groups died around the time that they were weaned/received Amitriptyline directly. Therefore, the extent of Asm inhibition was assessed in the group treated throughout development, but no reduction in Asm activity could be observed, although adult animals treated with the same dose showed an approximately 80 % reduction. In conclusion, Amitriptyline treatment could potentially be beneficial for the treatment of Farber Disease, if it was supplied in sufficient doses and before too much ceramide has accumulated. However, the results obtained in this study strongly caution against the use of any tricyclic antidepressants and other functional inhibitors of ASM in FD patients, given the previously undescribed toxicity of these compounds upon Ac-deficiency.

5.2 Asm inhibition for the treatment of RA

RA is a chronic autoinflammatory disorder with a high socioeconomic impact. Despite several symptomatic treatments, RA often progresses to disability and new treatment strategies are in high demand. This study newly identifies Asm as a key player in joint inflammation and introduces ASM as a new druggable target in RA. The role of Asm in joint inflammation was assessed with the murine antigen-induced arthritis model. Asm-deficient mice showed reduced arthritis severity (Fig. 25-26). A possible mechanism that explains the protection of Asm-deficient mice against arthritis could be lack of platelet activation and release of Asm from platelets upon contact with lymphocytes, preventing clustering of ß1-Integrin on lymphocytes and thereby extravasation. This potential mechanism is graphically summarized below.

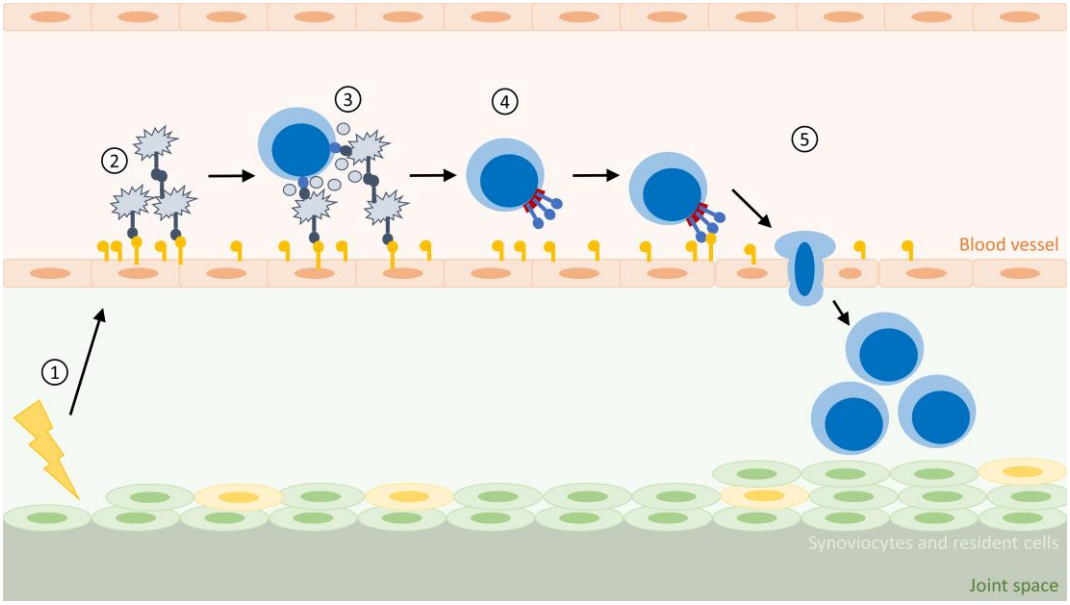

Figure 33: Proposed mechanism for regulation of arthritis severity by acid sphingomyelinase - An initiating event damages the joint (1). As a result, the endothelium is activated and recruits platelets (2). These then interact with circulating lymphocytes via release of Asm (3). Through the subsequent formation of ceramide-enriched platforms on the lymphocytes, ß1-Integrin is activated (4), enabling lymphocyte-adhesion to the activated endothelium and infiltration into the damaged joint (5).

The first steps of the proposed model (endothelial activation and platelet accumulation upon joint damage) have been reported previously (Schmitt-Sody, Metz, Klose, et al. 2007; Schmitt-Sody, Metz, Gottschalk, et al. 2007). The following steps – Asm release by platelets and subsequent cell extravasation – are new in the context of lymphocytes, but appear to be essentially identical to the mechanism my colleagues and I have previously described for melanoma metastasis (Becker et al. 2017; Carpinteiro et al. 2015; Carpinteiro et al. 2016). Unfortunately, it was not possible to investigate the activation status of ß1-Integrin on murine lymphocytes directly in the antigen-induced arthritis model, since no activation-specific antibody against murine ß1-Integrin is available. Instead, ß1-Integrin activation was analyzed in human PBMCs with the activation-specific anti-human ß1-Integrin antibody (clone HUTS-4). With the help of this antibody, sphingomyelinase-stimulation was shown to activate ß1-Integrin on lymphocytes (Fig. 30). Previous report show that sphingomyelinase-stimulation results in the formation of ceramide-enriched plasma membrane platforms and that these cluster ß1-Integrin molecules – a pre-requisite for integrin activation (Carpinteiro et al. 2015). The mechanistic details of ß1-Integrin activation upon sphingomyelinase-stimulation still require further definition: It is currently unclear whether ceramide only mediates the clustering of ß1-Integrin molecules and their activation is achieved through distinct signaling

pathways, or whether the interaction with ceramide modifies the conformation of ß1-Integrin directly and thereby results in activation.

Another possible explanation of the findings reported here would be any defect in Asm-deficient lymphocytes or lymphocyte stimulation that result in ß1-Integrin activation and/or prevents adhesion and/or emigration of lymphocytes *in vivo*. These upstream steps could potentially be bypassed by transfusion of pre-activated wild-type platelets into Asm-deficient mice, allowing the development of arthritis in Asm-deficient mice non-specifically. Further, arthritis could not be restored completely to Asm-deficient mice upon transfusion of Wt platelets (Fig. 29), which might indicate additional functions of Asm, for instance for emigration into the tissue. It may also reflect a technical problem due to incomplete reconstitution of platelet functions, because approximately 55 % of host platelets remain after transfusion (Carpinteiro et al. 2015). Thus, slightly more than half of all present platelets are still Asm-deficient and cannot release Asm to recruit lymphocytes to the joints.

It is also possible, however, that further endothelial and/or synovial Asm-effects are at play, which are not reconstituted upon Wt-platelet transfusion. A functional defect in Asm-deficient lymphocytes as the cause, however, seems improbable due to the results obtained here, as both proliferative and functional responses to the immunization antigen were unaffected by *Smpd1* knock-out (Fig. 28) and T- and B-cell populations did not differ between Wt- and *Smpd1*$^{-/-}$ mice in response to immunization (Fig. 27). The frequency of regulatory T cells was also not altered, which seems to contrast a previous study by Hollmann et al., which reported an increase of regulatory T cells in *Smpd1*$^{-/-}$ mice (Hollmann et al. 2016). Whereas the Hollmann-study analyzed untreated mice, this study considered only immunized mice, thus indicating that the immunization is a stimulus strong enough to overcome these baseline differences.

The data presented here also apparently contrast another study that reported a role of ASM in modulating T-helper cell responses (Bai et al. 2015). However, only FIASMAs were employed in this study, which can have diverse additional off-target effects (Glowinski and Axelrod 1964; Jang et al. 2009; Owens et al. 1997), including effects on different ion channels (Arita et al. 1987; Pancrazio et al. 1998; Park et al. 1998; Punke and Friederich 2007; Schofield et al. 1981; Wooltorton and Mathie 1995) and the induction and degradation of other lysosomal enzymes (Elojeimy et al. 2006). Importantly, exogeneous ceramide failed to rescue T-helper cells from ASM-inhibition in the Bai-study, arguing against a specific Asm-dependent effect in the regulation of T-helper cell responses (Bai et al. 2015).

Regarding platelets, reports concerning the role of Asm in platelet-degranulation vary. In their previous metastasis-experiments, my colleagues have observed no impairments in platelet-aggregometrical properties upon Asm-deficiency (Carpinteiro et al. 2015). One study, however, notes some changes in platelet function upon Asm-deficiency, including blunted ATP release, P-Selectin- and phosphatidylserine exposure and thrombin generation (Munzer et al. 2014). Functional properties like platelet αIIß3 activation and aggregation, activation-dependent Ca^{2+}-flux and bleeding time were not affected (Munzer et al. 2014). Therefore, it cannot be completely excluded that activation-dependent platelet functions are perturbed by *Smpd1* knock-out. Even if Asm-deficiency would cause a defect in classical platelet function, however, it is unclear how relevant this would be in this context, given that inhibitors of classical platelet functions do not ameliorate arthritis severity (Boilard et al. 2011; Boilard et al. 2010; Forrest et al. 2006; Garcia et al. 2011). Platelet-depletion, on the other hand, does (Boilard et al. 2010). Thus, it appears that platelet-activation in RA involves a mechanism that is distinct from the typical thrombosis pathway. The suppression of arthritis severity upon Asm-deficiency and Amitriptyline-treatment and the lack of arthritis reconstitution upon transfusion of Asm-deficient platelets to Asm-deficient mice reported in this study, suggests that release of Asm by platelets is this new mechanism. However, further studies are necessary to strengthen this hypothesis, i.e. a demonstration of Asm secretion by platelets, clustering and activation of ß1-Integrin on lymphocytes and enhanced adhesion of lymphocytes upon platelet and lymphocyte co-incubation. These studies will also help to distinguish whether the suggested hypothesis concerning Asm secretion by platelets is indeed the determinant of arthritis severity, or if arthritis severity is instead ameliorated by a defect in Asm-deficient lymphocyte or lymphocyte stimulation in Asm-deficient mice that results in ß1-Integrin activation and/or prevents adhesion and/or emigration of lymphocytes *in vivo*.

Given the findings of the present studies, ASM inhibition is an attractive new target for the treatment of RA in humans. FIASMAs have been clinically used for decades and are quite save and well suited for long-term therapy – a definite benefit compared to GCs, for instance, which should only be administered for the shortest possible time due to the potentially severe adverse effects (Saag 1997; van der Goes et al. 2010). The toxicity and tolerability of the current gold standard of care – MTX – also leaves a lot to be desired, given that the incidence rate of severe adverse events is up to 3-5 % and given its additional abortifacient and teratogenic properties (Zitnik and Cooper 1990). While new biological agents for the treatment of RA are making progress on their way into the clinic, these new treatments – if they are successful - will be quite expensive and their administration may also require *i.v.*

injections (e.g. Rituximab). Thus, Amitriptyline or other FIASMAs do not only have the advantage of being well tolerated, but are also easy to administer and inexpensive.

ASM inhibition may not only benefit RA patients, but also patients suffering from other chronic (auto-)inflammatory diseases, as the putative mechanism reported here is not joint-specific, but rather affects lymphocyte recruitment in general. Thus, future applications of FIASMAs could potentially also include diseases such as multiple sclerosis, psoriasis or inflammatory bowel disease. Moreover, the preliminary data on Sickle cell disease (Fig. 32) indicates that even some non-inflammatory diseases involving cell adhesion might be new targets for ASM inhibition.

References

Adams, C., V. Icheva, C. Deppisch, J. Lauer, G. Herrmann, U. Graepler-Mainka, S. Heyder, E. Gulbins, and J. Riethmueller. 2016. 'Long-Term Pulmonal Therapy of Cystic Fibrosis-Patients with Amitriptyline', *Cell Physiol Biochem*, 39: 565-72.

Alayoubi, A. M., J. C. Wang, B. C. Au, S. Carpentier, V. Garcia, S. Dworski, S. El-Ghamrasni, K. N. Kirouac, M. J. Exertier, Z. J. Xiong, G. G. Prive, C. M. Simonaro, J. Casas, G. Fabrias, E. H. Schuchman, P. V. Turner, R. Hakem, T. Levade, and J. A. Medin. 2013. 'Systemic ceramide accumulation leads to severe and varied pathological consequences', *EMBO Mol Med*, 5: 827-42.

Antonarakis, S. E., D. Valle, H. W. Moser, A. Moser, S. J. Qualman, and W. H. Zinkham. 1984. 'Phenotypic variability in siblings with Farber disease', *J Pediatr*, 104: 406-9.

Arenz, C. 2010. 'Small molecule inhibitors of acid sphingomyelinase', *Cell Physiol Biochem*, 26: 1-8.

Arita, M., A. Wada, H. Takara, and F. Izumi. 1987. 'Inhibition of 22Na influx by tricyclic and tetracyclic antidepressants and binding of [3H]imipramine in bovine adrenal medullary cells', *J Pharmacol Exp Ther*, 243: 342-8.

Ataga, K. I., A. Kutlar, J. Kanter, D. Liles, R. Cancado, J. Friedrisch, T. H. Guthrie, J. Knight-Madden, O. A. Alvarez, V. R. Gordeuk, S. Gualandro, M. P. Colella, W. R. Smith, S. A. Rollins, J. W. Stocker, and R. P. Rother. 2017. 'Crizanlizumab for the Prevention of Pain Crises in Sickle Cell Disease', *N Engl J Med*, 376: 429-39.

Awojoodu, A. O., P. M. Keegan, A. R. Lane, Y. Zhang, K. R. Lynch, M. O. Platt, and E. A. Botchwey. 2014. 'Acid sphingomyelinase is activated in sickle cell erythrocytes and contributes to inflammatory microparticle generation in SCD', *Blood*, 124: 1941-50.

Azuma, N., J. S. O'Brien, H. W. Moser, and Y. Kishimoto. 1994. 'Stimulation of acid ceramidase activity by saposin D', *Arch Biochem Biophys*, 311: 354-7.

Bai, A., E. Kokkotou, Y. Zheng, and S. C. Robson. 2015. 'Role of acid sphingomyelinase bioactivity in human CD4+ T-cell activation and immune responses', *Cell Death Dis*, 6: e1828.

Bao, X. H., J. M. Tian, T. Y. Ji, and X. Z. Chang. 2017. '[A case report of childhood Farber's disease and literature review]', *Zhonghua Er Ke Za Zhi*, 55: 54-58.

Bauer, J., G. Liebisch, C. Hofmann, C. Huy, G. Schmitz, F. Obermeier, and J. Bock. 2009. 'Lipid alterations in experimental murine colitis: role of ceramide and imipramine for matrix metalloproteinase-1 expression', *PLoS One*, 4: e7197.

Becker, K. A., N. Beckmann, C. Adams, G. Hessler, M. Kramer, E. Gulbins, and A. Carpinteiro. 2017. 'Melanoma cell metastasis via P-selectin-mediated activation of acid sphingomyelinase in platelets', *Clin Exp Metastasis*, 34: 25-35.

Beckmann, N., D. Sharma, E. Gulbins, K. A. Becker, and B. Edelmann. 2014. 'Inhibition of acid sphingomyelinase by tricyclic antidepressants and analogons', *Front Physiol*, 5: 331.

Beckmann, Nadine, Erich Gulbins, Katrin Anne Becker, and Alexander Carpinteiro. 2017. 'Sphingomyelinase, Acidic.' in Sangdun Choi (ed.), *Encyclopedia of Signaling Molecules* (Springer New York: New York, NY).

Ben-Yoseph, Y., R. Gagne, M. R. Parvathy, D. A. Mitchell, and T. Momoi. 1989. 'Leukocyte and plasma N-laurylsphingosine deacylase (ceramidase) in Farber disease', *Clin Genet*, 36: 38-42.

Bock, J., I. Szabo, N. Gamper, C. Adams, and E. Gulbins. 2003. 'Ceramide inhibits the potassium channel Kv1.3 by the formation of membrane platforms', *Biochem Biophys Res Commun*, 305: 890-7.

Boilard, E., K. Larabee, R. Shnayder, K. Jacobs, R. W. Farndale, J. Ware, and D. M. Lee. 2011. 'Platelets participate in synovitis via Cox-1-dependent synthesis of prostacyclin independently of microparticle generation', *J Immunol*, 186: 4361-6.

Boilard, E., P. A. Nigrovic, K. Larabee, G. F. Watts, J. S. Coblyn, M. E. Weinblatt, E. M. Massarotti, E. Remold-O'Donnell, R. W. Farndale, J. Ware, and D. M. Lee. 2010. 'Platelets amplify inflammation in arthritis via collagen-dependent microparticle production', *Science*, 327: 580-3.

Brady, R. O., J. N. Kanfer, M. B. Mock, and D. S. Fredrickson. 1966. 'The metabolism of sphingomyelin. II. Evidence of an enzymatic deficiency in Niemann-Pick diseae', *Proc Natl Acad Sci U S A*, 55: 366-9.

Brown, D. A., and E. London. 1998. 'Functions of lipid rafts in biological membranes', *Annu Rev Cell Dev Biol*, 14: 111-36.

Burrage, P. S., K. S. Mix, and C. E. Brinckerhoff. 2006. 'Matrix metalloproteinases: role in arthritis', *Front Biosci*, 11: 529-43.

Carpinteiro, A., K. A. Becker, L. Japtok, G. Hessler, S. Keitsch, M. Požgajova, K. W. Schmid, C. Adams, S. Müller, B. Kleuser, M. J. Edwards, H. Grassmé, I. Helfrich, and E. Gulbins. 2015. 'Regulation of hematogenous tumor metastasis by acid sphingomyelinase', *EMBO Mol Med*, 7: 714-34.

Carpinteiro, A., N. Beckmann, A. Seitz, G. Hessler, B. Wilker, M. Soddemann, I. Helfrich, B. Edelmann, E. Gulbins, and K. A. Becker. 2016. 'Role of Acid Sphingomyelinase-Induced Signaling in Melanoma Cells for Hematogenous Tumor Metastasis', *Cell Physiol Biochem*, 38: 1-14.

Case, J. P. 2001. 'Old and new drugs used in rheumatoid arthritis: a historical perspective. Part 2: the newer drugs and drug strategies', *Am J Ther*, 8: 163-79.

Chang, B. Y., M. M. Huang, M. Francesco, J. Chen, J. Sokolove, P. Magadala, W. H. Robinson, and J. J. Buggy. 2011. 'The Bruton tyrosine kinase inhibitor PCI-32765 ameliorates autoimmune arthritis by inhibition of multiple effector cells', *Arthritis Res Ther*, 13: R115.

Cohen, S., E. Hurd, J. Cush, M. Schiff, M. E. Weinblatt, L. W. Moreland, J. Kremer, M. B. Bear, W. J. Rich, and D. McCabe. 2002. 'Treatment of rheumatoid arthritis with anakinra, a recombinant human interleukin-1 receptor antagonist, in combination with methotrexate: results of a twenty-four-week, multicenter, randomized, double-blind, placebo-controlled trial', *Arthritis Rheum*, 46: 614-24.

Cojocaru, M., I. M. Cojocaru, I. Silosi, C. D. Vrabie, and R. Tanasescu. 2010. 'Extra-articular Manifestations in Rheumatoid Arthritis', *Maedica (Buchar)*, 5: 286-91.

Conran, N., C. F. Franco-Penteado, and F. F. Costa. 2009. 'Newer aspects of the pathophysiology of sickle cell disease vaso-occlusion', *Hemoglobin*, 33: 1-16.

Daniel, W. A., and J. Wojcikowski. 1997. 'Contribution of lysosomal trapping to the total tissue uptake of psychotropic drugs', *Pharmacol Toxicol*, 80: 62-8.

Danis, V. A., G. M. Franic, D. A. Rathjen, R. M. Laurent, and P. M. Brooks. 1992. 'Circulating cytokine levels in patients with rheumatoid arthritis: results of a double blind trial with sulphasalazine', *Ann Rheum Dis*, 51: 946-50.

Darroch, P. I., A. Dagan, T. Granot, X. He, S. Gatt, and E. H. Schuchman. 2005. 'A lipid analogue that inhibits sphingomyelin hydrolysis and synthesis, increases ceramide, and leads to cell death', *J Lipid Res*, 46: 2315-24.

Dayer, J. M., and E. Choy. 2010. 'Therapeutic targets in rheumatoid arthritis: the interleukin-6 receptor', *Rheumatology (Oxford)*, 49: 15-24.

Dhawan, S. S., and A. A. Quyyumi. 2008. 'Rheumatoid arthritis and cardiovascular disease', *Curr Atheroscler Rep*, 10: 128-33.

Dulaney, J. T., A. Milunsky, J. B. Sidbury, N. Hobolth, and H. W. Moser. 1976. 'Diagnosis of lipogranulomatosis (Farber disease) by use of cultured fibroblasts', *J Pediatr*, 89: 59-61.

Dworski, S., A. Berger, C. Furlonger, J. M. Moreau, M. Yoshimitsu, J. Trentadue, B. C. Au, C. J. Paige, and J. A. Medin. 2015. 'Markedly perturbed hematopoiesis in acid ceramidase deficient mice', *Haematologica*, 100: e162-5.

Dworski, S., P. Lu, A. Khan, B. Maranda, J. J. Mitchell, R. Parini, M. Di Rocco, B. Hugle, M. Yoshimitsu, B. Magnusson, B. Makay, N. Arslan, N. Guelbert, K. Ehlert, A. Jarisch, J. Gardner-Medwin, R. Dagher, M. T. Terreri, C. M. Lorenco, L. Barillas-Arias, P. Tanpaiboon, A. Solyom, J. S. Norris, X. He, E. H. Schuchman, T. Levade, and J. A. Medin. 2017. 'Acid Ceramidase Deficiency is characterized by a unique plasma cytokine and ceramide profile that is altered by therapy', *Biochim Biophys Acta*, 1863: 386-94.

Dyment, D. A., E. Sell, M. R. Vanstone, A. C. Smith, D. Garandeau, V. Garcia, S. Carpentier, E. Le Trionnaire, F. Sabourdy, C. L. Beaulieu, J. A. Schwartzentruber, H. J. McMillan, J. Majewski, D.

E. Bulman, T. Levade, and K. M. Boycott. 2014. 'Evidence for clinical, genetic and biochemical variability in spinal muscular atrophy with progressive myoclonic epilepsy', *Clin Genet*, 86: 558-63.

Edelmann, B., U. Bertsch, V. Tchikov, S. Winoto-Morbach, C. Perrotta, M. Jakob, S. Adam-Klages, D. Kabelitz, and S. Schütze. 2011. 'Caspase-8 and caspase-7 sequentially mediate proteolytic activation of acid sphingomyelinase in TNF-R1 receptosomes', *Embo j*, 30: 379-94.

Edwards, J. C., L. Szczepanski, J. Szechinski, A. Filipowicz-Sosnowska, P. Emery, D. R. Close, R. M. Stevens, and T. Shaw. 2004. 'Efficacy of B-cell-targeted therapy with rituximab in patients with rheumatoid arthritis', *N Engl J Med*, 350: 2572-81.

Ehlert, K., J. Roth, M. Frosch, N. Fehse, N. Zander, and J. Vormoor. 2006. 'Farber's disease without central nervous system involvement: bone-marrow transplantation provides a promising new approach', *Ann Rheum Dis*, 65: 1665-6.

Eliyahu, E., J. H. Park, N. Shtraizent, X. He, and E. H. Schuchman. 2007. 'Acid ceramidase is a novel factor required for early embryo survival', *Faseb j*, 21: 1403-9.

Elliott, M. J., R. N. Maini, M. Feldmann, A. Long-Fox, P. Charles, P. Katsikis, F. M. Brennan, J. Walker, H. Bijl, J. Ghrayeb, and et al. 1993. 'Treatment of rheumatoid arthritis with chimeric monoclonal antibodies to tumor necrosis factor alpha', *Arthritis Rheum*, 36: 1681-90.

Elojeimy, S., D. H. Holman, X. Liu, A. El-Zawahry, M. Villani, J. C. Cheng, A. Mahdy, Y. Zeidan, A. Bielwaska, Y. A. Hannun, and J. S. Norris. 2006. 'New insights on the use of desipramine as an inhibitor for acid ceramidase', *FEBS Lett*, 580: 4751-6.

Faarvang, K. L., C. Egsmose, P. Kryger, J. Podenphant, M. Ingeman-Nielsen, and T. M. Hansen. 1993. 'Hydroxychloroquine and sulphasalazine alone and in combination in rheumatoid arthritis: a randomised double blind trial', *Ann Rheum Dis*, 52: 711-5.

Farber, S., J. Cohen, and L. L. Uzman. 1957. 'Lipogranulomatosis; a new lipo-glycoprotein storage disease', *J Mt Sinai Hosp N Y*, 24: 816-37.

Fensom, A. H., P. F. Benson, B. R. Neville, H. W. Moser, A. E. Moser, and J. T. Dulaney. 1979. 'Prenatal diagnosis of Farber's disease', *Lancet*, 2: 990-2.

Ferlinz, K., G. Kopal, K. Bernardo, T. Linke, J. Bar, B. Breiden, U. Neumann, F. Lang, E. H. Schuchman, and K. Sandhoff. 2001. 'Human acid ceramidase: processing, glycosylation, and lysosomal targeting', *J Biol Chem*, 276: 35352-60.

Ferraz, M. B., G. R. Pinheiro, M. Helfenstein, E. Albuquerque, C. Rezende, L. Roimicher, L. Brandao, S. C. Silva, G. C. Pinheiro, and E. Atra. 1994. 'Combination therapy with methotrexate and chloroquine in rheumatoid arthritis. A multicenter randomized placebo-controlled trial', *Scand J Rheumatol*, 23: 231-6.

Filosto, M., M. Aureli, B. Castellotti, F. Rinaldi, D. Schiumarini, M. Valsecchi, S. Lualdi, R. Mazzotti, V. Pensato, S. Rota, C. Gellera, M. Filocamo, and A. Padovani. 2016. 'ASAH1 variant causing a mild SMA phenotype with no myoclonic epilepsy: a clinical, biochemical and molecular study', *Eur J Hum Genet*, 24: 1578-83.

Forestier, Jacques. 1932. 'THE TREATMENT OF RHEUMATOID ARTHRITIS WITH GOLD SALTS INJECTIONS', *The Lancet*, 219: 441-44.

Forrest, C. M., T. W. Stone, G. M. Mackay, L. Oxford, N. Stoy, G. Harman, and L. G. Darlington. 2006. 'Purine metabolism and clinical status of patients with rheumatoid arthritis treated with dipyridamole', *Nucleosides Nucleotides Nucleic Acids*, 25: 1287-90.

Fujiwaki, T., S. Hamanaka, M. Koga, T. Ishihara, R. Nishikomori, E. Kinoshita, and K. Furusho. 1992. 'A case of Farber disease', *Acta Paediatr Jpn*, 34: 72-9.

Fujiwaki, T., S. Hamanaka, S. Tate, F. Inagaki, M. Suzuki, A. Suzuki, and C. Mori. 1995. 'Tissue accumulation of sulfatide and GM3 ganglioside in a patient with variant Farber disease', *Clin Chim Acta*, 234: 23-36.

Gaffen, S. L. 2009. 'The role of interleukin-17 in the pathogenesis of rheumatoid arthritis', *Curr Rheumatol Rep*, 11: 365-70.

Galeazzi, M., L. Bazzichi, G. D. Sebastiani, D. Neri, E. Garcia, N. Ravenni, L. Giovannoni, J. Wilton, M. Bardelli, C. Baldi, E. Selvi, A. Iuliano, G. Minisola, R. Caporali, E. Prisco, and S. Bombardieri.

2014. 'A phase IB clinical trial with Dekavil (F8-IL10), an immunoregulatory 'armed antibody' for the treatment of rheumatoid arthritis, used in combination wilh methotrexate', *Isr Med Assoc J*, 16: 666.

Gan, J. J., V. Garcia, J. Tian, M. Tagliati, J. E. Parisi, J. M. Chung, R. Lewis, R. Baloh, T. Levade, and T. M. Pierson. 2015. 'Acid ceramidase deficiency associated with spinal muscular atrophy with progressive myoclonic epilepsy', *Neuromuscul Disord*, 25: 959-63.

Garcia, A. E., S. R. Mada, M. C. Rico, R. A. Dela Cadena, and S. P. Kunapuli. 2011. 'Clopidogrel, a P2Y12 receptor antagonist, potentiates the inflammatory response in a rat model of peptidoglycan polysaccharide-induced arthritis', *PLoS One*, 6: e26035.

Genovese, M. C. 2009. 'Inhibition of p38: has the fat lady sung?', *Arthritis Rheum*, 60: 317-20.

Genovese, M. C., M. Greenwald, C. S. Cho, A. Berman, L. Jin, G. S. Cameron, O. Benichou, L. Xie, D. Braun, P. Y. Berclaz, and S. Banerjee. 2014. 'A phase II randomized study of subcutaneous ixekizumab, an anti-interleukin-17 monoclonal antibody, in rheumatoid arthritis patients who were naive to biologic agents or had an inadequate response to tumor necrosis factor inhibitors', *Arthritis Rheumatol*, 66: 1693-704.

Genovese, M. C., R. F. van Vollenhoven, C. Pacheco-Tena, Y. Zhang, and N. Kinnman. 2016. 'VX-509 (Decernotinib), an Oral Selective JAK-3 Inhibitor, in Combination With Methotrexate in Patients With Rheumatoid Arthritis', *Arthritis Rheumatol*, 68: 46-55.

Glowinski, J., and J. Axelrod. 1964. 'INHIBITION OF UPTAKE OF TRITIATED-NORADRENALINE IN THE INTACT RAT BRAIN BY IMIPRAMINE AND STRUCTURALLY RELATED COMPOUNDS', *Nature*, 204: 1318-9.

Gorelik, A., K. Illes, L. X. Heinz, G. Superti-Furga, and B. Nagar. 2016. 'Crystal structure of mammalian acid sphingomyelinase', *Nat Commun*, 7: 12196.

Gourraud, P. A., P. Dieude, J. F. Boyer, L. Nogueira, A. Cambon-Thomsen, B. Mazieres, F. Cornelis, G. Serre, A. Cantagrel, and A. Constantin. 2007. 'A new classification of HLA-DRB1 alleles differentiates predisposing and protective alleles for autoantibody production in rheumatoid arthritis', *Arthritis Res Ther*, 9: R27.

Grassmé, H., P. L. Jernigan, R. S. Hoehn, B. Wilker, M. Soddemann, M. J. Edwards, C. P. Muller, J. Kornhuber, and E. Gulbins. 2015. 'Inhibition of Acid Sphingomyelinase by Antidepressants Counteracts Stress-Induced Activation of P38-Kinase in Major Depression', *Neurosignals*, 23: 84-92.

Grober, J. S., B. L. Bowen, H. Ebling, B. Athey, C. B. Thompson, D. A. Fox, and L. M. Stoolman. 1993. 'Monocyte-endothelial adhesion in chronic rheumatoid arthritis. In situ detection of selectin and integrin-dependent interactions', *J Clin Invest*, 91: 2609-19.

Gubner, R., S. August, and V. Ginsberg. 1951. 'Therapeutic suppression of tissue reactivity. II. Effect of aminopterin in rheumatoid arthritis and psoriasis', *Am J Med Sci*, 221: 176-82.

Guenther, G. G., E. R. Peralta, K. R. Rosales, S. Y. Wong, L. J. Siskind, and A. L. Edinger. 2008. 'Ceramide starves cells to death by downregulating nutrient transporter proteins', *Proc Natl Acad Sci U S A*, 105: 17402-7.

Gulbins, A., H. Grassmé, R. Hoehn, B. Wilker, M. Soddemann, M. Kohnen, M. J. Edwards, J. Kornhuber, and E. Gulbins. 2016. 'Regulation of Neuronal Stem Cell Proliferation in the Hippocampus by Endothelial Ceramide', *Cell Physiol Biochem*, 39: 790-801.

Gulbins, E., M. Palmada, M. Reichel, A. Luth, C. Bohmer, D. Amato, C. P. Müller, C. H. Tischbirek, T. W. Groemer, G. Tabatabai, K. A. Becker, P. Tripal, S. Staedtler, T. F. Ackermann, J. van Brederode, C. Alzheimer, M. Weller, U. E. Lang, B. Kleuser, H. Grassmé, and J. Kornhuber. 2013. 'Acid sphingomyelinase-ceramide system mediates effects of antidepressant drugs', *Nat Med*, 19: 934-8.

Hamada, M., K. Iikubo, Y. Ishikawa, A. Ikeda, K. Umezawa, and S. Nishiyama. 2003. 'Biological activities of alpha-mangostin derivatives against acidic sphingomyelinase', *Bioorg Med Chem Lett*, 13: 3151-3.

Han, Z., D. L. Boyle, K. R. Aupperle, B. Bennett, A. M. Manning, and G. S. Firestein. 1999. 'Jun N-terminal kinase in rheumatoid arthritis', *J Pharmacol Exp Ther*, 291: 124-30.

Haringman, J. J., D. M. Gerlag, A. H. Zwinderman, T. J. Smeets, M. C. Kraan, D. Baeten, I. B. McInnes, B. Bresnihan, and P. P. Tak. 2005. 'Synovial tissue macrophages: a sensitive biomarker for response to treatment in patients with rheumatoid arthritis', *Ann Rheum Dis*, 64: 834-8.

He, X., S. Dworski, C. Zhu, V. DeAngelis, A. Solyom, J. A. Medin, C. M. Simonaro, and E. H. Schuchman. 2017. 'Enzyme replacement therapy for Farber disease: Proof-of-concept studies in cells and mice', *BBA Clin*, 7: 85-96.

He, X., N. Okino, R. Dhami, A. Dagan, S. Gatt, H. Schulze, K. Sandhoff, and E. H. Schuchman. 2003. 'Purification and characterization of recombinant, human acid ceramidase. Catalytic reactions and interactions with acid sphingomyelinase', *J Biol Chem*, 278: 32978-86.

Heikkinen, T., U. Ekblad, and K. Laine. 2001. 'Transplacental transfer of amitriptyline and nortriptyline in isolated perfused human placenta', *Psychopharmacology (Berl)*, 153: 450-4.

Hirata, S., T. Matsubara, R. Saura, H. Tateishi, and K. Hirohata. 1989. 'Inhibition of in vitro vascular endothelial cell proliferation and in vivo neovascularization by low-dose methotrexate', *Arthritis Rheum*, 32: 1065-73.

Hollmann, C., S. Werner, E. Avota, D. Reuter, L. Japtok, B. Kleuser, E. Gulbins, K. A. Becker, J. Schneider-Schaulies, and N. Beyersdorf. 2016. 'Inhibition of Acid Sphingomyelinase Allows for Selective Targeting of CD4+ Conventional versus Foxp3+ Regulatory T Cells', *J Immunol*, 197: 3130-41.

Honorati, M. C., S. Neri, L. Cattini, and A. Facchini. 2006. 'Interleukin-17, a regulator of angiogenic factor release by synovial fibroblasts', *Osteoarthritis Cartilage*, 14: 345-52.

Horinouchi, K., S. Erlich, D. P. Perl, K. Ferlinz, C. L. Bisgaier, K. Sandhoff, R. J. Desnick, C. L. Stewart, and E. H. Schuchman. 1995. 'Acid sphingomyelinase deficient mice: a model of types A and B Niemann-Pick disease', *Nat Genet*, 10: 288-93.

Hueber, W., D. D. Patel, T. Dryja, A. M. Wright, I. Koroleva, G. Bruin, C. Antoni, Z. Draelos, M. H. Gold, P. Durez, P. P. Tak, J. J. Gomez-Reino, C. S. Foster, R. Y. Kim, C. M. Samson, N. S. Falk, D. S. Chu, D. Callanan, Q. D. Nguyen, K. Rose, A. Haider, and F. Di Padova. 2010. 'Effects of AIN457, a fully human antibody to interleukin-17A, on psoriasis, rheumatoid arthritis, and uveitis', *Sci Transl Med*, 2: 52ra72.

Hurwitz, R., K. Ferlinz, and K. Sandhoff. 1994. 'The tricyclic antidepressant desipramine causes proteolytic degradation of lysosomal sphingomyelinase in human fibroblasts', *Biol Chem Hoppe Seyler*, 375: 447-50.

Hurwitz, R., K. Ferlinz, G. Vielhaber, H. Moczall, and K. Sandhoff. 1994. 'Processing of human acid sphingomyelinase in normal and I-cell fibroblasts', *J Biol Chem*, 269: 5440-5.

Huston, J. P., J. Kornhuber, C. Mühle, L. Japtok, M. Komorowski, C. Mattern, M. Reichel, E. Gulbins, B. Kleuser, B. Topic, M. A. De Souza Silva, and C. P. Müller. 2016. 'A sphingolipid mechanism for behavioral extinction', *J Neurochem*, 137: 589-603.

Ingram, V. M. 1957. 'Gene mutations in human haemoglobin: the chemical difference between normal and sickle cell haemoglobin', *Nature*, 180: 326-8.

Ishizaki, J., K. Yokogawa, M. Hirano, E. Nakashima, Y. Sai, S. Ohkuma, T. Ohshima, and F. Ichimura. 1996. 'Contribution of lysosomes to the subcellular distribution of basic drugs in the rat liver', *Pharm Res*, 13: 902-6.

Jang, S. W., X. Liu, C. B. Chan, D. Weinshenker, R. A. Hall, G. Xiao, and K. Ye. 2009. 'Amitriptyline is a TrkA and TrkB receptor agonist that promotes TrkA/TrkB heterodimerization and has potent neurotrophic activity', *Chem Biol*, 16: 644-56.

Jones, E. E., S. Dworski, D. Canals, J. Casas, G. Fabrias, D. Schoenling, T. Levade, C. Denlinger, Y. A. Hannun, J. A. Medin, and R. R. Drake. 2014. 'On-tissue localization of ceramides and other sphingolipids by MALDI mass spectrometry imaging', *Anal Chem*, 86: 8303-11.

Kim, K. W., M. L. Cho, H. R. Kim, J. H. Ju, M. K. Park, H. J. Oh, J. S. Kim, S. H. Park, S. H. Lee, and H. Y. Kim. 2007. 'Up-regulation of stromal cell-derived factor 1 (CXCL12) production in rheumatoid synovial fibroblasts through interactions with T lymphocytes: role of interleukin-17 and CD40L-CD40 interaction', *Arthritis Rheum*, 56: 1076-86.

Klein, A., M. Henseler, C. Klein, K. Suzuki, K. Harzer, and K. Sandhoff. 1994. 'Sphingolipid activator protein D (sap-D) stimulates the lysosomal degradation of ceramide in vivo', *Biochem Biophys Res Commun*, 200: 1440-8.

Klinefelter, H. F., and A. Achurra. 1973. 'Effect of gold salts and antimalarials on the rheumatoid factor in rheumatoid arthritis', *Scand J Rheumatol*, 2: 177-82.

Koenders, M. I., E. Lubberts, B. Oppers-Walgreen, L. van den Bersselaar, M. M. Helsen, F. E. Di Padova, A. M. Boots, H. Gram, L. A. Joosten, and W. B. van den Berg. 2005. 'Blocking of interleukin-17 during reactivation of experimental arthritis prevents joint inflammation and bone erosion by decreasing RANKL and interleukin-1', *Am J Pathol*, 167: 141-9.

Kolzer, M., C. Arenz, K. Ferlinz, N. Werth, H. Schulze, R. Klingenstein, and K. Sandhoff. 2003. 'Phosphatidylinositol-3,5-Bisphosphate is a potent and selective inhibitor of acid sphingomyelinase', *Biol Chem*, 384: 1293-8.

Kolzer, M., N. Werth, and K. Sandhoff. 2004. 'Interactions of acid sphingomyelinase and lipid bilayers in the presence of the tricyclic antidepressant desipramine', *FEBS Lett*, 559: 96-8.

Kornhuber, J., M. Muehlbacher, S. Trapp, S. Pechmann, A. Friedl, M. Reichel, C. Muhle, L. Terfloth, T. W. Groemer, G. M. Spitzer, K. R. Liedl, E. Gulbins, and P. Tripal. 2011. 'Identification of novel functional inhibitors of acid sphingomyelinase', *PLoS One*, 6: e23852.

Kornhuber, J., W. Retz, and P. Riederer. 1995. 'Slow accumulation of psychotropic substances in the human brain. Relationship to therapeutic latency of neuroleptic and antidepressant drugs?', *J Neural Transm Suppl*, 46: 315-23.

Kornhuber, J., P. Tripal, M. Reichel, C. Mühle, C. Rhein, M. Muehlbacher, T. W. Groemer, and E. Gulbins. 2010. 'Functional Inhibitors of Acid Sphingomyelinase (FIASMAs): a novel pharmacological group of drugs with broad clinical applications', *Cell Physiol Biochem*, 26: 9-20.

Kornhuber, J., P. Tripal, M. Reichel, L. Terfloth, S. Bleich, J. Wiltfang, and E. Gulbins. 2008. 'Identification of new functional inhibitors of acid sphingomyelinase using a structure-property-activity relation model', *J Med Chem*, 51: 219-37.

Kosinska, M. K., G. Liebisch, G. Lochnit, J. Wilhelm, H. Klein, U. Kaesser, G. Lasczkowski, M. Rickert, G. Schmitz, and J. Steinmeyer. 2014. 'Sphingolipids in human synovial fluid--a lipidomic study', *PLoS One*, 9: e91769.

Kremer, J., M. C. Genovese, E. Keystone, P. C. Taylor, S. H. Zuckerman, G. Ruotolo, D. E. Schlichting, V. L. Crotzer, E. Nantz, S. D. Beattie, and W. L. Macias. 2016. 'Effects of Baricitinib on Lipid, Apolipoprotein, and Lipoprotein Particle Profiles in a Phase 2b Study in Patients with Active Rheumatoid Arthritis', *Arthritis Rheumatol*.

Kremer, J. M., P. Emery, H. S. Camp, A. Friedman, L. Wang, A. A. Othman, N. Khan, A. L. Pangan, S. Jungerwirth, and E. C. Keystone. 2016. 'A Phase IIb Study of ABT-494, a Selective JAK-1 Inhibitor, in Patients With Rheumatoid Arthritis and an Inadequate Response to Anti-Tumor Necrosis Factor Therapy', *Arthritis Rheumatol*, 68: 2867-77.

Kudoh, T., and D. A. Wenger. 1982. 'Diagnosis of metachromatic leukodystrophy, Krabbe disease, and Farber disease after uptake of fatty acid-labeled cerebroside sulfate into cultured skin fibroblasts', *J Clin Invest*, 70: 89-97.

Kuemmel, T. A., J. Thiele, R. Schroeder, and W. Stoffel. 1997. 'Pathology of visceral organs and bone marrow in an acid sphingomyelinase deficient knock-out mouse line, mimicking human Niemann-Pick disease type A. A light and electron microscopic study', *Pathol Res Pract*, 193: 663-71.

Kunwar, S., A. R. Devkota, and D. K. Ghimire. 2016. 'Fostamatinib, an oral spleen tyrosine kinase inhibitor, in the treatment of rheumatoid arthritis: a meta-analysis of randomized controlled trials', *Rheumatol Int*, 36: 1077-87.

Laffon, A., R. Garcia-Vicuna, A. Humbria, A. A. Postigo, A. L. Corbi, M. O. de Landazuri, and F. Sanchez-Madrid. 1991. 'Upregulated expression and function of VLA-4 fibronectin receptors on human activated T cells in rheumatoid arthritis', *J Clin Invest*, 88: 546-52.

Landre-Beauvais, A. J. 1800. 'The first description of rheumatoid arthritis. Unabridged text of the doctoral dissertation presented in 1800', *Joint Bone Spine*, 68: 130-43.

Lebre, M. C. , S. L. Jongbloed, S. W. Tas, T. J. Smeets, I.B. McInnes, and P. P. Tak. 2008. 'Rheumatoid arthritis synovium contains two subsets of CD83-DC-LAMP- dendritic cells with distinct cytokine profiles', *Am J Pathol*, 172: 940-50.

Levade, T., M. Leruth, D. Graber, A. Moisand, S. Vermeersch, R. Salvayre, and P. J. Courtoy. 1996. 'In situ assay of acid sphingomyelinase and ceramidase based on LDL-mediated lysosomal targeting of ceramide-labeled sphingomyelin', *J Lipid Res*, 37: 2525-38.

Levade, T., M. C. Tempesta, H. W. Moser, A. H. Fensom, K. Harzer, A. B. Moser, and R. Salvayre. 1995. 'Sulfatide and sphingomyelin loading of living cells as tools for the study of ceramide turnover by lysosomal ceramidase--implications for the diagnosis of Farber disease', *Biochem Mol Med*, 54: 117-25.

Levade, T., M. C. Tempesta, and R. Salvayre. 1993. 'The in situ degradation of ceramide, a potential lipid mediator, is not completely impaired in Farber disease', *FEBS Lett*, 329: 306-12.

Li, C. M., J. H. Park, X. He, B. Levy, F. Chen, K. Arai, D. A. Adler, C. M. Disteche, J. Koch, K. Sandhoff, and E. H. Schuchman. 1999. 'The human acid ceramidase gene (ASAH): structure, chromosomal location, mutation analysis, and expression', *Genomics*, 62: 223-31.

Lopes Pinheiro, M. A., J. Kroon, M. Hoogenboezem, D. Geerts, B. van Het Hof, S. M. van der Pol, J. D. van Buul, and H. E. de Vries. 2016. 'Acid Sphingomyelinase-Derived Ceramide Regulates ICAM-1 Function during T Cell Transmigration across Brain Endothelial Cells', *J Immunol*, 196: 72-9.

Lundberg, K., C. Bengtsson, N. Kharlamova, E. Reed, X. Jiang, H. Kallberg, I. Pollak-Dorocic, L. Israelsson, C. Kessel, L. Padyukov, R. Holmdahl, L. Alfredsson, and L. Klareskog. 2013. 'Genetic and environmental determinants for disease risk in subsets of rheumatoid arthritis defined by the anticitrullinated protein/peptide antibody fine specificity profile', *Ann Rheum Dis*, 72: 652-8.

Lundstrom, E., H. Kallberg, L. Alfredsson, L. Klareskog, and L. Padyukov. 2009. 'Gene-environment interaction between the DRB1 shared epitope and smoking in the risk of anti-citrullinated protein antibody-positive rheumatoid arthritis: all alleles are important', *Arthritis Rheum*, 60: 1597-603.

Masli, S., and B. Turpie. 2009. 'Anti-inflammatory effects of tumour necrosis factor (TNF)-alpha are mediated via TNF-R2 (p75) in tolerogenic transforming growth factor-beta-treated antigen-presenting cells', *Immunology*, 127: 62-72.

McInnes, I. B., C. D. Buckley, and J. D. Isaacs. 2016. 'Cytokines in rheumatoid arthritis - shaping the immunological landscape', *Nat Rev Rheumatol*, 12: 63-8.

McMurray, R. W. 1996. 'Adhesion molecules in autoimmune disease', *Semin Arthritis Rheum*, 25: 215-33.

Melet, J., D. Mulleman, P. Goupille, B. Ribourtout, H. Watier, and G. Thibault. 2013. 'Rituximab-induced T cell depletion in patients with rheumatoid arthritis: association with clinical response', *Arthritis Rheum*, 65: 2783-90.

Messemaker, T. C., T. W. Huizinga, and F. Kurreeman. 2015. 'Immunogenetics of rheumatoid arthritis: Understanding functional implications', *J Autoimmun*, 64: 74-81.

Mondal, R. K., M. Nandi, S. Datta, and M. Hira. 2009. 'Disseminated lipogranulomatosis', *Indian Pediatr*, 46: 175-7.

Moser, H. W.; Linke, T.; Fensom, A. H.; Levade, T.; Sandhoff K. 2001. 'Acid ceramidase deficiency: Farber lipogranulomatosis.' in C. R.; Childs Sly, W. S.; Beaudet, B.; Valle, A. L.; Kinzler, D.; Vogelstein, K. W. (ed.), *The Metabolic and Molecular Bases of Inherited Diseases* (McGraw-Hill Inc.: New York).

Mottonen, M., P. Isomaki, R. Saario, P. Toivanen, J. Punnonen, and O. Lassila. 1998. 'Interleukin-10 inhibits the capacity of synovial macrophages to function as antigen-presenting cells', *Br J Rheumatol*, 37: 1207-14.

Mühle, C., and J. Kornhuber. 2017. 'Assay to measure sphingomyelinase and ceramidase activities efficiently and safely', *J Chromatogr A*, 1481: 137-44.

Munzer, P., O. Borst, B. Walker, E. Schmid, M. A. Feijge, J. M. Cosemans, M. Chatterjee, E. M. Schmidt, S. Schmidt, S. T. Towhid, C. Leibrock, M. Elvers, M. Schaller, P. Seizer, K. Ferlinz, A. E. May, E. Gulbins, J. W. Heemskerk, M. Gawaz, and F. Lang. 2014. 'Acid sphingomyelinase regulates platelet cell membrane scrambling, secretion, and thrombus formation', *Arterioscler Thromb Vasc Biol*, 34: 61-71.

O'Connor, T. M., D. J. O'Halloran, and F. Shanahan. 2000. 'The stress response and the hypothalamic-pituitary-adrenal axis: from molecule to melancholia', *Qjm*, 93: 323-33.

Ohata, J., N. J. Zvaifler, M. Nishio, D. L. Boyle, S. L. Kalled, D. A. Carson, and T. J. Kipps. 2005. 'Fibroblast-like synoviocytes of mesenchymal origin express functional B cell-activating factor of the TNF family in response to proinflammatory cytokines', *J Immunol*, 174: 864-70.

Okudaira, C., Y. Ikeda, S. Kondo, S. Furuya, Y. Hirabayashi, T. Koyano, Y. Saito, and K. Umezawa. 2000. 'Inhibition of acidic sphingomyelinase by xanthone compounds isolated from Garcinia speciosa', *J Enzyme Inhib*, 15: 129-38.

Owens, M. J., W. N. Morgan, S. J. Plott, and C. B. Nemeroff. 1997. 'Neurotransmitter receptor and transporter binding profile of antidepressants and their metabolites', *J Pharmacol Exp Ther*, 283: 1305-22.

Pancrazio, J. J., G. L. Kamatchi, A. K. Roscoe, and C. Lynch, 3rd. 1998. 'Inhibition of neuronal Na+ channels by antidepressant drugs', *J Pharmacol Exp Ther*, 284: 208-14.

Park, J. H., and E. H. Schuchman. 2006. 'Acid ceramidase and human disease', *Biochim Biophys Acta*, 1758: 2133-8.

Park, T. J., S. Y. Shin, B. C. Suh, E. K. Suh, I. S. Lee, Y. S. Kim, and K. T. Kim. 1998. 'Differential inhibition of catecholamine secretion by amitriptyline through blockage of nicotinic receptors, sodium channels, and calcium channels in bovine adrenal chromaffin cells', *Synapse*, 29: 248-56.

Peister, A., J. A. Mellad, B. L. Larson, B. M. Hall, L. F. Gibson, and D. J. Prockop. 2004. 'Adult stem cells from bone marrow (MSCs) isolated from different strains of inbred mice vary in surface epitopes, rates of proliferation, and differentiation potential', *Blood*, 103: 1662-8.

Perrotta, C., L. Bizzozero, D. Cazzato, S. Morlacchi, E. Assi, F. Simbari, Y. Zhang, E. Gulbins, M. T. Bassi, P. Rosa, and E. Clementi. 2010. 'Syntaxin 4 is required for acid sphingomyelinase activity and apoptotic function', *J Biol Chem*, 285: 40240-51.

Pewzner-Jung, Y., O. Brenner, S. Braun, E. L. Laviad, S. Ben-Dor, E. Feldmesser, S. Horn-Saban, D. Amann-Zalcenstein, C. Raanan, T. Berkutzki, R. Erez-Roman, O. Ben-David, M. Levy, D. Holzman, H. Park, A. Nyska, A. H. Merrill, Jr., and A. H. Futerman. 2010. 'A critical role for ceramide synthase 2 in liver homeostasis: II. insights into molecular changes leading to hepatopathy', *J Biol Chem*, 285: 10911-23.

Preuss, S., F. D. Omam, J. Scheiermann, S. Stadelmann, S. Winoto-Morbach, P. von Bismarck, S. Adam-Klages, F. Knerlich-Lukoschus, D. Lex, D. Wesch, J. Held-Feindt, S. Uhlig, S. Schütze, and M. F. Krause. 2012. 'Topical application of phosphatidyl-inositol-3,5-bisphosphate for acute lung injury in neonatal swine', *J Cell Mol Med*, 16: 2813-26.

Punke, M. A., and P. Friederich. 2007. 'Amitriptyline is a potent blocker of human Kv1.1 and Kv7.2/7.3 channels', *Anesth Analg*, 104: 1256-64, tables of contents.

Qiu, H., T. Edmunds, J. Baker-Malcolm, K. P. Karey, S. Estes, C. Schwarz, H. Hughes, and S. M. Van Patten. 2003. 'Activation of human acid sphingomyelinase through modification or deletion of C-terminal cysteine', *J Biol Chem*, 278: 32744-52.

Quattrocchi, E., M. Ostergaard, P. C. Taylor, R. F. van Vollenhoven, M. Chu, S. Mallett, H. Perry, and R. Kurrasch. 2016. 'Safety of Repeated Open-Label Treatment Courses of Intravenous Ofatumumab, a Human Anti-CD20 Monoclonal Antibody, in Rheumatoid Arthritis: Results from Three Clinical Trials', *PLoS One*, 11: e0157961.

Rhein, C., P. Tripal, A. Seebahn, A. Konrad, M. Kramer, C. Nagel, J. Kemper, J. Bode, C. Mühle, E. Gulbins, M. Reichel, C. M. Becker, and J. Kornhuber. 2012. 'Functional implications of novel human acid sphingomyelinase splice variants', *PLoS One*, 7: e35467.

Rioja, I., K. A. Bush, J. B. Buckton, M. C. Dickson, and P. F. Life. 2004. 'Joint cytokine quantification in two rodent arthritis models: kinetics of expression, correlation of mRNA and protein levels and response to prednisolone treatment', *Clin Exp Immunol*, 137: 65-73.

Rosenstein, E. D., R. A. Greenwald, L. J. Kushner, and G. Weissmann. 2004. 'Hypothesis: the humoral immune response to oral bacteria provides a stimulus for the development of rheumatoid arthritis', *Inflammation*, 28: 311-8.

Roth, A. G., D. Drescher, Y. Yang, S. Redmer, S. Uhlig, and C. Arenz. 2009. 'Potent and selective inhibition of acid sphingomyelinase by bisphosphonates', *Angew Chem Int Ed Engl*, 48: 7560-3.

Rudnik-Schoneborn, S., S. Lutzenrath, J. Borkowska, A. Karwanska, I. Hausmanowa-Petrusewicz, and K. Zerres. 1998. 'Analysis of creatine kinase activity in 504 patients with proximal spinal muscular atrophy types I-III from the point of view of progression and severity', *Eur Neurol*, 39: 154-62.

Saag, K. G. 1997. 'Low-dose corticosteroid therapy in rheumatoid arthritis: balancing the evidence', *Am J Med*, 103: 31s-39s.

Sari, I., I. Turkcuer, T. Erurker, M. Serinken, M. Seyit, and A. Keskin. 2011. 'Therapeutic plasma exchange in amitriptyline intoxication: case report and review of the literature', *Transfus Apher Sci*, 45: 183-5.

Sarkar, S., L. A. Cooney, P. White, D. B. Dunlop, J. Endres, J. M. Jorns, M. J. Wasco, and D. A. Fox. 2009. 'Regulation of pathogenic IL-17 responses in collagen-induced arthritis: roles of endogenous interferon-gamma and IL-4', *Arthritis Res Ther*, 11: R158.

Scher, J. U., and S. B. Abramson. 2011. 'The microbiome and rheumatoid arthritis', *Nat Rev Rheumatol*, 7: 569-78.

Schett, G., M. Tohidast-Akrad, J. S. Smolen, B. J. Schmid, C. W. Steiner, P. Bitzan, P. Zenz, K. Redlich, Q. Xu, and G. Steiner. 2000. 'Activation, differential localization, and regulation of the stress-activated protein kinases, extracellular signal-regulated kinase, c-JUN N-terminal kinase, and p38 mitogen-activated protein kinase, in synovial tissue and cells in rheumatoid arthritis', *Arthritis Rheum*, 43: 2501-12.

Schissel, S. L., X. Jiang, J. Tweedie-Hardman, T. Jeong, E. H. Camejo, J. Najib, J. H. Rapp, K. J. Williams, and I. Tabas. 1998. 'Secretory sphingomyelinase, a product of the acid sphingomyelinase gene, can hydrolyze atherogenic lipoproteins at neutral pH. Implications for atherosclerotic lesion development', *J Biol Chem*, 273: 2738-46.

Schissel, S. L., G. A. Keesler, E. H. Schuchman, K. J. Williams, and I. Tabas. 1998. 'The cellular trafficking and zinc dependence of secretory and lysosomal sphingomyelinase, two products of the acid sphingomyelinase gene', *J Biol Chem*, 273: 18250-9.

Schmitt-Sody, M., P. Metz, O. Gottschalk, C. Birkenmaier, S. Zysk, A. Veihelmann, and V. Jansson. 2007. 'Platelet P-selectin is significantly involved in leukocyte-endothelial cell interaction in murine antigen-induced arthritis', *Platelets*, 18: 365-72.

Schmitt-Sody, M., P. Metz, A. Klose, O. Gottschalk, S. Zysk, J. Hausdorf, A. Veihelmann, and V. Jansson. 2007. 'In vivo interactions of platelets and leucocytes with the endothelium in murine antigen-induced arthritis: the role of P-selectin', *Scand J Rheumatol*, 36: 311-9.

Schofield, G. G., B. Witkop, J. E. Warnick, and E. X. Albuquerque. 1981. 'Differentiation of the open and closed states of the ionic channels of nicotinic acetylcholine receptors by tricyclic antidepressants', *Proc Natl Acad Sci U S A*, 78: 5240-4.

Schröder, A. E., A. Greiner, C. Seyfert, and C. Berek. 1996. 'Differentiation of B cells in the nonlymphoid tissue of the synvoial membrane of patients with rheumatoid arthritis', *Proc Natl Acad Sci U S A*, 93: 221-5.

Schuchman, E. H., and R. J. Desnick. 2017. 'Types A and B Niemann-Pick disease', *Mol Genet Metab*, 120: 27-33.

Schuchman, E. H., M. Suchi, T. Takahashi, K. Sandhoff, and R. J. Desnick. 1991. 'Human acid sphingomyelinase. Isolation, nucleotide sequence and expression of the full-length and alternatively spliced cDNAs', *J Biol Chem*, 266: 8531-9.

Segui, B., C. Bezombes, E. Uro-Coste, J. A. Medin, N. Andrieu-Abadie, N. Auge, A. Brouchet, G. Laurent, R. Salvayre, J. P. Jaffrezou, and T. Levade. 2000. 'Stress-induced apoptosis is not mediated by endolysosomal ceramide', *Faseb j*, 14: 36-47.

Semerano, L., E. Minichiello, N. Bessis, and M. C. Boissier. 2016. 'Novel Immunotherapeutic Avenues for Rheumatoid Arthritis', *Trends Mol Med*, 22: 214-29.

Seyler, T. M., Y. W. Park, S. Takemura, R. J. Bram, P. J. Kurtin, J. J. Goronzy, and C. M. Weyand. 2005. 'BLyS and APRIL in rheumatoid arthritis', *J Clin Invest*, 115: 3083-92.

Shtraizent, N., E. Eliyahu, J. H. Park, X. He, R. Shalgi, and E. H. Schuchman. 2008. 'Autoproteolytic cleavage and activation of human acid ceramidase', *J Biol Chem*, 283: 11253-9.

Silman, A. J., and J. E. Pearson. 2002. 'Epidemiology and genetics of rheumatoid arthritis', *Arthritis Res*, 4 Suppl 3: S265-72.

Simon, J., R. Surber, G. Kleinstäuber, P. K. Petrow, S. Henzgen, R. W. Kinne, and R. Bräuer. 2001. 'Systemic macrophage activation in locally-induced experimental arthritis', *J Autoimmun*, 17: 127-36.

Simons, K., and E. Ikonen. 1997. 'Functional rafts in cell membranes', *Nature*, 387: 569-72.

Singer, S. J., and G. L. Nicolson. 1972. 'The fluid mosaic model of the structure of cell membranes', *Science*, 175: 720-31.

Sólyom, Alexander, Nesrin Karabul, Boris Hügle, Calogera Simonaro, and Edward Schuchman. 2014. 'Polyarticular arthritis as presenting feature of farber disease: a lysosomal storage disease involving inflammation', *Pediatric Rheumatology*, 12: P285.

Sugita, M., M. Willians, J. T. Dulaney, and H. W. Moser. 1975. 'Ceramidase and ceramide synthesis in human kidney and cerebellum. Description of a new alkaline ceramidase', *Biochim Biophys Acta*, 398: 125-31.

Sutrina, S. L., and W. W. Chen. 1982. 'Metabolism of ceramide-containing endocytotic vesicles in human diploid fibroblasts', *J Biol Chem*, 257: 3039-44.

Teichgräber, V., M. Ulrich, N. Endlich, J. Riethmuller, B. Wilker, C. C. De Oliveira-Munding, A. M. van Heeckeren, M. L. Barr, G. von Kürthy, K. W. Schmid, M. Weller, B. Tümmler, F. Lang, H. Grassme, G. Döring, and E. Gulbins. 2008. 'Ceramide accumulation mediates inflammation, cell death and infection susceptibility in cystic fibrosis', *Nat Med*, 14: 382-91.

Teoh, H. L., A. Solyom, E. H. Schuchman, D. Mowat, T. Roscioli, M. Farrar, and H. Sampaio. 2016. 'Polyarticular Arthritis and Spinal Muscular Atrophy in Acid Ceramidase Deficiency', *Pediatrics*, 138.

Testai, F. D., M. A. Landek, R. Goswami, M. Ahmed, and G. Dawson. 2004. 'Acid sphingomyelinase and inhibition by phosphate ion: role of inhibition by phosphatidyl-myo-inositol 3,4,5-triphosphate in oligodendrocyte cell signaling', *J Neurochem*, 89: 636-44.

Tohyama, J., Y. Oya, T. Ezoe, M. T. Vanier, H. Nakayasu, N. Fujita, and K. Suzuki. 1999. 'Ceramide accumulation is associated with increased apoptotic cell death in cultured fibroblasts of sphingolipid activator protein-deficient mouse but not in fibroblasts of patients with Farber disease', *J Inherit Metab Dis*, 22: 649-62.

Torcoletti, M., A. Petaccia, R. M. Pinto, U. Hladnik, F. Locatelli, C. Agostoni, and F. Corona. 2014. 'Farber disease in infancy resembling juvenile idiopathic arthritis: identification of two new mutations and a good early response to allogeneic haematopoietic stem cell transplantation', *Rheumatology (Oxford)*, 53: 1533-4.

Trapp, S., G. R. Rosania, R. W. Horobin, and J. Kornhuber. 2008. 'Quantitative modeling of selective lysosomal targeting for drug design', *Eur Biophys J*, 37: 1317-28.

Tsuboi, K., Y. X. Sun, Y. Okamoto, N. Araki, T. Tonai, and N. Ueda. 2005. 'Molecular characterization of N-acylethanolamine-hydrolyzing acid amidase, a novel member of the choloylglycine hydrolase family with structural and functional similarity to acid ceramidase', *J Biol Chem*, 280: 11082-92.

van der Goes, M. C., J. W. Jacobs, M. Boers, T. Andrews, M. A. Blom-Bakkers, F. Buttgereit, N. Caeyers, M. Cutolo, J. A. Da Silva, L. Guillevin, J. R. Kirwan, J. Rovensky, G. Severijns, S. Webber, R. Westhovens, and J. W. Bijlsma. 2010. 'Monitoring adverse events of low-dose glucocorticoid therapy: EULAR recommendations for clinical trials and daily practice', *Ann Rheum Dis*, 69: 1913-9.

van Echten-Deckert, G., A. Klein, T. Linke, T. Heinemann, J. Weisgerber, and K. Sandhoff. 1997. 'Turnover of endogenous ceramide in cultured normal and Farber fibroblasts', *J Lipid Res*, 38: 2569-79.

Van Rompaey, L., R. Galien, E. M. van der Aar, P. Clement-Lacroix, L. Nelles, B. Smets, L. Lepescheux, T. Christophe, K. Conrath, N. Vandeghinste, B. Vayssiere, S. De Vos, S. Fletcher, R. Brys, G. van 't Klooster, J. H. Feyen, and C. Menet. 2013. 'Preclinical characterization of GLPG0634, a selective inhibitor of JAK1, for the treatment of inflammatory diseases', *J Immunol*, 191: 3568-77.

Vasiliauskaite-Brooks, I., R. Sounier, P. Rochaix, G. Bellot, M. Fortier, F. Hoh, L. De Colibus, C. Bechara, E. M. Saied, C. Arenz, C. Leyrat, and S. Granier. 2017. 'Structural insights into adiponectin receptors suggest ceramidase activity', *Nature*, 544: 120-23.

Verderio, C., L. Muzio, E. Turola, A. Bergami, L. Novellino, F. Ruffini, L. Riganti, I. Corradini, M. Francolini, L. Garzetti, C. Maiorino, F. Servida, A. Vercelli, M. Rocca, D. Dalla Libera, V. Martinelli, G. Comi, G. Martino, M. Matteoli, and R. Furlan. 2012. 'Myeloid microvesicles are a marker and therapeutic target for neuroinflammation', *Ann Neurol*, 72: 610-24.

Voican, C. S., E. Corruble, S. Naveau, and G. Perlemuter. 2014. 'Antidepressant-induced liver injury: a review for clinicians', *Am J Psychiatry*, 171: 404-15.

Wegner, N., R. Wait, A. Sroka, S. Eick, K. A. Nguyen, K. Lundberg, A. Kinloch, S. Culshaw, J. Potempa, and P. J. Venables. 2010. 'Peptidylarginine deiminase from Porphyromonas gingivalis citrullinates human fibrinogen and alpha-enolase: implications for autoimmunity in rheumatoid arthritis', *Arthritis Rheum*, 62: 2662-72.

Weinblatt, M. E., P. J. Maddison, K. J. Bulpitt, B. L. Hazleman, M. B. Urowitz, R. D. Sturrock, J. S. Coblyn, A. L. Maier, W. R. Spreen, V. K. Manna, and et al. 1995. 'CAMPATH-1H, a humanized monoclonal antibody, in refractory rheumatoid arthritis. An intravenous dose-escalation study', *Arthritis Rheum*, 38: 1589-94.

Westhovens, R., P. C. Taylor, R. Alten, D. Pavlova, F. Enriquez-Sosa, M. Mazur, M. Greenwald, A. Van der Aa, F. Vanhoutte, C. Tasset, and P. Harrison. 2016. 'Filgotinib (GLPG0634/GS-6034), an oral JAK1 selective inhibitor, is effective in combination with methotrexate (MTX) in patients with active rheumatoid arthritis and insufficient response to MTX: results from a randomised, dose-finding study (DARWIN 1)', *Ann Rheum Dis*.

Wong, P. K., J. M. Quinn, N. A. Sims, A. van Nieuwenhuijze, I. K. Campbell, and I. P. Wicks. 2006. 'Interleukin-6 modulates production of T lymphocyte-derived cytokines in antigen-induced arthritis and drives inflammation-induced osteoclastogenesis', *Arthritis Rheum*, 54: 158-68.

Wooltorton, J. R., and A. Mathie. 1995. 'Potent block of potassium currents in rat isolated sympathetic neurones by the uncharged form of amitriptyline and related tricyclic compounds', *Br J Pharmacol*, 116: 2191-200.

Xiong, Z. J., J. Huang, G. Poda, R. Pomes, and G. G. Prive. 2016. 'Structure of Human Acid Sphingomyelinase Reveals the Role of the Saposin Domain in Activating Substrate Hydrolysis', *J Mol Biol*, 428: 3026-42.

Xu, M., M. Xia, X. X. Li, W. Q. Han, K. M. Boini, F. Zhang, Y. Zhang, J. K. Ritter, and P. L. Li. 2012. 'Requirement of translocated lysosomal V1 H(+)-ATPase for activation of membrane acid sphingomyelinase and raft clustering in coronary endothelial cells', *Mol Biol Cell*, 23: 1546-57.

Xu, X., L. Blinder, J. Shen, H. Gong, A. Finnegan, J. W. Williams, and A. S. Chong. 1997. 'In vivo mechanism by which leflunomide controls lymphoproliferative and autoimmune disease in MRL/MpJ-lpr/lpr mice', *J Immunol*, 159: 167-74.

Yang, W., E. Schmid, M. K. Nurbaeva, K. Szteyn, C. Leibrock, J. Yan, M. Schaller, E. Gulbins, E. Shumilina, and F. Lang. 2014. 'Role of acid sphingomyelinase in the regulation of mast cell function', *Clin Exp Allergy*, 44: 79-90.

Yang, X. D., R. Tisch, S. M. Singer, Z. A. Cao, R. S. Liblau, R. D. Schreiber, and H. O. McDevitt. 1994. 'Effect of tumor necrosis factor alpha on insulin-dependent diabetes mellitus in NOD mice. I. The early development of autoimmunity and the diabetogenic process', *J Exp Med*, 180: 995-1004.

Yeager, A. M., K. A. Uhas, C. D. Coles, P. C. Davis, W. L. Krause, and H. W. Moser. 2000. 'Bone marrow transplantation for infantile ceramidase deficiency (Farber disease)', *Bone Marrow Transplant*, 26: 357-63.

Yokomatsu, T., T. Murano, T. Akiyama, J. Koizumi, S. Shibuya, Y. Tsuji, S. Soeda, and H. Shimeno. 2003. 'Synthesis of non-competitive inhibitors of sphingomyelinases with significant activity', *Bioorg Med Chem Lett*, 13: 229-36.

Yoshida, K., B. Smith, M. Craggs, and R. C. Kumar. 1997. 'Investigation of pharmacokinetics and of possible adverse effects in infants exposed to tricyclic antidepressants in breast-milk', *J Affect Disord*, 43: 225-37.

Yoshida, Y., and T. Tanaka. 2014. 'Interleukin 6 and rheumatoid arthritis', *Biomed Res Int*, 2014: 698313.

Yoshizaki, K., N. Nishimoto, M. Mihara, and T. Kishimoto. 1998. 'Therapy of rheumatoid arthritis by blocking IL-6 signal transduction with a humanized anti-IL-6 receptor antibody', *Springer Semin Immunopathol*, 20: 247-59.

Zampeli, E., P. G. Vlachoyiannopoulos, and A. G. Tzioufas. 2015. 'Treatment of rheumatoid arthritis: Unraveling the conundrum', *J Autoimmun*, 65: 1-18.

Zhang, Z., A. K. Mandal, A. Mital, N. Popescu, D. Zimonjic, A. Moser, H. Moser, and A. B. Mukherjee. 2000. 'Human acid ceramidase gene: novel mutations in Farber disease', *Mol Genet Metab*, 70: 301-9.

Zhou, J., M. Tawk, F. D. Tiziano, J. Veillet, M. Bayes, F. Nolent, V. Garcia, S. Servidei, E. Bertini, F. Castro-Giner, Y. Renda, S. Carpentier, N. Andrieu-Abadie, I. Gut, T. Levade, H. Topaloglu, and J. Melki. 2012. 'Spinal muscular atrophy associated with progressive myoclonic epilepsy is caused by mutations in ASAH1', *Am J Hum Genet*, 91: 5-14.

Zhou, Y. F., M. C. Metcalf, S. C. Garman, T. Edmunds, H. Qiu, and R. R. Wei. 2016. 'Human acid sphingomyelinase structures provide insight to molecular basis of Niemann-Pick disease', *Nat Commun*, 7: 13082.

Zitnik, R. J., and J. A. Cooper, Jr. 1990. 'Pulmonary disease due to antirheumatic agents', *Clin Chest Med*, 11: 139-50.

Appendix

Publications and conferences

Publications

Beckmann, N., Becker, KA., Schumacher, F., Wang, J., Becker, J., Kadow, S., Kramer, M., Kühn, C., Edwards, MJ., Kleuser, B., Gulbins, E., Carpinteiro, A. Acid sphingomyelinase deficiency ameliorates Farber disease. *Submitted for publication.*

Beckmann, N., Walter, S., Becker, KA., Becker, J., Kramer, M., Hessler, G., Weber, S., Göthert, J., Gulbins, E., Carpinteiro, A. Regulation of arthritis severity by the acid sphingomyelinase. *Submitted for publication.*

Beckmann, N., Gulbins, E., Becker, KA., Carpinteiro, A. (2016). Sphingomyelinase, Acidic. Encyclopedia of Signaling Molecules, 2nd edition. New York: Springer Science+Business media, LLC, 2016.

Becker, KA.*, Beckmann, N.*, Adams, C., Hessler, G, Kramer, M., Gulbins, E., Carpinteiro, A. (2016). Melanoma cell metastasis via P-selectin-mediated activation of acid sphingomyelinase in platelets. *Clin Exp Metastasis, 34 (1): 25-35.* * These authors contributed equally to the work.

Carpinteiro, A., Beckmann, N., Seitz, A., Hessler, G., Wilker, B., Soddemann, M., Helfrich, I., Edelmann, B., Gulbins, E., Becker, KA. (2016). Role of acid sphingomyelinase-induced signaling in melanoma cells for hematogenous tumor metastasis. *Cell Physiol Biochem*, 38 (1): 1-14.

Beckmann, N., Sharma, D., Gulbins, E., Becker, KA., Edelmann, B. (2014). Inhibition of acid sphingomyelinase by tricyclic antidepressants and analogons. *Frontiers in Physiology*, 5: 331.

Weirauch, U., Beckmann, N., Thomas, M., Grünweller, A., Huber, K., Bracher, F., Hartmann, RK., Aigner, A. (2013). Functional role and therapeutic potential of the pim-1 kinase in colon carcinoma. *Neoplasia*, 15 (7): 783-794.

Conferences

Sphingolipids Conference, February 10th-14th 2017, Jackson Hole, USA: Two talks ("Acid ceramidase deficiency: Starved to death?" and "Arthritis and acid sphingomyelinase").

Retreat of the BIOME graduate school, November 3rd-4th 2016, Hamminkeln, Germany: Poster prize winner ("The role of acid sphingomyelinase in murine antigen-induced arthritis").

3rd Conference on the Molecular Medicine of Sphingolipids, September 18th-23rd 2016, French Lick, USA: Short talk ("The role of acid sphingomyelinase in murine antigen-induced arthritis") and poster presentation ("Characterization of an acid ceramidase knockout mouse").

Research day at the University of Duisburg-Essen, November 20th 2015, Essen, Germany: Poster presentation ("Characterization of an acid ceramidase knockout-mouse").

2nd Conference on the Molecular Medicine of Sphingolipids, September 16th-19th 2014, Kloster Banz, Germany.

Acknowledgements

First, I would like to thank Prof. Dr. Erich Gulbins for giving me the opportunity to work on these exciting projects under his excellent scientific guidance.

I am also very grateful for the academic support of Dr. Katrin Becker-Flegler and Dr. Alexander Carpinteiro and for their patience, encouragement and council throughout my PhD time and for sharing their enthusiasm for science with me.

I would like to thank my collaboration partners, Dr. Fabian Schumacher at the Department of Toxicology/Institute of Nutritional Science in Potsdam, Jan Becker at the Institute of Pathology in Cologne and Dr. Jiang Wang at the Department of Pathology and Laboratory Medicine in Cinncinnati, Ohio, for their time and effort.

I would also like to thank our partner lab at the Department of Surgery in Cincinnati, Ohio - particularly Dr. Peter Jernigan, Dr. Aaron Seitz and Prof. Dr. Michael J. Edwards - for highly motivating symposia and thought-provoking discussions.

I would also like to thank the members of the thesis committee for taking the time to evaluate my PhD thesis.

A huge thank you is also owed to my past and present colleagues and friends at the Department of Molecular Biology, for helping me out and creating a positive and fun work environment: Salina Begum, Hannelore Disselhoff, Dr. Bärbel Edelmann, Dr. Heike Grassmé, Karen Hung, Dr. Stephanie Kadow, Simone Keitsch, Anne Koch, Claudine Kühn, Dr. Cao Li, Jie Ma, Sigefried Moyrer, Eyad Naser, Helga Pätsch, Dr. Huiming Peng, Bettina Peter, Bärbel Pollmeier, Andrea Riehle, Carolin Sehl, Dr. Deepa Sharma, Matthias Soddeman, Shaghayegh Tavakoli, Barbara Wilker, Dr. Elisa Venturini and Yuqing Wu. In particular, I would also like to thank Gabriele Hessler and Melanie Kramer, who always offered a helping hand and a listening ear and provided excellent technical support.

Finally, I would like to thank my family and friends, particularly my parents and my fiancé, for their unconditional love and friendship and their unfaltering belief in me.

Curriculum Vitae

Der Lebenslauf ist in der Online-Version aus Gründen des Datenschutzes in enthalten.

Declarations

Erklärung:

Hiermit erkläre ich, gem. § 6 Abs. (2) g) der Promotionsordnung der Fakultät für Biologie zur Erlangung des Dr. rer. nat., dass ich das Arbeitsgebiet, dem das Thema „Identification of novel clinical applications for acid sphingomyelinase inhibitors“ zuzuordnen ist, in Forschung und Lehre vertrete und den Antrag von Nadine Beckmann befürworte.

Essen, den _____ _____

Prof. Dr. E. Gulbins - Unterschrift des wissenschaftl. Betreuers
Mitglied der Universität Duisburg-Essen

Erklärung:

Hiermit erkläre ich, gem. § 7 Abs. (2) d) + f) der Promotionsordnung der Fakultät für Biologie zur Erlangung des Dr. rer. nat., dass ich die vorliegende Dissertation selbständig verfasst und mich keiner anderen als der angegebenen Hilfsmittel bedient, bei der Abfassung der Dissertation nur die angegebenen Hilfsmittel benutzt und alle wörtlichen oder inhaltlich übernommen Stellen als solche gekennzeichnet habe.

Essen, den _____ _____

Unterschrift der Doktorandin

Erklärung:

Hiermit erkläre ich, gem. § 7 Abs. (2) e) + g) der Promotionsordnung der Fakultät für Biologie zur Erlangung des Dr. rer. nat., dass ich keine anderen Promotionen bzw. Promotionsversuche in der Vergangenheit durchgeführt habe und dass diese Arbeit von keiner anderen Fakultät/Fachbereich abgelehnt worden ist.

Essen, den _____ _____

Unterschrift der Doktorandin